INTEGRATED RENEWABLE ENERGY OPTIONS

FOR HVAC-COOLING SYSTEMS

by

Amani Shaheen Ali Al Hammadi

A Thesis Presented to the Faculty of the
American University of Sharjah
College of Engineering
in Partial Fulfillment
of the Requirements
for the Degree of

Master of Science in
Mechanical Engineering

Sharjah, United Arab Emirates

June 2013

Approval Signatures

We, the undersigned, approve the Master's Thesis of Amani Shaheen Al Hammadi.

Thesis Title: Integrated Renewable Energy Options for HVAC-Cooling Systems

Signature	**Date of Signature**
_____	_____
Dr. Mohamed Gadalla Professor, Department of Mechanical Engineering Thesis Advisor	
_____	_____
Dr. Naif Darwish Professor, Department of Chemical Engineering Thesis Committee Member	
_____	_____
Dr. Essam Wahba Associate Professor, Department of Mechanical Engineering Thesis Committee Member	
_____	_____
Dr. Ibrahim Deiab Interim Head, Department of Mechanical Engineering	
_____	_____
Dr. Hany El Kadi Associate Dean, College of Engineering	
_____	_____
Dr. Leland Blank Interim Dean, College of Engineering	
_____	_____
Dr. Khaled Assaleh Director of Graduate Studies	

Acknowledgements

I have been indebted in the preparation of this thesis to my advisor, Professor Mohamed Gadalla, whose patience, kindness, and academic experience have been invaluable to me. I am extremely grateful to him for encouraging and supporting me during the preparation of this thesis.

Besides my advisor, I would like to thank the rest of my thesis committee: Professor Naif Darwish and Dr. Esam Wahba, for their time, insightful comments and feedback.

Finally, I am forever grateful to my parents for their understanding, endless patience, and encouragement when it was most required.

Abstract

The demand for energy is increasing at an unexpected rate all over the world. Most of the present worldwide energy usage is based on fossil fuel and results in continuous depletion of this resource. Conventional Heating Ventilation and Air conditioning (HVAC) cooling systems are the dominant source of power consumption. These systems have some problems such as low performance, high emissions, and high costs. So, more economically and environmentally friendly HVAC systems are desired which can provide the required power while saving energy and having high performance and low emissions to the environment. In this thesis, fuel cells and solar collectors are integrated with absorption cooling systems for sustainable development. This thesis examines the Coefficient of Performance (COP) and/or overall efficiency of a Proton Exchange Membrane Fuel Cell (PEMFC), Flat Plate Solar Collector (FPSC), Parabolic Trough Solar Collector (PTSC), and Photovoltaic-Thermal Collector (PV/T) integrated with Double Effect and Triple Effect Absorption Systems (DEAS and TEAS) to produce 10 kW of cooling capacity. A computer program is developed using Engineering Equation Solver (EES) software. The software is used to obtain all required thermodynamic properties of a water-lithium bromide (H_2O/LiBr) solution and to carry out detailed energy and exergy analyses for each integrated system. The analyses show that the PEMFC system integrated with DEAS results in the highest COP. This is followed by the PV/T integrated with TEAS. The maximum energetic and exergetic COPs obtained for PEMFC integrated with DEAS are 2.70 and 2.30, respectively, while those obtained for PV/T integrated with TEAS are 2.32 and 2.06, respectively. However, the integration of PEMFC, PTSC, and PV/T with DEAS results in improved COP where the maximum energetic and exergetic COPs obtained are 2.94 and 2.50, respectively. Thus, this hybrid system is considered to be the optimum design from the performance point of view. This research provides a new interpretation of how alternative energy is utilized in operating HVAC cooling systems and presents a new insight into the most sustainable integrated systems that can be applied in residential and commercial buildings in the UAE.

Search Terms: HVAC, PEM Fuel Cell, Flat Plate Solar Collector, Parabolic Trough Solar Collector, PV/T, Double Effect, Triple Effect

Table of Contents

List of Figures

Figure Page

List of Tables

Table Page

Nomenclature

a	Membrane water activity
A	Area (cm^2)
C	Variable of top loss coefficient
C_b	Bond conductance($m.K/W$)
C_f	Conversion factor of the thermal power plant
COP	Coefficient of Performance
Cp	Average specific heat of hydrogen ($kJ/kg \cdot K$)
cc	Distance between the centers of two neighboring tubes (m)
d	Variable of top loss coefficient
D	Diameter (m)
Dr	Solution distribution ratio
E	Energy (kW)
f	Variable of top loss coefficient
F	Faraday's constant ($C/mole$)
F'	Collector efficiency factor
F_{fi}	Standard fin efficiency
F_R	Heat removal factor
h	Specific enthalpy (kJ/kg)
h_c	Convection heat transfer coefficient ($W/m^2.K$)
h_r	Radiation heat transfer coefficient ($W/m^2.K$)
h_{fi}	Heat transfer coefficient between the working fluid and tube wall($W/m^2.K$)
h_{p2}	Penalty factor
HHV	Higher Heating Value (kJ/kg)
i	Current density (A/cm^2)
I	Solar radiation (W/m^2)
I_D	Direct incident solar radiation (W/m^2)
i_{max}	Maximum current density (A/cm^2)
i_o	Exchange current density (A/cm^2)
$\dot{I}$	Rate of irreversibility(kW)
k	Specific heat ratio for air and hydrogen
kt	Thermal conductivity
L	Length (m)
M	Molecular weight ($g/mole$)
m	Variable of standard fin efficiency
$\dot{m}$	Mass flow rate of refrigerant (kg/s)
n	Number of electrons

n_{fc}	Number of PEM fuel cells
N	Number of glass cover
Nus	Nusselt number
$\dot{Q}$	Rate of heat transfer (kW)
P	Pressure (kPa)
p	Partial pressure (kPa)
Pr	Prandtl number
U	Heat loss coefficient
R	Universal gas constant ($J/mole.K$)
r_{HL}	Heat loss ratio
ρ	Density (kg/cm^3)
R_{Ohmic}	Ohmic resistance of PEM fuel cell (Ωcm^2)
Re	Reynolds number
s	Specific entropy ($kJ/kg.K$)
$\dot{S}$	Rate of entropy generation (kW)
T	Temperature ($°C$)
T_{fm}	Average working fluid temperature ($°C$)
t_{mem}	Membrane thickness (cm)
v	Specific volume (m^3/kg)
V	Voltage (V)
v_{act}	Activation overpotential
v_{Ohmic}	Ohmic overpotential
v_{Conc}	Concentration overpotential
w	Width (m)
W	Work (kJ)
$\dot{W}$	Power (kW)
x	Mole fraction
$\dot{X}$	Rate of exergy

Greek Letters

α	Transfer coefficient
α_p	Solar absorbtance of collector plate
β	Collector tilt angle (deg)
β_1, β_2	Constant and variable of concentration overpotential
β_c	Packing factor of solar cell
ϵ	Effectiveness
ε	Emissivity
ΔG	Gibbs free energy ($J/mole$)
ΔS	Change in Entropy ($J/mole.K$)

ΔT	Temperature difference
λ_{mem}	Membrane water content
μ	Dynamic viscosity ($Pa \cdot s$)
υ	Kinematic viscosity (mm^2/s)
δ	Thickness (m)
η	Efficiency
σ	Stephen-Boltzman constant ($5.67 \times 10^{-8} W/m^2.K^4$)
σ_{mem}	Membrane conductivity
τ_g	Solar transmittance of glazing
ω	Velocity (m/s)
ζ	Stoichiometry

Subscripts

a	Aperture
A	Anode
Abs	Absorber
amb	Ambient
b	Bottom
c	Cover
C	Cathode
cell	PEM fuel cell
$Cond$	Condenser
des	Destructed
e	Edge
el	Electrical
en	Energy
$Evap$	Evaporator
ex	Exergy
g	Glass
gen	Generation
HG	High temperature generator
$HHEX$	High heat exchanger
i	The *i*th state, component
$irrev$	Irreversible
L	Overall
LG	Low temperature generator
$LHEX$	Low heat exchanger
MG	Medium temperature generator
$MHEX$	Medium heat exchanger

o	Dead state condition
ov	Overall
p	Absorber plate
PEM	Proton exchange Membrane
r	Receiver
ref	Reference
ro	Receiver outside
ri	Receiver inside
co	Cover outer
$reac$	Reactant
rev	Reversible
s	Sun
sat	Saturation
sys	System
th	Thermal
tot	Total
u	Useful
w	Water

Superscripts

CH	Chemical
PH	Physical

Abbreviations

COP	Coefficient of Performance
$DEAS$	Double Effect Absorption System
FP	Flat Plate
$FPSC$	Flat Plate Solar Collector
LHV	Lower Heating Value
$PEMFC$	Proton Exchange Membrane Fuel Cell
PT	Parabolic Trough
$PTSC$	Parabolic Trough Solar Collector
PV/T	Photo-Voltaic Thermal
sat	Saturation
sys	System
$TEAS$	Triple Effect Absorption System
th	Thermal
tot	Total

Chapter 1 Introduction

Most of the present worldwide energy usage is based on conventional energy sources (e.g., fossil fuels) which results in continuous depletion of these resources. World demand for fossil fuels, starting with oil, is expected to exceed annual production, probably within the next two decades. International economic and political crises and conflicts can also be initiated by shortages of oil or gas [1]. In addition, such resources have risks associated with their use, as they are all potentially vulnerable to adverse weather conditions or human acts. This is due to the fact that burning fossil fuels releases harmful emissions which affect the local, regional, and global environment. Conventional cooling systems are the main consumer of the power produced by the electrical grids. As a result, serious moves should be taken in order to reduce energy consumption and develop sustainable, environmentally friendly cooling systems.

The world trend nowadays is to employ renewable energy sources in energy production systems in order to achieve the most productive output from an economic and environmental perspective. These systems are known as advanced thermodynamic systems that lead to the achievement of high power efficiency with reduced environmental emissions [2].

Renewable energy can be utilized to solve issues related to the high demand on electricity generated by electrical grids and can also lessen the environmental impact by releasing fewer emissions into the atmosphere. Renewable energy can contribute significantly to the residential and commercial buildings in the United Arab Emirates in terms of power and environmental impact. Fuel cells and solar collectors are among the alternatives that are utilized as sources of electricity for cooling systems in the proposed research due to their suitability and applicability to both the UAE environment and HVAC cooling systems.

1.1 Need for the Research

In this section, the purpose behind conducting such research is illustrated. The significance of the research for sustainable building operations is also presented.

1.1.1 Problem statement.

The demand for energy is increasing at an unexpected rate all over the world where energy consumption in residential applications, mainly HVAC systems, is the major factor in increasing power consumption, especially in the Gulf region.

Conventional HVAC systems that use the vapor compression refrigeration principle along with fossil fuels as a source of energy have some issues such as high energy consumption rates, low performance, high emissions, and high costs. Therefore, new technologies have to be implemented in order to come up with better systems that lead to the achievement of high power efficiency with reduced environmental emissions and reduced cost.

The high energy consumption and high costs of conventional HVAC systems make it a crucial area for study aiming at lowering the consumption by integrating alternative systems running on renewable energy sources to decrease the load on the electrical grids. In addition, conventional sources of energy such as fossil fuels release harmful emissions to the environment. Therefore, renewable energy can be useful both in terms of energy consumption and environmental safety.

This research aims to improve HVAC cooling systems using PEMFC, FPSC, PTSC, and PV/T integrated with Double and Triple Effect Absorption Systems (DEAS and TEAS). These fuel cells and solar thermal and photovoltaic collectors have been chosen based on their contribution to sustainable building operations.

1.1.2 Significance of the research.

Fossil fuel sources are limited and are going to be depleted as the worldwide demand increases. It has been predicted that crude oil and natural gas will be significantly depleted within the next 40 years. World demand for fossil fuels is expected to exceed annual production, probably within the next two decades.

While the global growth of the rate of energy consumption is 4%, the percentage in the UAE is more than double (around 10%). Statistics for 2007 have shown that Dubai's power consumption was about 25 Gigawatts (GW), while the power requirement is 26 GW. In addition, the average individual's electricity usage, according to the Dubai Electricity and Water Authority (DEWA) is 20,000 kilowatt hours (kWh) annually. Air conditioning systems were found to be the major factor in increasing power consumption in the country since they consume more than 75% of electricity generated at peak load time. As a result, the UAE government aims to shift 7% of the needed power to renewable energy sources by the year 2020, according to [1] and [2].

The burning of fossil fuels releases harmful emissions to the atmosphere known as greenhouse gases that contribute to global warming. Global warming is the increase in the average temperature of the Earth's air and oceans since the mid 20^{th} century. Greenhouse gases, in addition to their harmful effect on the environment, have a crucial impact on public health and welfare. The United States has been ranked as the highest producer of CO_2 emissions (5,762,050 thousand metric tons of carbon dioxide) followed by China. The UAE was ranked 38, accounting for 72,309.8 thousand metric tons of carbon dioxide for the year 2007. Besides the harmful emissions, coal mining creates several environmental issues in the form of erosion and habitat besides destruction; in addition, toxic ash remains after coal burning and is disposed into landfills. Likewise, oil drilling has a significant impact on marine organisms and the building of roads. Structures and pipelines to support oil recovery operations can impact the wildlife in natural areas, according to [3]-[5].

From an economic point of view, non-renewable energy sources have finite deposits. This creates special concern about their exploitation, use, consumption, and recycling in order to prevent their shortage or unavailability for future generations. Future shortages in fossil fuels will lead to price increases, which furthers the need for alternative resources of energy [6].

Energy shortages and environmental problems caused by conventional energy generation systems, as well as the rapid increase in world population, create a strong need for clean energy sources. Renewable energy has a great potential to solve environmental issues because of its lack of carbon-based emissions that release warming and polluting

agents into the atmosphere. They therefore add no contribution to global warming, nor polluting emissions. In addition, as there are no harmful emissions released by renewable energy, it has indirect benefits on health and its costs. It is also characterized by the absence of noise as there are no combustion engines with associated moving parts used in producing such energy. So, renewable energy sources are essential to the sustainability of human life, wildlife, and building operations.

Moreover, from an economic point of view, renewable energy is less expensive than non-renewable energy and can be used repeatedly without wearing down. However, the devices used in processing the energy are not free. Moreover, the financial cost of its applications is not always cheap, but compared with non-renewable energy, it is more cost effective in the capital cost as well as in the long run. Moreover, renewable energy has indirect advantages on the expenditure spent on human health and environment destruction issues that are associated with the utilization of non-renewable energy, as mentioned by [7]-[9].

Examples of renewable energy are solar energy, fuel cells, wind, flowing water (hydroelectric), tidal (ocean), biofuels, and geothermal energy. Fuel cells and solar energy are good alternatives and have been chosen to be implemented in the absorption systems proposed in this research. They are distinguished as clean and green forms of energy because of their minimal impact on the environment. Moreover, they are cost effective as they are abundant and available in the UAE, especially solar energy, as the UAE is characterized by a sunny climate.

1.2 Background and Motivation

In this section, a background of absorption refrigeration systems, fuel cells, and solar energy is presented.

1.2.1 Absorption cooling system.

In absorption cooling systems, heat energy is absorbed with the use of two fluids as the working medium. In comparison with the compression refrigeration system in which the compression of the refrigerant is done by a compressor, the compression in the absorption system is achieved by absorbing the refrigerant by an absorbent. As the

refrigerant is absorbed, it gets converted from a vapor to a liquid so its volume is reduced. As a result, the power consumed in the absorption system is much less than that required by the compression system. In the absorption system, the pump requires a very small amount of power for its operation and it remains almost the same even for higher capacities of refrigeration. In the compression system, the compressor requires large quantities of power which increase as the size of the refrigeration system increases. Moreover, unlike the compression system which can be run by electric power only, the absorption system runs mainly on the extra or waste heat available in the system which makes it suitable to be operated by renewable energy sources such as the heat generated by a solar cell, or the waste heat produced by a fuel cell.

Economically speaking, the running cost of the absorption system is much less than that of the compression system as the electrical power required to operate the pump is very small. Also, no extra power in the pure electric form is required since the extra heat or energy that would have otherwise gone wasted is utilized. On the other hand, the compression system can run only on electric power and it requires a large amount of power, which has become very expensive. Also, the refrigerant used in absorption systems which is mostly water along with the absorbent are cheaply and easily available compared with the expensive halocarbons that are used in compression systems.

From foundations and maintenance points of view, the compressor in the compression systems is operated at very high speeds, which makes high vibrations and noise and requires a very strong foundation to sustain them. Conversely, absorption systems operate silently as there are no major moving parts. In addition, the compressor in the compression system requires maintenance regularly unlike the small pump in the absorption system that fails rarely.

In contribution to the environment and health, unlike compression systems which release harmful gases due to the burning of the halocarbon refrigerants, absorption systems have no greenhouse effect.

Although absorption systems have advantages over compression systems, their initial capital cost is much higher than compression systems although their running cost is lower. Moreover, in the lithium bromide absorption system, lithium bromide is corrosive in nature which reduces the overall life of the system. In case of an ammonia system,

ammonia is corrosive to copper. Nevertheless, copper is used with the halocarbon refrigerants in the compression systems and they are quite safe, thus ensuring a long life for the refrigeration system. So, compression systems have a longer life than absorption systems. In addition, the working pressures of the absorption systems are very low which requires the system to be sealed thoroughly so that no atmospheric gases enter the system. Also, in the absorption system, heat has to be rejected from a number of parts such as the condenser and the absorber, compared to the compression system in which the heat is given up only from the condenser. Finally, the Coefficient of Performance (COP) of the absorption system is very low compared to the compression system. For instance, the COP of the double effect lithium bromide absorption system is about 1.3 while that of the compression system used for the air conditioning applications is about 4 to 5, according to [10] and [11].

Due to the advantages of the absorption refrigeration system mentioned herein, this system has been chosen to be integrated with renewable energy sources to replace the conventional compression system.

1.2.2 Fuel cells.

A fuel cell is an electrochemical device that converts chemical energy directly into electrical energy without the need for converting heat into mechanical energy. Through electrochemical reactions, fuel cells produce electricity, water, and heat by the combination of a fuel (on the anode side) and oxygen (on the cathode side) in the presence of an electrolyte. The reactants flow into the cell, and the reaction products flow out of it, while the electrolyte remains within it.

The purpose of a fuel cell is to produce an electrical current that can be directed outside the cell to do work. Because of the way electricity behaves, this current returns to the fuel cell, completing an electrical circuit. Fig. 1.1 illustrates the operation of the fuel cell.

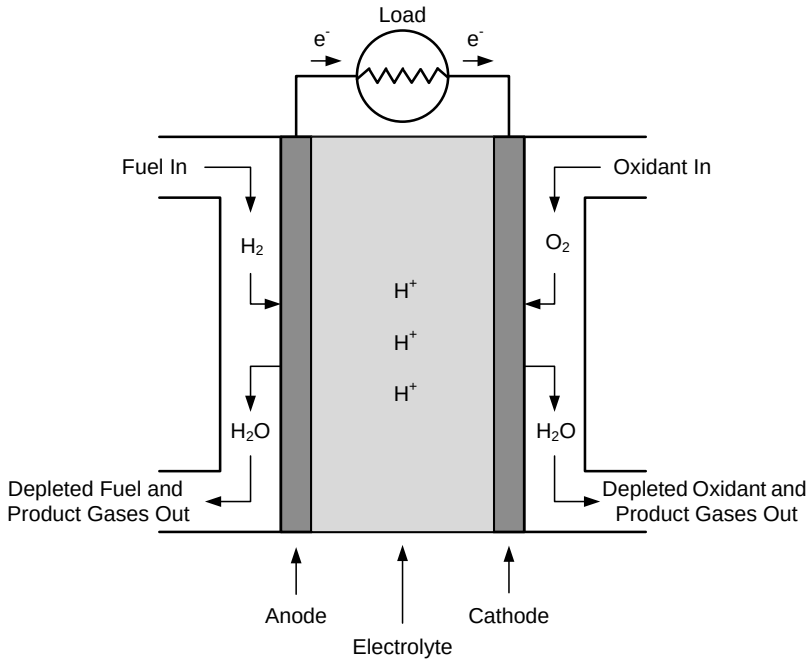

Fig. 1.1 Working principle of fuel cells (adapted from [12]).

There are several types of fuel cells, and each operates a bit differently. But in general terms, hydrogen atoms enter the fuel cell at the anode where a chemical reaction strips them of their electrons. The hydrogen atoms are ionized and carry a positive electrical charge. The negatively charged electrons provide the current through wires to do work. If alternating current is needed, the direct current produced by the fuel cell must be routed through a conversion device called an inverter.

Oxygen enters the fuel cell at the cathode and, in some fuel cell types, it combines with electrons returning from the electrical circuit and hydrogen ions that have traveled through the electrolyte from the anode. In other cell types the oxygen picks up the electrons and then travels through the electrolyte to the anode, where it combines with hydrogen ions. Whether they combine at the anode or cathode, together hydrogen and oxygen form water, which drains from the cell. As long as the fuel cell is supplied with hydrogen and oxygen, it will generate electricity.

The electrolyte plays a key role as it permits only the appropriate ions to pass between the anode and cathode. If free electrons or other substances could travel through the electrolyte, they would disrupt the chemical reaction.

Even better, since fuel cells create electricity chemically, rather than by combustion, they are not subject to the thermodynamic laws that limit a conventional power plant. Therefore, fuel cells are more efficient in extracting energy from a fuel. Waste heat from some cells can also be harnessed, boosting the system's efficiency further, as mentioned by [12]-[14].

Fuel cells are a very promising technology as they can generate electrical power and at the same time produce water and waste heat. Also, the high efficiency conversion from chemical energy to electrical energy without the need of combustion makes them economically attractive. Fuel cells have a variety of options in the type of fuel and catalyst and their associated parameters according to the operating temperature, pressure of the system, and required power output. Moreover, they are quiet in operation which makes them attractive for residential areas where noise pollution is undesirable [15].

Fuel cells are classified either according to the type of electrolyte that determines the operating temperature range of the fuel cell, or according to the type of fuel used in the cell. Aqueous electrolytes are limited to temperatures of about 200°C or lower because of their high vapor pressure and rapid degradation at higher temperatures. The operating temperature also plays an important role in determining the degree of fuel processing required. In low temperature fuel cells, all the fuel must be converted to hydrogen before entering the fuel cell. In addition, the anode catalyst in low temperature fuel cells (mainly platinum) is strongly poisoned by carbon monoxide (CO). However, in high temperature fuel cells, CO can be internally converted to hydrogen or even directly oxidized electrochemically [15]. So, based on the operating temperature of the fuel cell, each type can contribute to a range of applications starting with small portable devices, passing through vehicles and cars, and ending with stationary power generation plants. A brief description of these types, classified based on the type of electrolyte, follows herein.

1.2.2.1 Polymer Exchange Membrane Fuel Cells (PEMFCs).

The PEMFC uses a solid phase polymer membrane as the cell electrolyte which provides excellent resistance to gas crossover and has a high current density and a relatively low operating temperature (ranging from 60 to 100 °C). The low operating temperature means that it does not take very long for the fuel cell to warm up and begin

generating electricity. Because the cell electrolyte is a polymer film and the cell operates at relatively low temperatures, issues such as sealing, assembly, and handling are less complex than most other fuel cells. The need to handle corrosive acids or bases is eliminated in this system. The low operating temperature makes PEMFC the most suitable type of fuel cells for powering automobiles such as cars and light vehicles as they need fast start up.

PEMFCs are also used for stationary applications, especially for small-scale distributed generation. System efficiency typically ranges from 25 to 32% based on the Lower Heating Value (LHV). By recovering waste heat from the cooling water, the overall thermal efficiency can be raised to about 70%. On the other hand, PEMFC has some disadvantages as the low and narrow operating temperature range makes thermal management difficult, especially at very high current densities. However, this disadvantage can be overcome by lowering operating current density [12]-[15].

For its advantages, PEMFC is used in this research as a heat source for the absorption system to produce 10 kW of cooling capacity.

1.2.2.2 Alkaline Fuel Cells (AFCs).

AFCs use highly concentrated potassium hydroxide (KOH) as the electrolyte in fuel cells operating at high temperatures (up to 250 °C). They use less concentrated KOH for fuels cells at lower temperatures (less than 120 °C). AFC is one of the most developed fuel cell technologies and it is the cell that flew man to the moon. NASA had used alkaline fuel cells since the mid-1960s in the Apollo-series missions and on the Space Shuttle. AFCs consume hydrogen and pure oxygen producing potable water, heat, and electricity. They are among the most efficient fuel cells, having the potential to reach 80% efficiency. AFCs can operate on pressures up to 5 atm. They have excellent performance on hydrogen and oxygen compared to other types of fuel cells due to their active O_2 electrode kinetics and their flexibility to use a wide range of electro-catalysts and electrodes which do not have to be made of precious metals. Also, the activation overvoltage at the cathode is usually less with an acid electrolyte fuel cell.

A drawback of AFCs is the sensitivity of the electrolyte to CO_2which requires the use of highly pure H_2 as a fuel. As a result, a highly effective CO and CO_2 removal

system is required. However, a scrubber can be used to treat the inlet ambient stream to minimize CO_2 entering the cell or a separator can be used in the fuel processor to obtain a pure stream of H_2. In comparison to other fuel cells, AFC has high performance which leads to the plausibility of developing the technology for terrestrial, stationary power applications [13]-[15].

1.2.2.3 Phosphoric Acid Fuel Cells (PAFCs).

Phosphoric acid is used as the electrolyte in PAFCs, which typically operate at higher temperatures than PEMFCs (around 150 to 220 °C). As a result, PAFCs have a longer warm-up time. This makes them unsuitable for use in cars. However, PAFCs have the potential for use in small stationary power-generation systems. Although the present practice is to operate at atmospheric pressure, the operating pressure of PAFCs surpasses 8 atm.

Development of PAFCs has slowed down in the past ten years, in favor of PEMFCs that were thought to have better cost potential. However, PAFC development continues. PAFCs are much less sensitive to CO than PEMFCs and AFCs. PAFCs have demonstrated system efficiency of 37 to 42% (based on the LHV of natural gas fuel), which is higher than most PEMFC systems can achieve. In addition, the waste heat from PAFCs can be readily used in most commercial and industrial cogeneration applications.

Cathode-side oxygen reduction is slower in PAFCs and requires the use of platinum catalyst. Although less complex than PEMFCs, PAFCs still require extensive fuel processing. Finally, the highly corrosive nature of phosphoric acid requires the use of expensive materials in the stack. Due to the above mentioned drawbacks, PAFCs are not preferred for implementation in absorption systems [13].

1.2.2.4 Molten Carbonate Fuel Cells (MCFCs).

The defining characteristic of a MCFC is the material used for the electrolyte which is a molten mixture of alkali metal carbonates. The electrolyte is usually a binary mixture of lithium and potassium, or lithium and sodium carbonates. MCFCs operate at relatively high temperatures (in the range of 600-700 °C) which allows them to attain high efficiencies. Their high operating temperature also allows them to utilize different

types of fuel. Also, both CO and certain hydrocarbons can be used as fuels for the MCFC, as they are converted to hydrogen within the stack which results in improving the system efficiency to 40-50%. In addition, no expensive electro-catalysts are needed as the nickel electrodes used in MCFCs provide sufficient activity.

The development of MCFCs has been focused on large stationary and marine applications, where the relatively large size and weight of MCFCs and slow start-up time do not matter. MCFCs are under development for use with a wide range of conventional and renewable fuels. After PEMFCs, MCFCs have been demonstrated most extensively in stationary applications.

The main challenge for MCFC developers stems from the very corrosive and mobile electrolyte, which requires the use of nickel and high-grade stainless steel. The higher temperatures promote material problems, impacting mechanical stability and stack life [13]. Thus, MCFCs are not considered for integration with the absorption refrigeration system in this research.

1.2.2.5 Solid Oxide Fuel Cells (SOFCs).

SOFCs have become a valid option for energy generation due to their attractive features such as their solid-state components. Unlike the high temperature MCFCs, SOFCs have a solid state electrode, as well as a solid state anode, cathode, and cell interconnects. This type of fuel cells operates at very high temperatures (between 800 and 1000 °C). Due to its high temperature of operation, it is an effective source of byproduct heat which can be used for cogeneration. Also, due to this high temperature of operation, it does not require precious metals on the anode or the cathode.

Another advantage of SOFCs is the ability to use a wide variety of fuels which makes it a promising technology. Although its operational temperature makes it impractical for smaller applications, SOFCs in general are very promising fuel cells for use in the distributed or centralized power generation industry. Thus, these fuel cells are best suited for large stationary power generators that could provide electricity for factories or towns. However, the high temperature of SOFCs has its drawbacks. There are thermal expansion mismatches among materials, and sealing between cells becomes difficult. The high operating temperature places severe constraints on materials selection

and results in difficult fabrication processes. Corrosion of metal stack components is also a challenge. These factors limit stack-level power density, thermal cycling, and stack life[16]-[18].

Among the above mentioned fuel cells, PEMFCs are the type best-suited for small stationary applications. Thus, PEMFCs have been chosen to be integrated with the absorption system in this research.

1.2.3 Solar energy.

The energy in sunlight is in the form of electromagnetic radiation from the infrared (long) to the ultraviolet (short) wavelengths. The solar energy striking the Earth's surface depends on weather conditions, as well as the location and orientation of the surface, but overall, it averages about $1kW/m^2$ under clear skies with the surface directly perpendicular to the sun's rays. Energy from sunlight can be converted directly into electricity by a device called a solar cell which uses a photovoltaic effect in the conversion process. It does this without using chemical reactions or moving parts. Assemblies of cells are used to make solar panels, solar modules, or photovoltaic arrays. The major applications of solar energy can be classified into two categories: solar thermal systems, which convert solar energy to thermal energy, and photovoltaic (PV) systems, which convert solar energy to electrical energy. Usually, these two systems are combined to form the photovoltaic thermal (PV/T) solar system [19].

1.2.3.1 Solar thermal collectors.

A solar thermal collector is a device composed of solar cells designed to collect heat by absorbing sunlight via fluid circulation and convert it into a more usable or storable form. In the solar thermal system, external electrical energy is required to circulate the working fluid through the system.

Solar thermal collectors are classified into two main categories: non-concentrating and concentrating. In the non-concentrating collectors, the collector area (the area that intercepts the solar radiation) is the same as the absorber area (the area absorbing the radiation) so that the whole solar panel absorbs the light.

Flat plate and evacuated tube solar collectors are examples of non-concentrating collectors and are used to collect heat for domestic hot water and space heating or cooling by integrating them with absorption chillers [20].

Flat Plate Solar Collectors (FPSC).

Flat plate collectors are the most common type of solar thermal collectors. They consist of a transparent cover or "glazing" that allows solar energy to pass through but reduces heat losses, a heat-transport fluid (air, antifreeze, or water) flowing through tubes to remove heat from the absorber, a dark flat plate absorber designed to absorb sunlight and release the energy as heat which is absorbed by the working fluid and trapped by the glazing, and a heat-insulating backing. Fluid is circulated through the tubing to transfer heat from the absorber to an insulated fluid tank. Fluid flows into a lower corner of the collector and becomes heated before exiting through a higher corner. The typical range of operating temperatures of flat plate solar collectors is 80 –150 °C[21].

Evacuated Tube Solar Collectors (ETSC).

Evacuated tube collectors are made up of long, clear glass tubes containing a colored glass or metal tube to absorb the sunlight. The space between the outer glass tube and the inner absorber tube is evacuated (contains almost no air), which greatly reduces convection and conduction heat loss to the outside. This allows them to achieve greater efficiency than FPSCs, especially in colder conditions. This advantage is largely lost in warmer climates, except in cases where very hot water is desirable. Evacuated tubes are more expensive per unit area than other collectors, and are ideal for cold climates or buildings that use hot water as an energy source for air conditioning or heating. In comparison with FPSCs, FPSCs are more cost effective in all sunlight conditions, up to 76% on clear days. For systems that require a very high temperature rise, evacuated tubes outperform flat plates in all conditions. However, if winters are mostly sunny, FPSCs tend to be the most cost effective overall [22] and [23].

Due to this, FPSCs among the non-concentrating collectors are used in the proposed solar thermal powered HVAC cooling system in this research. Examples of

concentrating collectors are the parabolic trough and parabolic dish collectors and are illustrated as follows.

Parabolic Trough Solar Collectors (PTSC).

This type of collector is generally used in solar power plants. A curved, mirrored trough is used to concentrate solar radiation on an insulated tube or heat pipe(also called a receiver, absorber or collector), running the length of the trough, positioned at the focal point of the reflector, containing coolant which transfers heat from the collector to a thermally-driven system.

The receiver may be enclosed in a glass vacuum chamber. The vacuum significantly reduces convective heat loss. A fluid passes through the receiver and becomes very hot. Common fluids are synthetic oil, molten salt and pressurized steam. The fluid containing the heat is transported to a heat engine where about a third of the heat is converted to electricity. The trough is parabolic along one axis and linear in the orthogonal axis. The trough tilts east to west so that the direct radiation remains focused on the receiver as the sun moves throughout the day. However, seasonal changes in the angle of sunlight parallel to the trough do not require adjustment of the mirrors since the light is simply concentrated elsewhere on the receiver. Thus the trough design does not require tracking on a second axis [24] and [25].

Parabolic Dish Solar Collectors (PDSC).

PDSCs are considered the most powerful type of collectors. These collectors focus all the sunlight that strikes the dish onto a single point on the dish, where a receiver captures the heat and transforms it into a useful form. This geometry may be used in solar furnaces and solar power plants.

The advantage of a dish system is that it can achieve much higher temperatures due to the higher concentration of light. Higher temperatures lead to better electricity conversion, a task which the dish system performs very efficiently. Also, losses due to atmosphere between the dish and its focal point are minimal, as the dish is generally designed specifically to be small enough that this factor is insignificant on a clear, sunny

day. However, there are also some disadvantages. Heat to electricity conversion requires moving parts, which results in higher maintenance costs. In general, a centralized approach for this conversion is better than the decentralized concept in the dish design. Second, the engine is part of the moving structure, which requires a rigid frame and strong tracking system. Furthermore, parabolic mirrors are used instead of flat mirrors and tracking must be dual-axis.

Compared to a parabolic trough which concentrates light on a line, a parabolic dish concentrates light on a point. A practical application of a parabolic dish is a flashlight lens, which is used to transform a point source of light into a parallel beam. However, parabolic troughs are used in solar power plants to produce superheated steam and generate electricity because their fabrication and tracking equipment are less expensive than that of the dish. Due to the advantages of parabolic troughs over the parabolic dishes and their applicability for space cooling, they have been implemented in the design of a solar thermal-based HVAC-cooling system for higher operating temperatures [26].

1.2.3.2 Solar photo-voltaic collectors (PV).

Photovoltaics is the field of technology and research related to the application of solar cells in producing electricity for practical use. In the PV system, the electrical efficiency of the system decreases rapidly as the PV module temperature increases. Therefore, in order to achieve higher electrical efficiency, the PV module should be cooled by removing the heat. A common PV module converts 4-17% of the incoming solar radiation into electricity depending on the type of solar cells in use and the working conditions. More than 50% of the incident solar energy is converted into heat after deducting the reflected portion.

In order to eliminate an external electrical source and cool the PV module, the PV module should be combined with a solar air/water heater collector. This type of system is called a solar Photo-Voltaic Thermal (PV/T) collector system [20].

1.2.3.3 Solar photo-voltaic thermal collectors (PV/T).

A PV/T collector is a combination of photovoltaic (PV) and solar thermal components/systems that produces electricity and heat from one integrated component or system. The PV/T collector produces thermal and electrical energy simultaneously. Besides the higher overall energy performance, PV/T systems demand less physical space and equipment cost through the use of common frames and brackets as compared to the separated PV and solar thermal system placed side-by-side [27].

In this research, a solar PV/T collector is used to produce heat and electricity to drive a triple-effect absorption cooling system.

1.2.3.4 Meteorological data of the UAE.

In order to conduct a thermodynamic analysis on the solar powered absorption cooling system, data on solar irradiance and ambient air temperature is required. Thus, the monthly average solar irradiance and ambient temperature of the UAE are provided in Table 1.1 [28,29].

Table 1.1 Monthly average values of direct beam solar irradiance and averaged measured temperature of the UAE ([28] and [29]).

Month	**Direct Solar Irradiance (W/m^2)**	**Inlet Air Temperature °C**
Jan	490	18.7
Feb	603	22.8
Mar	470	24.7
Apr	480	27.5
May	605	33.0
Jun	565	34.4
Jul	530	35.1
Aug	617	35.9
Sep	615	33.6
Oct	595	30.5
Nov	593	26.5
Dec	520	22.3

1.3 Literature Review

The aim of this section is to provide basic background and review existing literature on absorption refrigeration, fuel cells, solar thermal, and photovoltaic technologies. Moreover, recent developments in the implementation of fuel cells, solar thermal, and photovoltaic technologies in HVAC systems are reviewed in order to shed light on the latest evolutions in the field. Research options are discussed to provide a solid background for the systems proposed.

The literature review covers the different configurations and working fluids used in absorption systems to come up with the most efficient configuration and working fluid that can be utilized in HVAC systems. Then, literature discussing Proton Exchange Membrane Fuel Cells (PEMFCs) are reviewed to determine the most significant parameters that should be considered in analyzing such systems. The review also covers the solar thermal, Photo-Voltaic (PV), and Photo-Voltaic Thermal (PV/T) systems to build a background on their specifications and operating conditions. The implementation of fuel cells as well as solar thermal and PV/T collectors in absorption systems is also covered to shed light on the recent developments in these areas. In addition, available literature discussing the integration of HVAC systems with hybrid systems composed of fuel cells and solar energy has been reviewed.

1.3.1 Absorption cooling system.

A literature review on absorption cooling systems covering different configurations is conducted in this section. Also, the different forms of working fluid pairs used in absorption systems are reviewed and evaluated.

Industrial processes use a huge amount of thermal energy by burning fossil fuels for the production of steam or heat, where heat is released to the surroundings as waste after the processes. A heat-operated refrigeration system such as an absorption refrigeration system can be used to convert the waste heat to useful energy. Such systems reduce the electricity purchased from utility companies for conventional vapor compression refrigeration systems. In addition, problems related to global environmental change, such as the so called greenhouse effect caused by CO_2 emissions released from the combustion of fossil fuels in the utility power plants, are reduced. Moreover, most

vapor compression refrigeration systems use chlorofluorocarbon (CFC) and hydrochlorofluorocarbon (HCFC) refrigerants because of their thermo-physical properties. CFCs are well-known as the main cause of depletion of the ozone layer. This has stimulated interest in the development of absorption systems. Absorption refrigeration systems can employ natural refrigerants such as water, ammonia, and methanol, and can be activated by hot water, steam, and direct-fired natural gas instead of electricity. Thus, low-grade thermal energy can be used to drive absorption chillers where solar energy, geothermal energy, fuel cells, and waste heat from industry processes can be used as energy sources for these systems instead of fossil fuels. However, vapor compression refrigeration systems still dominate all market sectors. Thus, in order to promote the use of absorption systems, further development is required to improve their performance and reduce costs.

The coefficient of performance (COP) of lithium bromide (H_2O/LiBr) absorption chillers, defined by the ratio of the refrigeration capacity and the driving heat input, is in the range of $0.7 < COP < 1.5$ depending on the cycle configuration and the temperature of the driven heat [30] and [31].

1.3.1.1 Configurations of absorption system

Absorption systems can be modeled in various configurations, some of which are the single, double, and triple effect configuration. The following section looks at these in more detail.

Single effect absorption system.

The single effect is the simplest configuration of absorption technology. Karamangil et al. [32] conducted a thermodynamic analysis of a single-stage absorption refrigeration system with different refrigerant–absorbent pairs using a software package and compared the theoretical performance of the cycles. The effect of the operating temperature, effectiveness of the solution, and selection of working fluid pair on the system performance were examined using the developed package. It was concluded that the performance of the cycles increases with increasing generator and evaporator temperatures, but decreases with increasing condenser and absorber temperatures. The

performance of the system was affected by the solution heat exchanger (SHE) more than the refrigerant heat exchanger (RHE) and solution–refrigerant heat exchanger (SRHE). Specifically, the use of SHE improved the system COP up to 66%, while RHE and SRHE had an effect of only 14% and 6%, respectively. Thus, the SRHE was not considered practically significant according to the researchers. Furthermore, the analysis showed that the generator temperature had a great effect on the COP. In general, single-effect technology has a low COP but can operate at low temperature of waste heat applications, resulting in no cost expense for energy input.

Double effect absorption system.

For higher temperatures of waste heat applications, double-effect technology is proposed. The COP of the double effect technology is in the range between 1.0 and 1.5 which is much higher than that of the single effect. However, double effect technology requires significantly higher driving temperatures: between 120 °C and 170 °C.

The double effect cycle is made by adding high and low heat exchangers between the generator and the absorber of the single effect cycle. The generator is then divided into two sections: high and low generators forming double solution circuits. The two cycles are connected through the condenser and low generator. The low generator and condenser of the double effect system operate at almost the same conditions of those in a single effect system. However, the double effect system operates at a much higher temperature of heat input than that of the single effect system. This configuration increases the availability of the double effect technology, as a result of the higher temperature of input heat can be utilized which results in higher COP [33] and [34].

Double effect systems can be designed in different configurations according to the method of connecting the solution circuits. Parallel and series flows of refrigerant are the common configurations of this technology.

Kaushik and Arora [35] did energy and exergy analyses of single effect and series flow double effect lithium bromide/water ($LiBr/H_2O$) absorption systems. They found that the coefficient of performance (COP) of the single effect system lay in the range of 0.6–0.75 and the corresponding COP value for the series flow double effect system lay in the range of 1–1.28 (a 60–70% increase). Also, their exergy analysis showed that the

irreversibility is highest in the absorber in both systems when compared to other system components. Moreover, an increase in the generator temperature increased the COP and the exergetic efficiency in both single and series flow double effect systems up to an optimum generator temperature. On the other hand, an increase in the evaporator temperature caused the COP to increase while the exergetic efficiency decreased. Also, increasing the absorber temperature resulted in reducing the performance of the system significantly as compared to increasing the condenser temperature.

Arun et al.[36] did a comparative study of double effect parallel flow and series flow absorption refrigeration systems with lithium bromide as the working fluid. An analysis was conducted on the parallel flow cycle based on the concept of equilibrium temperature in the low pressure generator. The COP of the double effect parallel flow cycle along with its sensitivity to operating conditions were determined and compared with those of series flow cycle. It was found that the maximum attainable COP for the parallel flow cycle was greater than that for the series flow cycle over the entire range of operating conditions considered. Compared to the series flow system, performance of the parallel flow system is more sensitive to the effectiveness of low pressure heat exchanger and evaporator temperature variation and less sensitive to variations in condenser and absorber temperatures. For both parallel and series flow cycles, maximum COP increases with higher evaporator temperatures and effectiveness of the heat exchanger, as well as with lower condenser and absorber temperatures. This analysis revealed that the sensitivity of maximum COP is greater at lower temperatures at the evaporator, condenser, and absorber. In addition, it is more sensitive to evaporator temperature than condenser and absorber temperatures. The researchers suggest incorporating a large low pressure heat exchanger for parallel flow, and a large high pressure heat exchanger for series flow, as COP is more sensitive to the respective effectiveness.

Gomri and Hakimi [37] presented an exergy analysis of a double effect $LiBr/H_2O$ absorption refrigeration system. The results showed that the performance of the system increased with increasing low pressure generator (LPG) temperature, but decreased with increasing high pressure generator (HPG) temperature. Also, the absorber had the highest exergy loss, followed by the HPG, which therefore makes the absorber and HPG the most important components of the double effect refrigeration system which need to

be developed. In addition, exergy loss rates in the pump and solution valves were very small, so their effects on the total exergy loss rate were negligible. Results also showed that COP and exergetic efficiency initially increase sharply with increasing the temperature of LPG and then they become almost constant at high values of LPG temperature. So, up to a certain limit, increasing LPG temperature does not significantly improve the COP and exergetic efficiency. In this study, it was concluded that for condenser and absorber cooling water temperature (27 °C/32 °C) and chilled water temperature (12 °C/7 °C), the best COP and exergetic efficiency were obtained for LPG temperatures between 78 °C and 81 °C and HPG temperatures between 125 °C and 135 °C.

Rabah [38] also did a comparative study between single effect and double effect absorption refrigeration systems with identical cold output. The results showed that the COP of the double effect system (in the range of 1.22–1.42) is approximately twice the COP of the single effect system (in the range of 0.73–0.79), while the exergetic efficiency of the double effect system (in the range of 14.3–25.1%.) is slightly higher that that of the single effect system (in the range of 12.5–23.2%). In addition, the COP of the cycle increases with increasing generator and evaporator temperatures, but decreases with increasing condenser temperatures. The comparison also showed that the condenser and generator thermal loads of single effect systems were greater than those for the double effect systems.

Triple effect absorption system.

As the COP of double effect systems can reach around 1.5 and is almost close to the maximum, triple effect systems are proposed to attain higher efficiency. Aghdam et al. [39] presented energy and exergy analyses of triple effect series and parallel flow absorption refrigeration systems with $LiBr/H_2O$ as the working fluid pair. For both series and parallel flow systems, the results showed that the COP of the system increases slightly when temperatures of the high temperature generator and evaporator are increased, while the exergetic efficiency decreases. Moreover, there is a relative preference of triple effect parallel flow system over the series flow system. Compared to the double and single effect systems, the COP of the triple effect system is about 50%

more than that of the double effect system and about 2.2 times that of the single effect system. Also, the results showed that most of the irreversibilities occur in generators and absorbers due to mixing losses in series and parallel flow systems.

Kaita [40] carried out a simulation analysis for three kinds of triple effect absorption systems: parallel flow, series flow, and reverse flow, in order to investigate the coefficient of performance, the maximum pressure and temperature of each cycle, and pressure and temperature of the high temperature generator. The results showed that the COP of the parallel flow cycle was the highest among the cycles, while the maximum pressure and temperature in the reverse flow cycle were lower than those of other cycles. This is advantageous in terms of adapting to regulations and resisting corrosion. In addition, a heat recovery of the condensed refrigerant leaving low temperature generator can be achieved by installing a heat exchanger which could improve the COP by 0.03–0.05. Moreover, Kaita compared the three configurations in terms of factors such as number of solution pumps and controllability of the solution flow. The overall comparison led to the preference of the parallel flow cycle compared to series and reverse flow cycles.

1.3.1.2 Working fluids for absorption systems.

An absorption refrigeration system uses different combinations of refrigerant–absorbent known as solution pairs. The absorbent acts as a secondary fluid to absorb the primary fluid which is the refrigerant in its vapor phase. Ammonia/water (NH_3/H_2O) and lithium bromide/water ($LiBr/H_2O$) solutions are the most widely used working fluid pairs in absorption systems. For large capacity industrial applications requiring low temperatures for process cooling, the NH_3/H_2O absorption system is generally used. However, $LiBr/H_2O$ systems are used where moderate temperatures are required (e.g., air conditioning and chilling applications) and this system is more efficient than NH_3/H_2O [32].

A thermodynamic analysis of a single stage absorption refrigeration system with different working fluids was done by Karamangil et al.[32]. Their study showed that the system with the $LiBr/H_2O$ mixture had a higher COP but could operate in a more narrow range of generator temperatures, because of its crystallization possibility, compared to the

systems using ammonia-based mixtures. So, although the lithium bromide/water solution is the most commonly used working fluid, precautions have to be taken to prevent crystallization of lithium bromide.

In conclusion, a lithium bromide/water ($LiBr/H_2O$) absorption chiller is an environmentally-friendly air conditioning system that avoids the global warming potential (GWP) and the ozone depleting potential (ODP) caused by CFC and HCFC gases used by the conventional vapor compression refrigeration cycle of air conditioning systems. Moreover, double effect and triple effect systems with parallel flow cycles are the best configurations to be integrated with renewable energy options.

1.3.2 Fuel cells.

Fuel cells offer clean, quiet, and efficient electrochemical energy conversion. Among high efficiency technologies, fuel cells are among the most promising as they have high efficiency and very low environmental impact. They are considered an alternative to combustion-based cogeneration and traditional, centralized power generation. As fuel cells have no moving parts, and do not involve combustion, in ideal conditions they can achieve up to 99.99% reliability, according to [41] and [42].

For low temperature fuel cells, the electrical efficiencies are between 30-40%, and are expected to rise to a maximum of 45% by the time they enter the market. Likewise, high temperature fuel cells are expected to have an electrical efficiency of around 55% at the time they enter the market [43]. From an environmental point of view, the application of fuel cells in automotive vehicles can reduce carbon dioxide emissions about 40-60% and nitrogen dioxide emissions about 50-90%. Although fuel cells hold a great promise for delivering clean and efficient power for automotive and residential applications, they are still in their developmental infancy, and a great deal of research is necessary before they can be considered as viable power systems [44].

Fuel cell technology offers the possibility to excel in today's automobile power techniques in terms of environmental compatibility, consumer profit, costs of maintenance, and efficiency. The key concern is economic. This will be decided by the cost of fuel cell systems if they are to be used as power generators for future electric vehicles [45].

Compared to other micro-cogeneration technologies, fuel cells show the highest electrical efficiency, and are promising systems for residential and small-scale cogeneration applications. The main reason for their high performance is their modular construction. Therefore, their efficiency is hardly influenced by its size [46].

Fuel cells can provide lower cost electricity, heating, and air conditioning for homes and offices independent of the power grid; however, they can be hooked into the grid as a backup or as a source of electricity for peak demands[47]. Another application of fuel cells is in remote homes and other sites where stringing wire from the nearest utility is too expensive. With fuel cells, the occasional delivery of power can get through without the noise of a typical engine-powered generator.

The overall efficiency of HVAC systems can be enhanced greatly through a beneficial use of fuel cell exhaust heat [48]. For fuel cells used in commercial building applications, the use of absorption technology is highly encouraged due to the fact that absorption chillers can use thermal energy to produce chilled water for cooling.

According to Hearn [49], fuel cells' residential cogeneration application has been introduced to the market in Japan where 480 residential cogeneration systems were placed in homes in 2005. In these fuel cells, waste heat is used to provide hot water. 93% of the natural gas lower heating value (LHV) is converted to useful heat or electricity, fuel cell stack electricity is also provided to the household. The production of hot water in typical residential cogeneration is around 1.4 kW for every kilowatt of electricity. Additionally, cogeneration units can be sized for one kilowatt to hundreds or even thousands of kilowatts[40].

Kakaras et al. [50] stated that in order to evaluate fuel cell operation in a commercial office building, typical electricity (power consumption) and heating and cooling loads of the building have to be examined. In their project of stationary co-generation fuel cell systems in Greece, the resulted profiles for 24-hour demand in summer and winter showed that the air conditioning electricity loads were significant in the summer period. Based on these results, the concept of trigeneration configuration that is applied in absorption chillers using the heat rejected by fuel cells could be examined. It was found that the cost of the absorption chiller is 750 to 800 € per ton of

capacity and the COP is 0.7. Electrical and thermal efficiencies of fuel cells were considered as 37% and 50% on the LHV of natural gas respectively [50].

Many configurations can be achieved for an integrated fuel cell system and air conditioning. An interesting one is that proposed by Seong et al. [51], where the air conditioning has a variable load that undergoes a rapid change in power instantaneous consumption. The fuel cell system stores the generated electricity if the instantaneous power consumption of the air conditioner is lowered and supplies the stored electricity together with the generated electricity to the air conditioner if the instantaneous power consumption is increased.

A study conducted by Ferguson and Ugursal [42] showed that the performance of fuel cell-based cogeneration systems is affected by two critical factors: cell size and operating strategy. So, in order to understand the impact of these parameters on the performance of residential fuel cell-based cogeneration systems, further studies and comprehensive models with the ability of modeling electric storage are highly encouraged.

According to Romey et al. [52], low temperature fuel cells are suitable for transportation applications. However, in the stationary field, the requirements regarding temperature limit the range of applications of low temperature fuel cells to water for domestic use as the industry usually requires higher temperatures. However, low temperature fuel cells can be used for small scale stationary applications.

Based on these studies, it is clear that fuel cell technology is highly encouraged to be applied in future energy systems. For HVAC applications, they can provide electricity to power air conditioning systems, cover domestic hot water needs, and provide heating and cooling requirements. A literature review on each type of fuel cell is provided in the following sections.

1.3.2.1 Proton Exchange Membrane Fuel Cells (PEMFCs).

PEMFCs, one of the low temperature fuel cells, have gained international attention as alternative to the combustion engine in the automotive and stationary markets due to features such as their adaptable size and low operating temperatures. The typical operating temperature of PEMFCs is in the range of 60–100 °C. PEMFCs have achieved

over 30,000 hours of continual operation in stationary applications, and 50% power is achieved in 16 seconds at ambient temperatures of 20˚C [49].

Generally, applications of PEMFCs in stationary markets are foreseen in the next coming years and those for the residential applications (in the size of 0.5–10 kW) are under development in Europe, the US, and Japan [44]. Hearn [49] stated that PEMFCs' coolant loop can provide hot water to the residence at 60˚C as sustained temperatures above 90˚C are out of reach in the present production of PEMFCs stack technology (in 2006). Therefore, according to Hearn [49], results of PEMFC laboratory stacks at temperatures of 160˚C are subject to recent publications. The importance of higher PEMFCs technology is the opportunity it provides to use the coolant in residential and commercial buildings.

Lipman et al. [53] examined the economics of producing electricity from PEMFC systems under various operating conditions, including the possibility of using fuel cell vehicles (FCVs) to produce power when they are parked at office buildings and residences. The analysis showed that the economics of both stationary fuel cells and FCV-based power vary significantly in terms of input variables such as the price of natural gas, electricity prices, fuel cell and reformer system costs, and fuel cell system durability levels. The results showed that stationary PEMFC systems can supply electricity for offices and homes in California at competitive rates at potential future installed capital costs of the order $1200/kW for a 5 kW home system and $700/kW for a 250 kW commercial system, assuming somewhat favorable natural gas costs of $6/GJ (Gigajoule) for residences and $4/GJ for commercial buildings. FCV-based power at individual residences does not appear to be as attractive, at least where FCV power can only be used directly or banked with the utility and not sold in greater quantities [53].

From an economic point of view, the investment costs for PEMFCs will likely be reduced because of the expected mass production of PEMFCs for vehicle propulsion. As a result, PEMFC co-generation systems for stationary applications will become economical for one- and multiple-family dwellings. Thus, a concept of a PEMFC cogeneration system for terraced or detached houses has been developed and theoretical and practical investigations have been performed [52].

In short, PEMFCs have emerged as the technology of choice for low temperature, moderate power applications. For the integration with absorption systems, double effect parallel flow configuration can be implemented, as PEMFCs operate at low temperatures.

1.3.2.2 Alkaline Fuel Cells (AFCs).

With the growing interest in fuel cells, the Alkaline Fuel Cell (AFC) has proven to be a good alternative. The long lifetime and the possibility to use non-noble catalysts gives it advantages over all other fuel cell systems [50].

The AFC was the first fuel cell technology to be put to practical use and make the generation of electricity from hydrogen feasible. It had been used widely in the U.S. space program to produce electricity and water onboard spacecraft where it could provide high-energy conversion efficiency with no moving parts and high reliability [46], [51]. However, most of the current research and development are directed towards PEMFCs for residential applications. Nevertheless, AFC technology is very competitive for power applications, especially for small-scale cogeneration applications [51].

McLean et al. [54] conducted a review of AFC technology focusing about on its power density and lifetime performance. They stated that because of the rapid development of PEMFCs, AFCs have fallen out of favor with the technical community although they were popular in the 1970s and 1980s. AFCs appear to compete favorably with ambient air PEMFCs as they can provide high power densities and achieve long lifetimes in certain applications.

Contamination of AFCs due to the presence of CO_2 is an issue for sustained system operation. CO_2 in the cathode air stream definitely poisons the electrolyte and in turn can cause some designs of electrodes to become clogged with carbonate. Development of new means of CO_2 removal from the oxidant stream for an AFC system would address many operational issues associated with AFC stacks. Contamination due to impure hydrogen is another problem that may prohibit the use of AFCs with reformed hydrogen streams, though this contamination seems to be totally reversible [55].

A literature review of AFCs done by McLean et al. [51] revealed that AFCs were the first fuel cell technology to be put into practical service and make the generation of electricity from hydrogen feasible. Starting with applications in space, the alkaline fuel

cell provided high energy conversion efficiency with no moving parts and high reliability. Also, AFCs were used as the basis for the first experiments with vehicular applications of fuel cells. Current AFC systems have been demonstrated to easily meet the 5000 hour lifetime required for traction applications. However, despite their early success, the current research and development activities are more directed towards PEMFCs for vehicular applications. In practice, the AFC is very well-developed, simple to operate with a built-in cooling system, and has excellent reliability [56].

According to Duerr et al. [57], the Centre of Economic Renewable Power Delivery (CERPD) at the University of Strathclyde has developed various fuel cell systems for stationary and vehicular applications over the last 5 years. Duerr et al. have designed and built reliable and cost efficient hybrid fuel cell/battery systems, which could replace existing conventional technology in the near future. A domestic scale combined heat and power (CHP) alkaline fuel cell (AFC) system has been developed. A small AFC stack was used to satisfy the average load demand of the domestic load profile of a stationary application whereas the load peaks were supplied by a battery system working in parallel with the AFC stack.

Also more research is devoted to high temperature fuel cells as the Solid Oxide Fuel Cell (SOFC) and the Phosphoric Acid Fuel Cell (PAFC) which show some interesting prospectives in new power cycles for electricity plants. In spite of the limited development efforts for AFC technology, it is still competitive with other fuel cells for power applications. Further improvement in the AFC technology is still possible and will strengthen this position [50], [51].

Overall, it appears that the AFC continues to have potential to succeed in certain market applications, but needs some further development to address potential solutions for the sensitivity of the AFC to CO_2 in the oxidant stream [54].

1.3.2.3 Phosphoric Acid Fuel Cells (PAFCs).

Bizzarri and Morini [41] mentioned that for a four 200 kW PAFCs hybrid plant implemented for the operation of a hospital HVAC system, the electricity produced from the fuel cells could almost provide the monthly needs except during the summer. However, even in this season, the fuel cells could supply around 70% of the electrical

need. The heat recovered from the four cells could be exploited to supply some of the needed heat, while the remainder could be provided by high efficiency gas-fired boilers so that the production of the boilers could be lowered by 17% in January and up to 45% in October. Regarding primary energy, it was found that the hybrid system would lower the hospital's primary energy needs by more than 4925 MWh/year. In a conventional system, CO_2 emissions associated with the production of 1 kWh of electricity are estimated at 0.7 kg while in fuel cells system the value reduces to 0.19 kg CO_2/kWh. Moreover, using heat recovery for thermal usage with a reduction in boiler use lowers pollution. Hence, CO_2 emissions associated with all processes associated with the electrical and thermal requirements decreased from 6999 to 3163 tons/year [41].

Regarding maintenance, fuel cells require some regular upkeep such as periodic filter changeout and maintenance for pump and fans no more than once a year [47]. An economic analysis for the hybrid fuel cell system showed that the electricity cost is 0.085 €/kWh. Likewise, 0.34 (€/Sm^3)[1] worth of natural gas is required to feed cogeneration systems while 0.51 €/Sm^3 is needed for the conventional system. The annual interest rate is assumed at 3% and the excepted life of the system is assumed to be 7 years[41].

Mohamed [58] discusses the use of commercially-available PAFCs to operate air conditioning systems for big buildings in Kuwait. The proposed fuel cell system, which is usually delivered with a built-in heat exchanger for hot water, is operated by natural gas and uses a propylene glycol-water loop to recover thermal energy. The PAFC has a 200 kW nominal electric power capacity, and produces thermal energy of 105 kW at 120 °C, and 100 kW at 60 °C. In his study, it was suggested that a combined mechanical vapor compression and absorption water chiller is operated by fuel cells to utilize the fuel cells' full output as electric power and waste heat. Also, it is proposed to use a cold storage technique in order to meet the required cooling capacity to supply cold water during as the power output of PAFC is not enough to carry the full load. This allows fuel cell power output to supply the needed energy for the average as well as the peak air conditioning system capacity. The economy of the proposed solution is very promising once the cost of the fuel cell becomes $2000/kW or lower.

[1]Standard cubic meters per hour, measured at standard metric conditions.

1.3.2.4 Solid Oxide Fuel Cells (SOFCs).

An analysis of an integrated system that combines a SOFC power generation system with an absorption heating and cooling system done by Zink et al. [59] showed that such a system has the capacity to produce electric power, heating, and/or cooling for buildings. The total system efficiencies in different modes are expected to reach 87% or more. Such a system demonstrates great advantages in both technical and environmental aspects. With the present development trends in fuel cells, it is likely that initial costs for the SOFCs will reach commercially-viable levels within the next decade. The economic and environmental analysis of the proposed system illustrates how it is superior to current power and heat supply technologies.

Baniasadi and Alemrajabi [60] in their research of combining SOFCs with a recovery cycle for the sake of electric power, cooling load, and domestic hot water demand of a hotel, stated that hot exhaust gases of SOFCs are potentially applicable in heat recovery systems. Results of the research showed that for energy generation and heat recovery cycles, a maximum efficiency of 83% (based on fuel lower heating value, LHV), all the electrical energy and cooling load, and 40% of hot water demand could be provided by this cycle. Moreover, about 49% of the input exergy could be efficiently recovered for energy requirements of a building.

Alanne et al. [61], in their study of SOFCs as an energy source for residential applications, showed that SOFC technology is an alternative to heating systems based on oil and electrical furnaces and is a major competitor for such systems.

1.3.3 Solar energy.

Solar thermal energy is the most abundant renewable source of energy and is available in both direct and indirect forms. The sun emits energy at a rate of 3.8×10^{23} kW, of which approximately 1.8×10^{14} kW is intercepted by the earth. About 60% of this amount, or 1.08×10^{14}, reaches the surface of the earth. The rest is reflected back into space and absorbed by the atmosphere. About 0.1% of this energy, when converted at an efficiency of 10%, would generate four times the world's total generating capacity of about 3000 GW. It is also worth noting that the total annual solar radiation falling on the earth is more than 7500 times the world's total annual primary energy consumption of

450 EJ (Exa Joule = 10^{18} joule). The annual solar radiation reaching the earth's surface, approximately 3,400,000 EJ, is an order of magnitude greater than all the estimated (discovered and undiscovered) non-renewable energy resources, including fossil fuels and nuclear energy. Due to the fact that the efficiency of solar thermal and photovoltaic collectors is generally low at the time being, the effectiveness of solar cooling would be closely related to the availability of solar irradiation, climatic conditions, and geographic location [1] and [62].

Using solar energy for generating both electrical energy and water-heating applications has been an attractive proposal for many years. Many combinations of solar electricity generation and heat generation systems have been studied to cover the bulk requirements of residential houses. Generally, depending on the type of solar cells used, some of the 80–95% of the collected energy is not converted to electricity and therefore, constitute a loss and at the same time heat the modules. Hence, large area solar modules absorb considerable amounts of solar radiation that also generate excessive heat. This excessive heating of modules serves to lower the conversion efficiency of the modules by about 3–6% for 1°C. Many systems have been designed to remove this excessive heat and to utilize it as a source of energy for some other applications [63].

Solar energy as heat can be used as an energy source for building HVAC systems so that energy is conserved and the environment is protected by avoiding CO_2 emissions released through burning fossil fuels for electrical power production purposes. Due to large surfaces exposed to solar radiation, buildings offer an ideal platform for distributed solar energy production compared to other energy-consuming utilities [64].

Kim and Ferreira [65] stated that as cooling demand increases with the intensity of solar radiation, solar refrigeration has been considered as a logical solution. During the 1970 oil crisis, solar refrigeration received great interest. There were many projects for development or demonstration of solar refrigeration technologies and solar refrigeration continued to be an important issue in the 1980s. The study conducted by Kim and Ferreira presented different technologies to deliver refrigeration from solar energy and showed that solar thermal with a single-effect absorption system appears to be the best option, closely followed by the solar thermal with a single-effect adsorption system, and by the solar thermal with a double-effect absorption system.

Qu et al. [66] mentioned that solar thermal energy can be used in an absorption cycle, a desiccant cycle, or a mechanical process for cooling purposes. However, a solar absorption cycle is more reliable, feasible, and quiet in comparison with solar desiccant cycles and mechanical processes.

Thirugnanasambandam et al. [1] did an economic comparison of a solar-powered single, double effect vapor absorption air-conditioning system and a vapor compression system using the present worth comparison method along with the equivalent annual comparison method. They suggested that a double effect solar air-conditioning system is more suitable for HVAC applications.

Fong et al. [62] conducted a comparative study for five types of solar cooling systems for a typical office in subtropical Hong Kong, which is known for its hot and humid summers. The solar cooling systems include solar electric compression refrigeration, solar mechanical compression refrigeration, solar absorption refrigeration, solar adsorption refrigeration, and solar solid desiccant cooling. In addition, different installation strategies and types of solar collectors were compared for each kind of solar cooling system. The key performance indicators were solar fraction, coefficient of performance, solar thermal gain, and primary energy consumption. It was found that the performance of the five refrigeration systems from highest to lowest is as follows: solar electric compression, solar absorption, solar adsorption, solar solid desiccant cooling, and solar mechanical compression refrigeration. Solar electric compression refrigeration makes use of solar electric gain while solar absorption refrigeration adopts solar thermal gain. These two solar cooling systems would have even better performance through the continual advancement of the solar collectors. They provide a promising application potential of solar cooling for buildings.

Yoshie et al. [67] proposed a new HVAC system for condominiums that makes use of solar heat and outdoor cool air by integrating solar collectors with the balcony handrail, the 24-h ventilation system, and under-floor space. They have carried out experiments and computational fluid dynamics (CFD) studies on a solar heat collector integrated with the balcony handrail and calculated dynamic thermal load on a model condominium. The results showed that the proposed system has high performance, both for energy saving and thermal comfort.

Ortiz et al. [68] did a numerical model for a solar thermal-assisted HVAC system in a 7000 m^2 educational building in a high desert climate to predict its performance and optimize its parameters. The system was composed of a solar collector array, hot storage, cold storage, absorption chiller, chilled water heat exchanger, steam heat exchanger, solar heat exchanger, and air handling units. The system was used for space heating in the winter and electricity production in the summer. The modes of operation of the system depended on the time of the day and on the season of the year. It was found that using solar energy can cover over 90% of the total heating requirements and solar cooling can reduce the need to use external cooling energy by 33-43%.

Johnston [69] did a study on a building-integrated solar energy system installed on Chinese-style buildings in which the panels were mounted on the walls and roofs. He came to the conclusion that potential savings of up to 15% in space heating, and up to 55% in air conditioning energy demand can be achieved.

1.3.3.1 Solar thermal collectors.

A literature review on flat plate, parabolic trough, vacuum tube, and evacuated tube solar collectors is provided in this section.

Flat Plat Collectors (FPSC).

Farahat et al. [70] developed an exergetic optimization of flat plate solar collectors in order to determine their optimal performance and design parameters by carrying out a detailed energy and exergy analysis though a simulation program. The results showed that the exergetic efficiency increases with increasing the incident solar energy per unit area of the absorber plate while it decreases rapidly when the ambient temperature and the wind speed increase. Since these parameters change during the day (and to attain the maximum exergetic efficiency), the solar collector operating conditions should change during the day and the design of solar collector should be based on the daily average of these parameters.

Marcos et al. [71] designed and tested an experimental solar space heating and cooling facility. The design was based on a new type of flat plate solar collector. The solar facility comprised a 48 m^2 (with a net area of 42 m^2) solar collector field, a 25 kW

plate heat exchanger, a 1500 L storage tank, a 4.5-kW air-cooled absorption chiller, and several fan coils. The facility had been used to heat and cool an 80 m^2 lab (the average area of Spanish homes). The system could meet 65.3% and 46% of the space heating and cooling demand, respectively. The savings in CO_2 emissions compared to conventional air conditioning ranged from 556.9 kg of CO_2 (compared to a heat pump) to 2658.1 kg of CO_2 (compared to coal-fuelled systems). The potential emissions reduction based on this concept for the Spanish households is 19.8 million tons of CO_2.

Parabolic Trough Collectors (PTSC).

Mazloumi et al. [72] in their simulation of a solar single-effect lithium bromide–water absorption cooling system mentioned that the required heat energy of the generator could be provided by a solar parabolic trough collector with direct water and an insulated thermal storage tank. The largest collector area and storage tank capacity were required for a day in July to supply the cooling loads of a typical house with a maximum load of 17.5 kW. The researchers concluded that the collector mass flow rate has a negligible effect on the minimum required collector area while it has a significant effect on the optimum capacity of the storage tank. The minimum required collector area could supply the cooling loads for the sunshine hours of a day in July. The operation of the system has also been considered after sunset by storing the solar energy.

A great deal of work has been conducted on solar HVAC systems, especially solar-powered absorption cooling systems. Qu et al. [66] developed a solar thermal absorption cooling and heating system that incorporates 52 m^2 of high temperature linear parabolic trough solar collectors, a 16 kW double effect water lithium bromide ($LiBr/H_2O$) absorption chiller, and a heat recovery heat exchanger with circulation pumps and control valves for the purpose of generating chilled and heated water for space cooling and heating. The system could supply 39% of cooling and 20% of heating energy for a building space if the system included a properly-sized storage tank and short low diameter connecting pipes. Also, they concluded that the PTSC has high solar efficiency compared to various flat plates and evacuated tube collectors when the solar field operates at a high temperature. However, building characteristics and load profiles, climate conditions and incident solar radiation profiles, physical limitations of the

situation, and the economics of the energy supply should all be considered in the design and operation of a solar absorption cooling and heating system [66].

A system studied by Mammoli [73] was made of PTSC which heats water in a large hot storage tank to be delivered to an absorption chiller for space cooling or directly to heating coils for space heating. Large chilled water storage tanks are used to cool the building along with the absorption chiller and are charged off-peak and discharged during the day. The system comprises a parabolic trough solar collector, a $LiBr/H_2O$ double-effect absorption chiller, a thermal storage unit, a heat recovery space from electric heat pumps, a generator, a heat exchanger, fans and pump motors with variable frequency drives (VFDs), and a direct digital control (DDC) system.

Masson and Qu [74] have developed an integrated solar cooling system with parabolic trough collectors, a double effect absorption chiller, and hot/cold water storage tanks. They suggested optimizing the system based on different parameters such as volume and insulation thickness of the cold/hot storage tank.

Wang and Zhai [75] developed a solar absorption air-conditioning system driven by parabolic trough solar collectors. In this system, chilled water produced by the solar cooling system is stored in a cold storage water tank. This means that chilled water produced by the solar cooling system in the spring could be stored for later use in the summer. It was reported that the cooling output could attain 266 kW with a corresponding thermal COP of 0.8. The solar COP was 0.2–0.3 and the average solar collecting efficiency exceeded 40%.

Vacuum Tube Solar Collectors (VTSC).

Eicker and Pietruschka [34] designed a simulation model for a solar thermal absorption chiller combined with a stratified storage tank, steady-state or dynamic collector model, and hourly resolved building loads. Vacuum tube collectors were used with sizes between 1.7 and 3.6 m^2 per kW cooling load to cover 80% of the cooling load. The results showed that buildings with the same maximum cooling load and different load time series required collector areas varying by more than a factor of 2 to achieve the same solar fraction. The best solar thermal efficiency was 45% for high full load hours of nearly 2000 h. The total system cost for commercially-available solar cooling systems

is between 180 and 270 €/MWh, depending on the cooling load file and the chosen control strategy. The total costs are dominated by the costs for the solar thermal system and the chiller itself. For a more moderate climate with low cooling energy demand, the costs can rise as high as 680 €/MWh.

Agyenim et al. [76] studied the performance of a domestic scale prototype experimental solar thermal absorption cooling system based on a $LiBr/H_2O$ absorption chiller that consists of a 12 m^2 vacuum tube solar collector, a 4.5 kW $LiBr/H_2O$ single effect absorption chiller fired by hot water to produce chilled water, a 40 kW heat exchanger, a 1000 L cold storage tank, and a 6 kW fan coil unit. The performance of the individual components in the system were studied based on the physical measurements of the daily solar radiation, ambient temperature, inlet and outlet fluid temperatures, mass flow rates, and electrical consumption by component. The system was used to supply cooling to an 82 m^3 office. The results of the study showed that the system's average thermal COP was 0.58 based on the thermal cooling power output per unit solar thermal energy available. The system's average ambient temperature was24 °C while the electrical COP 3.64 with an average chiller inlet temperature of 77.1 °C.

In order to improve the COP of the system, thermal storage is required to store excess energy where for every kW of chilled water, a storage capacity of 180 and 250 L is required. Although the developed system is not commercially competitive for cooling applications due to large costs, it is technologically competitive compared with the current vapor compression systems. To promote the system's commercial competition, it is recommended that the system be integrated into domestic hot water (DHW) and space heating systems to meet the heat demand during the winter [76].

Evacuated Tube Solar Collector (ETSC).

According to Wang and Zhai [75], the largest solar cooling system in China is the demonstration project at Beiyuan, which was constructed in 2005. In this system, heating pipe-evacuated tubular solar collectors were installed on the roof. As the solar cooling system is the thermal driving source, solar collectors of this type are characteristic of high thermal efficiency as well as frost-resistance.

Based on the literature review of solar thermal collectors, FPSC and PTSC have been chosen to be integrated with the double effect and triple effect absorption cooling systems, respectively.

1.3.3.2 Solar photo-voltaic collectors (PV).

Photovoltaic (PV) technology is one of the finest ways to harness solar power. Vast research is being carried out on this technology, and a significant improvement in its performance has been achieved[77].

Tiwari et al. [78] conducted a review of available literature on thermal modeling of photovoltaic modules. Even though commercial PV modules are available and being widely deployed, it is suggested to carry out more research to improve cost-effectiveness and performance and target well-known issues to increase their competitiveness. Different PV modules have demonstrated substantial improvements and transformations over the past 40 years and are expected to undergo developments in the following decades. PV cells and modules have therefore been under development. PV modules can be used in buildings, transportation, standalone devices, agriculture, medical refrigeration, and street lights [78].

Building Integrated Photovoltaic (BIPV) adoption varies greatly by, and within, countries depending upon the climate, environment, electricity industry structure, government policies, local product offerings, market stimulation mechanisms, consumer demand, existing industrial capabilities, and the forms of tariff arrangement for grid-connected PV power generation. BIPV modularity results in short installation times, and the lack of moving parts reduces the need for maintenance [79].

In building integrated PV systems, an overall energy scheme must be developed for the building at the beginning of the construction project because the energy requirements for a building are initially determined and affected decisively in the drawing board stage by the layout of the building shape, orientation, and use. This will help in easily selecting the most suitable solar energy techniques according to cost-effectiveness. Doing so will avoid some problems associated with solar thermal energy systems such as the losses resulting from the conversion of heat to cooling capacity in the case of space

cooling. If not considered properly in the design stage, this process has the capacity to completely offset any advantage gained from the solar system.

On the other hand, solar PV energy can easily displace a large fraction of traditional heating sources in the case of space heating. Typically, an absorption chiller is used to utilize the heat produced by the solar thermal array for cooling. The system also includes hot and cold thermal storage and an evaporative cooling tower to dispose of the rejected heat from the chiller [73],[80].

The incorporation of PV modules can be used in both existing and new buildings. It can be used as a shading system, window pane, building exterior paneling, and for many other purposes [80].

Bazilian et al. [81] conducted a thermographic analysis on a residential-scale building integrated photovoltaic (BiPV) cogeneration system that is based on roofing technology with a heat recovery unit in which a PV array is acts as a roofing element as well as a power producer. They concluded that convection of the air behind the panels can aid PV panel cooling and provide a heat source for space heating. In addition, the heat recovery unit utilizes the waste heat from the back of the array while cooling PV cells. Also, waste heat from the system array can be utilized to increase the system's efficiency and in turn, its economics.

1.3.3.3 Solar photo-voltaic thermal collectors (PV/T).

Joshi and Tiwari [82]conducted exergy and energy analyses of a hybrid photovoltaic–thermal (PV/T) parallel plate air collector. For the performance of a PV/T collector to be evaluated, the value of electricity versus heat from the collector should be determined. Their analysis showed an increase of about 2–3% exergy due to thermal energy in addition to its 12% electrical output from PV/T system, which makes an overall electrical efficiency of about 14–15% of the PV/T system.

Charalambous et al. [83] in their literature review found that PV/T efficiencies could range from over 70% for a perfect collector to less than 60% for a low-quality collector. Air PV/T collectors are generally less efficient than liquid ones.

Moreover, since the sheet and tube design is the easiest to manufacture and is only 2% less efficient, it is the most promising of design concepts. The thermal

performance of a coverless PV/T collector is reduced especially at high temperatures due to heat losses from the top. However, the coverless PV/T collectors have a better electrical performance. The optimum PV/T collector flow rate was found to be in the range of 0.001–0.008 kg/s.m^2, whereas a value of 0.015 kg/s.m^2 was also reported. Thus, optimum flow rate studies need to be investigated further.

PV/T collectors are very promising devices and further work should be carried out aiming at improving their efficiency and reducing their costs, making them more competitive. This would aid the global expansion and utilization of this environmentally-friendly renewable energy device [84].

A literature review conducted by Thirugnanasambandam et al. [1] realized a new approach of domestic heating and cooling by using solar PV/T collectors with an efficiency of 9% via studying the performance of the collector in varying geographical regions with different total surface areas. They confirmed that PV/T technology offers a feasible solution for the problem of domestic heating and cooling.

The thermal and electrical parameters of a PV/T air collector include solar cell temperature, back surface temperature, outlet air temperature, open-circuit voltage, short circuit current, maximum power point voltage, and maximum power point current, among others [85].

In this research, a PV/T collator is integrated with a triple effect parallel flow absorption cooling system to produce 10 kW of cooling load.

1.3.3.4 Working fluids for solar collectors.

Air or water can be used as the working fluid for FPSCs and PV/Ts. However, water collectors are generally more efficient than air ones as water has a high heat transfer rate due to high thermal conductivity. Therefore, water is used as the working fluid in FPSCs as it has a simple configuration and will be used for thermal output only. On the other hand, air is used in the PV/T system so that the device is more compact, lightweight, and easy to install as it is a combination of solar thermal and PV collectors. In addition, the use of air avoids the need for special heat transfer fluids (oil or glycol) to withstand freezing conditions. Also, corrosion and leakage though joints and ducts are less of a concern [83].

The working fluid in the concentrating solar collectors could be water or a commercial oil. In this research, Therminol 66 oil was selected as the working fluid for the PTSC. It can be used in both thermal solar systems and thermal storage tanks. Therminol 66 is a high-performance, highly stable synthetic heat transfer fluid due to the unique stability of the polyphenyl structure. It operates at temperatures in the range of 85°C to 400°C and is intended for use in systems operating at or near atmospheric pressure within its recommended operating temperature range. It is suitable for most process heating and cooling or waste heat recovery applications. Therminol 66 offers potential savings in both capital and operating costs [86].

1.3.3.5 Thermal energy storage.

As time delays, available power production, availability of energy and its consumption, and intermittency are major problems associated with solar energy, thermal storage is used as an attractive and economical energy management resource [68],[72].

Thermal energy storage (TES) units guarantee a more efficient usage of the collected solar energy. According to Viorel [87], a small TES unit discharges more rapidly during time periods with higher thermal loads. However, the larger TES units provide heat during longer time periods, even if the heat flux they supply is generally smaller. The maximum heat flux is extracted from the TES unit during the morning. The study showed that a photovoltaic array is able to provide all of the energy required to drive a space heating system in mid-summer on clear days. The results also showed that the operation of the solar system at temperatures close to and below room temperature would decrease the collector losses and allow more energy to be collected. The operation of a TES unit is similar to the common heat exchangers. However, the TES unit is either being charged or discharged at any given time, so that its operation is essentially unsteady. Energy storage is important when the energy source is intermittent, as is the case with solar energy.

1.3.4 Hybrid energy (fuel cells/PVT) based HVAC system.

For hybrid energy systems, the photovoltaic panel group constitutes the primary energy supplier of the system while the fuel cell group is the secondary supplier if the

area is sunny throughout the year [88]. As is the case with all solar energy systems, non-solar supplementary sources of energy are required to meet the demand when solar energy is insufficient [69].

Medrano et al. [89] studied the integration of an advanced Distributed Generation (DG) of Combined Cooling, Heat, and Power (CCHP) composed of three types of DG technologies (high-temperature fuel cells, micro-turbines, and photovoltaic solar panels) into four types of commercial buildings (small office building, medium office building, hospital, and college/school). They showed that the high-temperature fuel cell performance is best matched with the hospital energy loads, resulting in a 98% DG capacity factor, 85% DG heat recovery factor, and $860,000 in energy savings (6 years payback). Also, the introduction of thermally-driven double-effect absorption cooling in the college building with the high-temperature fuel cell significantly reduces the building's electricity-to-thermal load ratio and boosts the heat recovery factor from 37% to 97%.

In this research, PTSCs along with PV/Ts are integrated with a 10 kW triple effect absorption cooling system.

1.4 Scope and Objectives

The scope of the research is to improve cooling systems using alternative sources of renewable energy and methods of operation by developing different integrated hybrid systems to come up with a novel renewable energy-based absorption refrigeration system for sustainable building operations.

The main objective of this research is to propose alternative cooling systems by integrating selected renewable energy sources with an absorption refrigeration system that can solve the high energy demand and high emissions issues associated with conventional cooling systems.

The research specifically aims to:

1. Identify the problems related to the energy used in conventional HVAC systems.
2. Develop the following integrated systems:

- PEMFC-Based HVAC Cooling System
- FPSC-Based HVAC Cooling System
- PTSC-Based HVAC Cooling System
- PV/T-Based HVAC Cooling System
- PEMFC-FPSC-PV/T-Based HVAC Cooling System

3. Examine the operating principles and design parameters of PEMFC, FPSC, PTSC, PV/T, DEAS and TEAS.
4. Perform thermodynamic (energy and exergy) analyses of the integrated systems.
5. Conduct a parametric study to investigate the effect of variation in design parameters on the systems' efficiency, performance, heat gain, and output power.
6. Compare the integrated systems in order to determine the most efficient design that can provide the required power, has high efficiency, is cost effective, and can be applied in residential and commercial buildings in the UAE.

1.5 Research Methods and Materials

The methodology used in the research starts with the design of PEMFC, FPSC, PTSC, PVT, DEAS and TEAS using Microsoft Visio. Then, these systems are modeled to determine their properties and output data using Engineering Equation Solver (EES). Afterward, energy analysis is carried out to investigate the overall performance of the subsystems. Exergetic analysis is also conducted as it is a powerful tool for developing, evaluating and improving energy conversion systems. These subsystems are then combined and analyzed as integrated systems where the overall performance of the integrated systems is well examined.

Finally, a parametric study is conducted to study the effect of the variation in operating parameters on the performance of the integrated systems. This helps in determining the operating conditions that provide the best performance and select the optimum integrated system.

1.6 Thesis Organization

Chapter one outlines the need for the research, giving the problem statement and significance of the research. Also, it covers background information about fuel cells and solar energy along with absorption systems. A comprehensive literature review is conducted and the scope along with the objectives are stated briefly. Research methods and materials followed in the research are also provided. Finally, brief research results and a summary of key findings are presented.

Chapter two provides schematic diagrams of the proposed integrated systems along with the systems' descriptions. Chapter three covers modeling and analysis of the integrated systems. Chapter four presents detailed results obtained from thermodynamic analysis and parametric study of the different systems and also provides a discussion of results for the systems' performance. Finally, conclusions and recommendations of the present research are provided in chapter five for further development of the proposed systems.

Chapter 2 Configurations of Integrated Systems

In this chapter, schematic diagrams of the integrated systems are provided and the operational principle of each system is explained in detail.

2.1 Absorption Cooling System

Descriptions and schematic diagrams of double effect and triple effect absorption cooling systems with parallel flow configuration are provided in this section.

2.1.1 Double Effect Absorption System (DEAS).

In the double effect parallel flow absorption cycle, Fig. 2.1, a lithium bromide/water ($LiBr/H_2O$) solution leaves the absorber as a weak solution at state 1 and is distributed to two generators, low and high temperature generators (LTG and HTG, respectively). The weak solution coming from the absorber at state 11 is heated through the high temperature heat exchanger (HHEX) to leave as a strong solution at state 12. The strong solution at state 12 passes through the HHEX in order to preheat the weak solution at state 19 coming from the LHEX. The strong solution from the LTG (state 18) with the strong solution coming from the HHEX (state 13) passes through the low temperature heat exchanger (LHEX) to preheat the weak solution from the absorber (state 2) and leave at state 4. The strong solution at state 5 enters the expansion valve where the pressure and the temperature are dropped to enter the absorber at state 6. In the absorber, the strong solution (state 6) absorbs the water vapor leaving the evaporator (state 10).

Meanwhile, the heat input to the HTG from an external heat source is used to boil off water vapor (state 15) from the $LiBr/H_2O$ solution at state 11. The water vapor generated in the HTG (state 15) supplies energy to boil off water vapor (state 7) from the $LiBr/H_2O$ solution (state 14) in the LTG. The water at state 7 goes directly into the condenser while at state 16 it enters the expansion valve where a drop in the pressure and temperature occurs. Water vapor from both generators (states 7 and 16) is cooled down in the condenser. The water at state 17 mixes with the water at state 7 to leave at state 8

as saturated liquid water. The saturated water then passes through the expansion valve and leaves at state 9 where a drop in the pressure and temperature is achieved to enter the evaporator. In the evaporator, heat is added so that the saturated liquid water gets evaporated at low pressure (state 10), thereby providing cooling to the space to be cooled. The water leaves the evaporator as saturated vapor water and enters the absorber where it mixes with the solution and leaves at state 1 as a weak solution to enter the pump and repeat the cycle.

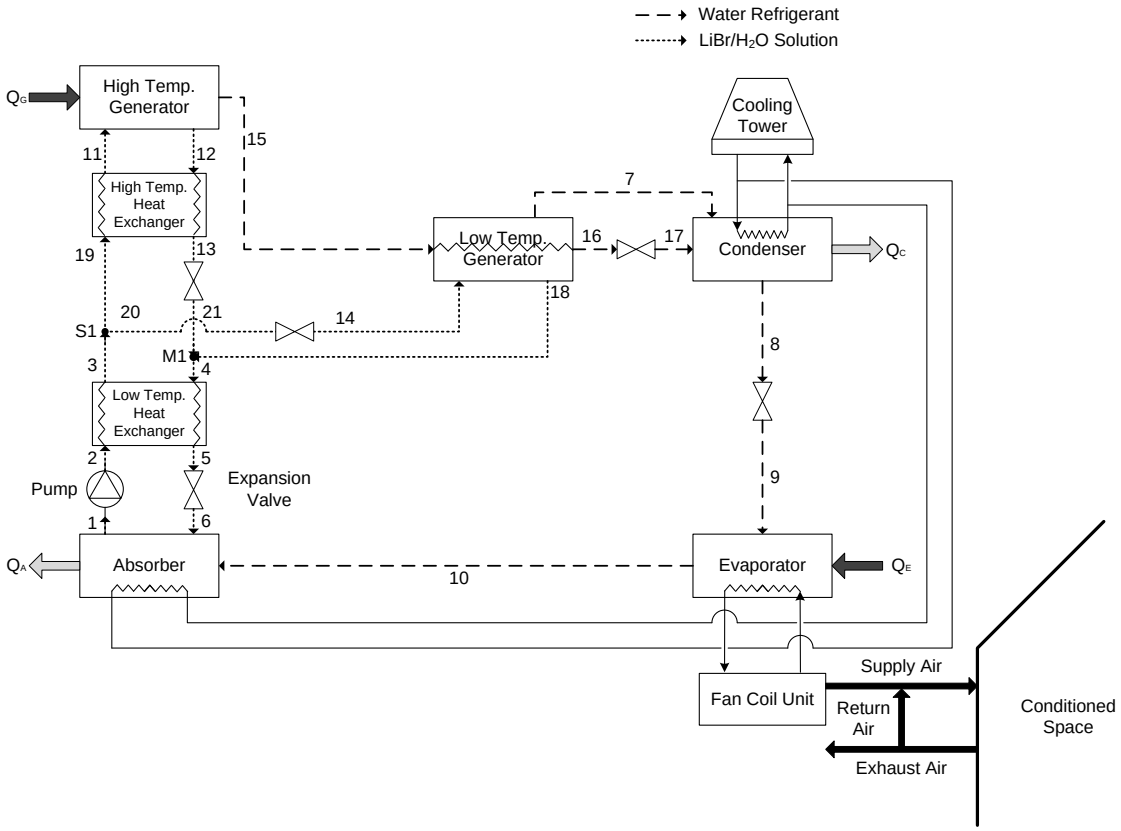

Fig. 2.1 Schematic diagram of the double effect parallel flow absorption cooling system.

2.1.2 Triple Effect Absorption System (TEAS).

In the triple effect parallel flow absorption cycle (Fig. 2.2), the weak solution leaving the absorber at state 1 is distributed to three generators, low, medium, and high temperature generators (LTG, MTG, and HTG respectively). The weak solution coming from the absorber at state 11 is heated through the high temperature heat exchanger (HHEX) to leave as a strong solution at state 12. The strong solution at state 12 provides heat in the HHEX and mixes with the medium solution coming from state 28 and leaves at state 29. The medium solution from state 29 then provides heat in the medium temperature heat exchanger (MHEX) and mixes with the medium solution from state 18 to leave at state 4 as medium solution lower in temperature than that at state 29. This medium solution then enters the low temperature heat exchanger (LHEX) where it preheats the weak solution coming from state 2. The medium solution at state 5 enters the expansion valve where the pressure and the temperature are dropped to enter the absorber at state 6.

The heat input to the HTG from an external heat source is used to boil off water vapor (state 15) from the $LiBr/H_2O$ solution at state 11. The water vapor coming out from the HTG at state 15 enters the MTG where it heats the weak solution at state 25 and leaves as water vapor at state 24. The vapor at state 24 enters the LTG and heats the weak solution coming from state 14 and leaves as water vapor at state 7 and state 16. Water at state 7 goes directly into the condenser while at state 16 it enters the expansion valve where a drop in the pressure and temperature occurs. Water vapor from both generators (states 7 and 16) is cooled down in the condenser. The water at state 17 mixes with the water at state 7 to leave at state 8 as saturated liquid water. The saturated water then passes through the expansion valve and leaves at state 9 where a drop in the pressure and temperature is achieved to enter the evaporator. In the evaporator, heat is added so that the saturated liquid water gets evaporated at low pressure (state 10), thereby providing cooling to the space to be cooled. The water leaves the evaporator as saturated vapor water and enters the absorber where it mixes with the solution and leaves at state 1 as a weak solution to enter the pump and repeat the cycle.

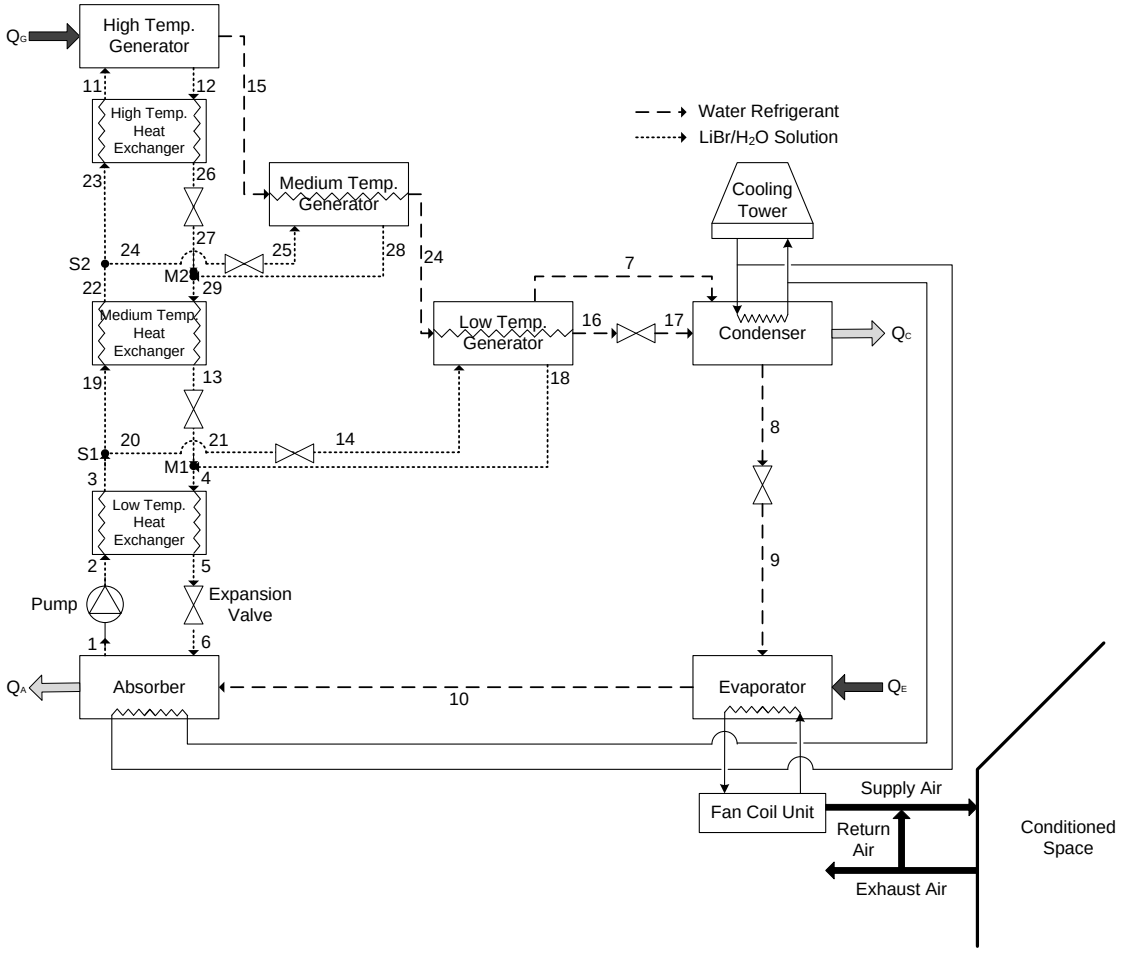

Fig. 2.2 Schematic diagram of the triple effect parallel flow absorption cooling system.

2.2 PEMFC-Based HVAC-Cooling System.

A schematic diagram of the PEMFC-based HVAC-cooling system is provided in Fig. 2.3. The PEMFC unit consists of an anode, cathode, and electrolyte along with hydrogen cylinders as fuel. In the PEMFC, the fuel is hydrogen and the charge carrier is the proton. At the anode, the hydrogen is supplied to the hydrogen flow plate where the molecules are stripped of their electrons and the positively-charged protons diffuse through one side of the membrane and migrate toward the cathode. On the other hand, the electrons flow through an external circuit from the anode to the cathode and produce electric power as the membrane electrolyte allows hydrogen protons to pass through but prohibits the passage of electrons. At the cathode, oxygen from the air is supplied and combined with the electrons and the hydrogen protons to form water. The generated power and heat are then supplied to the HTG of the DEAS and a small amount of the power produced is used to run the solution pump. Also, the excess water generated from the fuel cell unit can be utilized for domestic water usage.

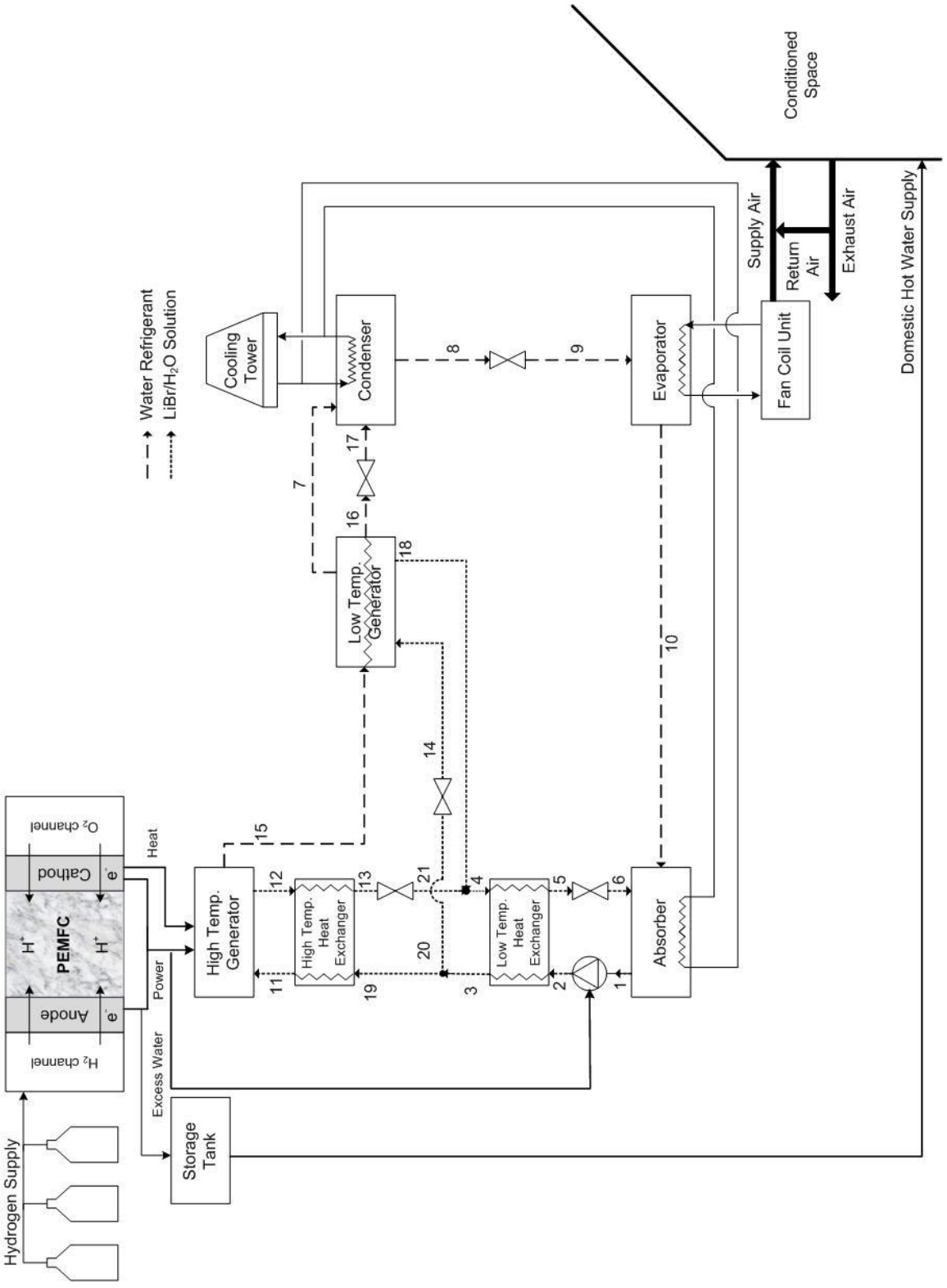

Fig. 2.3 Schematic diagram of PEMFC-based HVAC-cooling system.

2.3 FPSC-Based HVAC-Cooling System.

Fig. 2.4 shows a schematic diagram of the solar-powered absorption cooling system. The system consists of a single cover liquid-based flat plate solar collector of area 0.5m^2 tilted35° from the horizontal with water as the working fluid, and a 0.5 m^3 hot water storage tank used to operate a 10 kW cooling capacity double effect parallel flow LiBr/H_2O absorption chiller.

The FPSC is composed of an insulated metal box with a glass cover which serves as a heat trap by admitting shortwave solar radiation and retaining longwave thermal radiation and a dark-colored absorber plate used to heat liquid water. When the solar radiation passes through the transparent cover and strikes the blackened absorber surface of high absorptivity, a large portion of this energy is absorbed by the absorber plate and converted into heat energy and also transferred to the water flowing through the collector tubes. The water is heated to a temperature considerably less than that of the boiling point so that it is integrated with a double-effect absorption system as it is best suited to low temperature applications. The FPSC is fixed in position as it requires no tracking of the sun.

A closed-circuit stainless steel storage tank is used to store the heated water where part of it is fed directly to the HTG and the remaining is stored for later use for absorption system operation or to cover domestic hot water demand. In the closed circuit, the water stored in the storage tank is circulated directly from the storage tank through the FPSC.

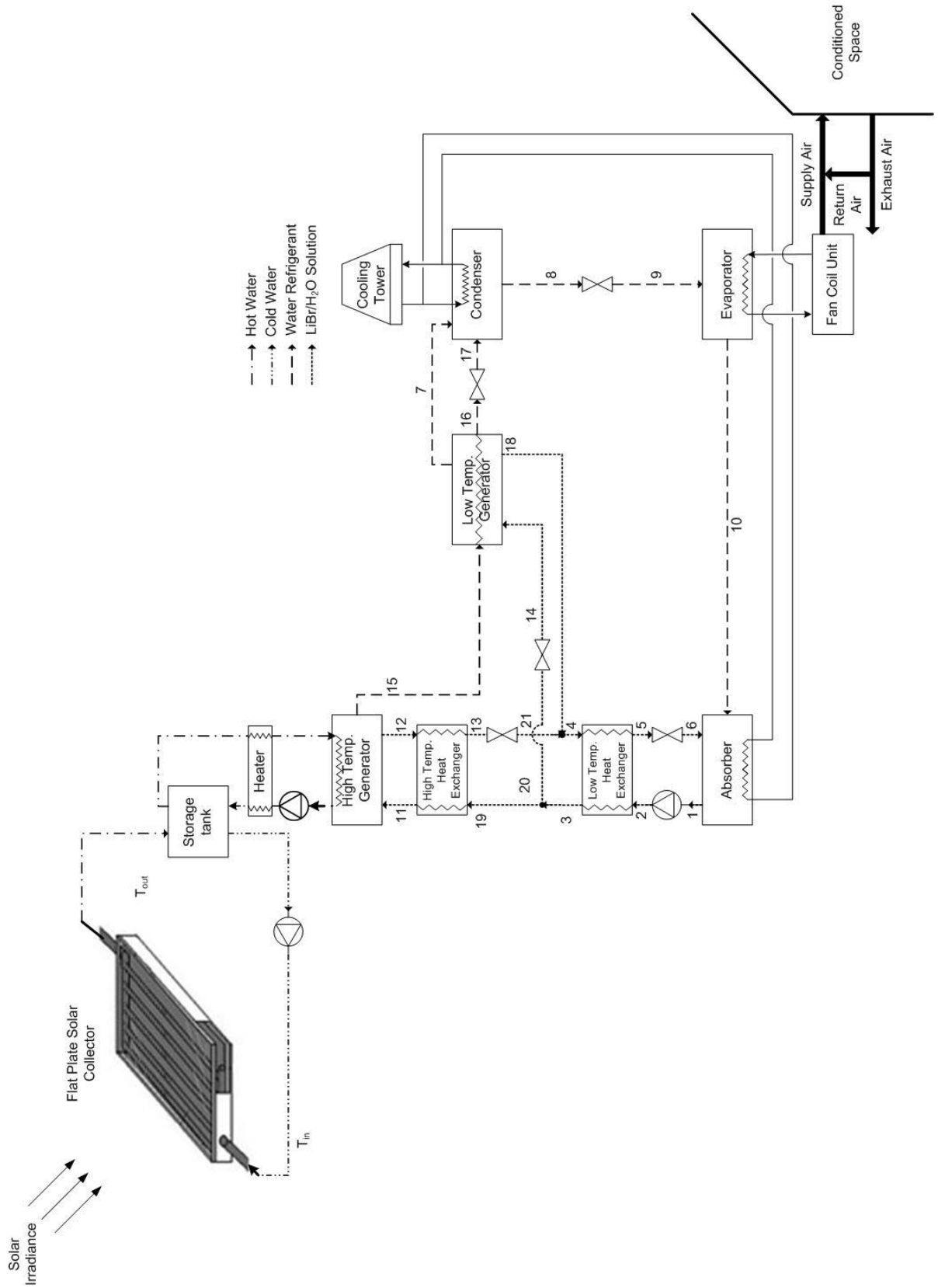

Fig. 2.4 Schematic diagram of the FPSC-based HVAC-cooling system.

2.4 PTSC-Based HVAC-Cooling System.

A schematic diagram of the proposed PTSC-based HVAC-cooling system is shown in Fig. 2.5. The system is composed of a 10 m^2 PTSC, a circulating pump, and a 0.5 m^3 hot oil storage tank used to provide the required heat input to the generator used to drive a 10 kW cooling capacity triple effect parallel flow $LiBr/H_2O$ absorption chiller. The PTSC considered in this system uses Therminol-66 oil as the working fluid as it can be used in both thermal solar systems and thermal storage tanks.

When the solar radiation falls on the PTSC, only part of the radiation is absorbed by the collector and the remaining is reflected to the surroundings. A metal black tube, covered with a glass tube to reduce heat losses that can take place by radiation and convection, is placed along the focal line of the receiver. When the parabola is pointed toward the sun, the parallel rays that fall on the reflector are reflected onto the receiver tube.

The radiation absorbed by the PTSC causes Therminol-66 oil pumped from the oil storage tank to the receiver to be heated up. The heated oil then flows back into the storage tank where the heat gained by the PTSC from the solar radiation is accumulated. Hot oil from the storage tank is then used as a heat source to drive the HTG of the TEAS. The oil storage tank temperature, taken as a heat source temperature, changes through the day; however it could be controlled by a differential thermostat controller.

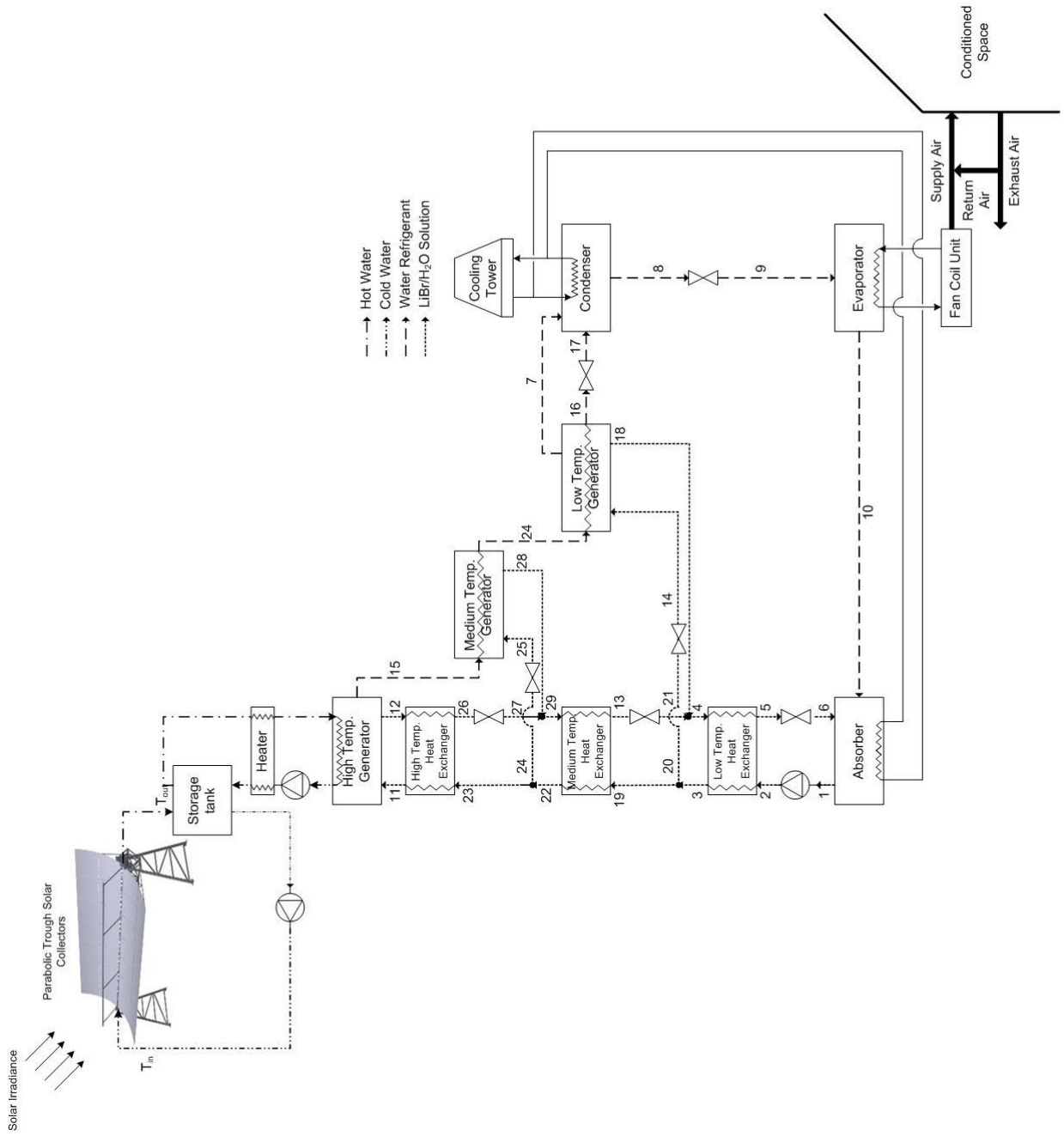

Fig. 2.5 Schematic diagram of the PTSC-based HVAC-cooling system.

2.5 PV/T-Based HVAC-Cooling System.

A schematic diagram of the PV/T-based HVAC-cooling system is shown in Figure 2.6. A glass-to-glass PV module is considered in this system. A parallel flat plate is provided below the glass base of the solar cells to regulate the passage of the working fluid. In this system, air is used as the working fluid. Solar radiation is absorbed by the solar cells and the black surface while the flowing air inside the duct is heated by convective heat from the black surface and heat conducted from the solar cells through the glass cover placed below the solar cells. Part of the solar radiation is converted into electrical energy and the remaining is converted into thermal energy available from the black surface. Power and heat generated by the PV/T system are used to drive the TEAS by supplying power and heat to the HTG.

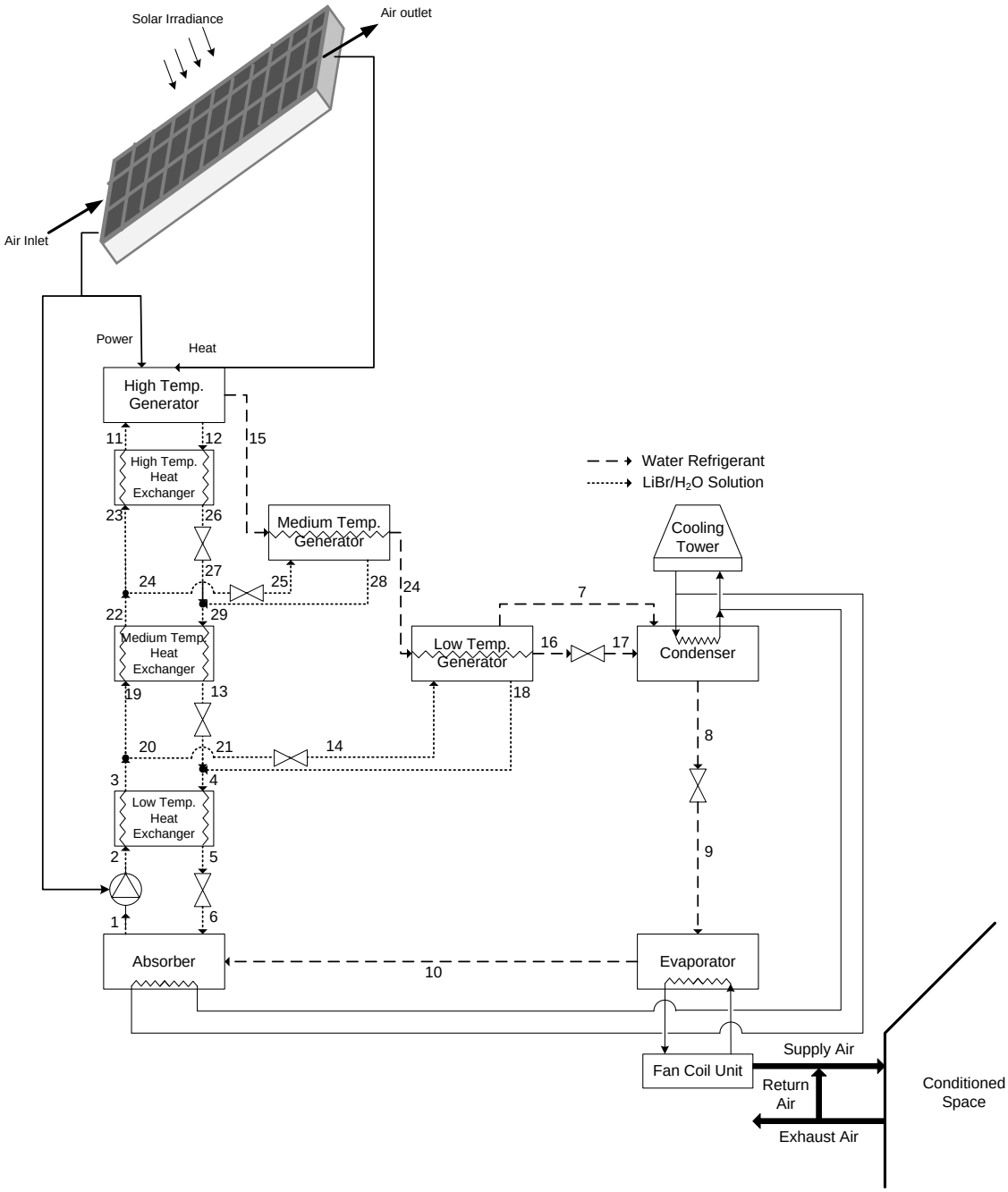

Fig. 2.6 Schematic diagram of the PV/T-based HVAC-cooling system.

2.6 Hybrid PEMFC-PTSC-PV/T-Based HVAC-Cooling System.

A schematic diagram of the hybrid PEMFC-PTSC-PV/T-based HVAC-cooling system is shown in Fig.2.7. The generated power from PEMFC and PV/T is used to power the High Temperature Generator (HTG) and a small amount of this power is supplied to run the solution pump. Also, heat generated by the PEMFC, PTSC, and PV/T is used as a heat source to drive the HTG of the DEAS. Also, the excess water generated from the PEMFC unit can be utilized for domestic water usage.

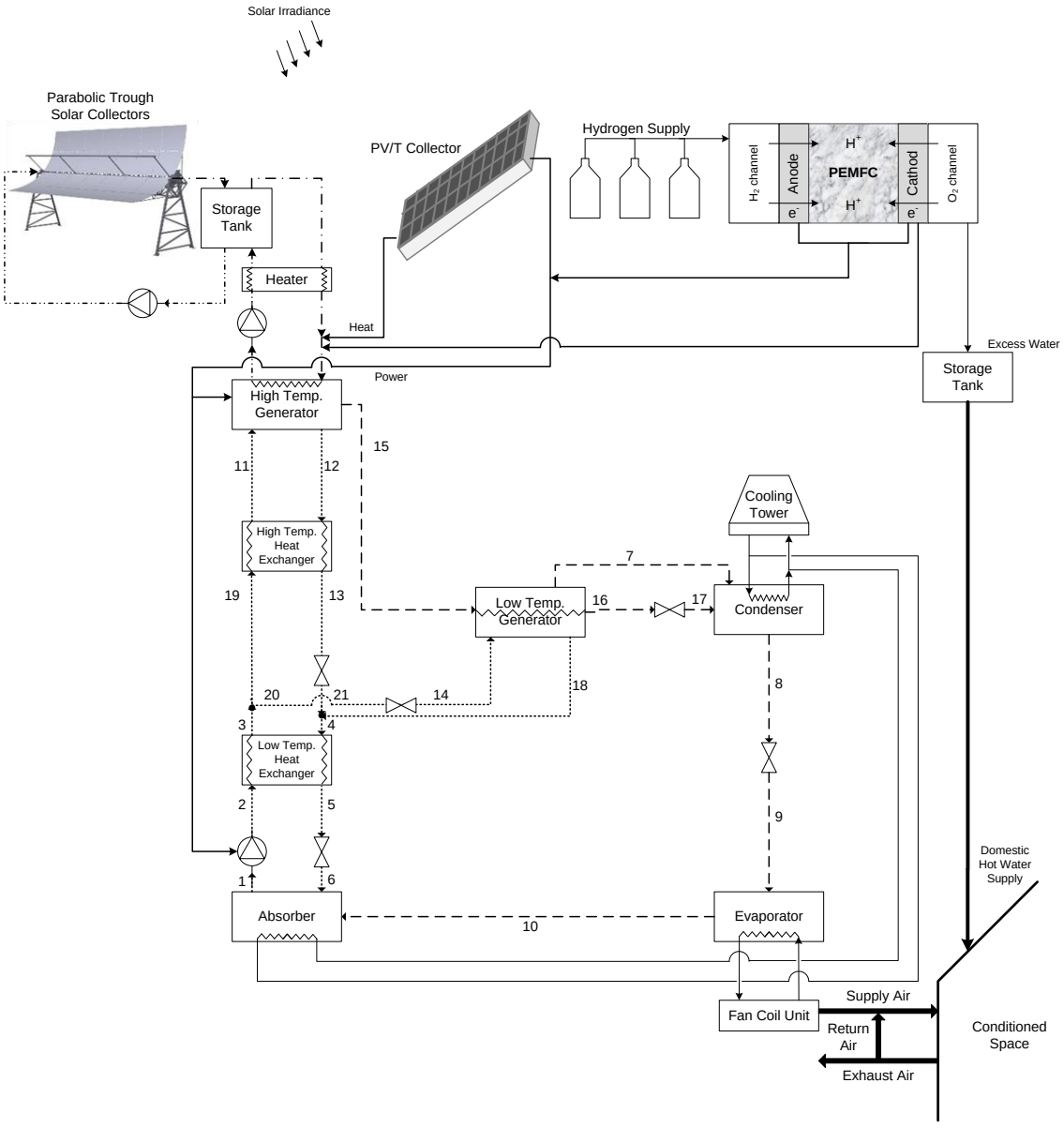

Fig. 2.7 Schematic diagram of the hybrid PEMFC-PTSC-PV/T-based HVAC-cooling system.

Chapter 3 Systems Modeling and Analysis

In order to study the performance of the integrated systems, mathematical and thermodynamic models are developed. The mathematical model helps in identifying the operating conditions of the system. The thermodynamic model demonstrates thermodynamic behavior of the system and provides a prospective idea of the overall performance of the system. The thermodynamic model covers energy and exergy analyses. As the first law of thermodynamics does not provide the best possible performance of system, second law analysis is required as it provides the true indicator of the performance of an energy system from a thermodynamic point of view so that the efficiency of a system is best described by its exergetic efficiency. All the analyses conducted herein are programmed using Engineering Equation Solver (EES) software.

First, modeling and analysis of the DEAS and TEAS are conducted. The models of the PEMFC, FPSC, PTSC and PV/T are provided in the subsequent sections.

3.1 Modeling of Absorption Systems

Mass, concentration, energy and exergy balances are presented in detail to model double effect and triple effect absorption cooling systems (DEAS and TEAS).In order to simulate the DEAS and TEAS, several assumptions are made, including the following:

a. The analysis is made under steady conditions.
b. The refrigerant (water) at the outlet of the condenser is saturated liquid.
c. The refrigerant (water) at the outlet of the evaporator is saturated vapor.
d. The lithium bromide solution at the absorber outlet is a weak solution and it is at the absorber temperature.
e. Pressure losses in the pipelines and all heat exchangers are negligible.
f. Heat exchange between the system and surroundings, other than that prescribed by heat transfer at the HTG, evaporator, condenser and absorber, does not occur.
g. The system produces chilled water.
h. The system rejects heat to cooling water at the condenser and absorber.

3.1.1 Double Effect Absorption System (DEAS).

The design and operating parameters of the double effect absorption cooling system are listed in Table 3.1.

Table 3.1 Design and operating parameters of DEAS.

Parameter	Symbol	Unit	Value
Mass flow rate of refrigerant	$\dot{m}$	kg/s	1.8 [90]
Absorber temperature	T_A	$°C$	42 [90]
Temperature of HTG	T_{HG}	$°C$	145 [90]
Temperature of LTG	T_{LG}	$°C$	95 [90]
Condenser temperature	T_C	$°C$	40 [90]
Evaporator temperature	T_E	$°C$	4 [90]
Effectiveness of HHEX	ε_{HHEX}	$-$	0.9 [91]
Effectiveness of LHEX	ε_{LHEX}	$-$	0.9 [91]
Solution distribution ratio	Dr	$-$	0.5 [92]
Temperature difference in HHEX	ΔT_{HHEX}	$°C$	65 [92]
Dead state temperature	T_o	$°C$	25
Dead state pressure	P_o	kPa	101.325

Mass, concentration, energy, and exergy balances at each component are illustrated as follows.

For High Temperature Generator (HTG)

$$\dot{m}_{12} + \dot{m}_{15} = \dot{m}_{11} \tag{3.1}$$

$$\dot{m}_{12} \cdot x_{12} + \dot{m}_{15} \cdot x_{15} = \dot{m}_{11} \cdot x_{11} \tag{3.2}$$

$$\dot{m}_{12} \cdot h_{12} + \dot{m}_{15} \cdot h_{15} = \dot{m}_{11} \cdot h_{11} + \dot{Q}_{HG} \tag{3.3}$$

$$\dot{S}_{gen,HG} = \dot{m}_{12} \cdot s_{12} + \dot{m}_{15} \cdot s_{15} - \dot{m}_{11} \cdot s_{11} - \left[\frac{\dot{Q}_{HG}}{T_{HG}} \right] \tag{3.4}$$

$$\dot{X}_{dest,HG} = T_o \cdot \dot{S}_{gen,HG} \tag{3.5}$$

For Low Temperature Generator (LTG)

$$\dot{m}_{14} + \dot{m}_{15} = \dot{m}_7 + \dot{m}_{16} + \dot{m}_{18} \tag{3.6}$$

$$\dot{m}_{14} \cdot x_{14} + \dot{m}_{15} \cdot x_{15} = \dot{m}_7 \cdot x_7 + \dot{m}_{16} \cdot x_{16} + \dot{m}_{18} \cdot x_{18} \tag{3.7}$$

$$\dot{m}_{14} \cdot h_{14} + \dot{m}_{15} \cdot h_{15} = \dot{m}_7 \cdot h_7 + \dot{m}_{16} \cdot h_{16} + \dot{m}_{18} \cdot h_{18} \tag{3.8}$$

$$\dot{S}_{gen,LG} = \dot{m}_7 \cdot s_7 + \dot{m}_{16} \cdot s_{16} + \dot{m}_{18} \cdot s_{18} - \dot{m}_{14} \cdot s_{14} - \dot{m}_{15} \cdot s_{15} - \left[\frac{\dot{Q}_{LG}}{T_{LG}} \right] \tag{3.9}$$

$$\dot{X}_{dest,LG} = T_o \cdot \dot{S}_{gen,LG} \tag{3.10}$$

For High Heat Exchanger (HHEX)

$$\dot{Q}_{HHEX} = \dot{m}_{19} \cdot \left(h_{11} - h_{19} \right) \tag{3.11}$$

$$\dot{Q}_{HHEX} = \dot{m}_{13} \cdot \left(h_{12} - h_{13} \right) \tag{3.12}$$

For Low Heat Exchanger (LHEX)

$$\dot{Q}_{LHEX} = \dot{m}_5 \cdot \left(h_4 - h_5 \right) \tag{3.13}$$

$$\dot{Q}_{LHEX} = \dot{m}_2 \cdot \left(h_3 - h_2 \right) \tag{3.14}$$

For absorber

$$\dot{m}_1 = \dot{m}_6 + \dot{m}_{10} \tag{3.15}$$

$$\dot{m}_1 \cdot x_1 = \dot{m}_6 \cdot x_6 + \dot{m}_{10} \cdot x_{10} \tag{3.16}$$

$$\dot{m}_1 \cdot h_1 + \dot{Q}_A = \dot{m}_6 \cdot h_6 + \dot{m}_{10} \cdot h_{10} \tag{3.17}$$

$$\dot{S}_{gen,A} = \dot{m}_{10} \cdot s_{10} + \dot{m}_6 \cdot s_6 - \dot{m}_1 \cdot s_1 - \left[\frac{\dot{Q}_{Abs}}{T_{Abs}} \right] \tag{3.18}$$

$$\dot{X}_{dest,Abs} = T_o \cdot \dot{S}_{gen,Abs} \tag{3.19}$$

For evaporator

$$\dot{m}_{10} = \dot{m}_9 \tag{3.20}$$

$$\dot{m}_{10} \cdot x_{10} = \dot{m}_9 \cdot x_9 \tag{3.21}$$

$$\dot{m}_{10} \cdot h_{10} = \dot{m}_9 \cdot h_9 + \dot{Q}_E \tag{3.22}$$

$$\dot{S}_{gen,E} = \dot{m}_{10} \cdot s_{10} - \dot{m}_9 \cdot s_9 - \left[\frac{\dot{Q}_{Evap}}{T_{Evap}} \right] \tag{3.23}$$

$$\dot{X}_{dest,Evap} = T_o \cdot \dot{S}_{gen,Evap} \tag{3.24}$$

For condenser

$$\dot{m}_8 = \dot{m}_7 + \dot{m}_{17} \tag{3.25}$$

$$\dot{m}_8 \cdot x_8 = \dot{m}_7 \cdot x_7 + \dot{m}_{17} \cdot x_{17} \tag{3.26}$$

$$\dot{m}_8 \cdot h_8 + \dot{Q}_C = \dot{m}_7 \cdot h_7 + \dot{m}_{17} \cdot h_{17} \tag{3.27}$$

$$\dot{S}_{gen,C} = \dot{m}_{17} \cdot s_{17} + \dot{m}_7 \cdot s_7 - \dot{m}_8 \cdot s_8 - \left[\frac{\dot{Q}_{Cond}}{T_{Cond}} \right] \tag{3.28}$$

$$\dot{X}_{dest,Cond} = T_o \cdot \dot{S}_{gen,Cond} \tag{3.29}$$

Separation point 1 (S1)

$$\dot{m}_3 = \dot{m}_{19} + \dot{m}_{20} \tag{3.30}$$

Mixing point 1 (M1)

$$\dot{m}_{21} + \dot{m}_{18} = \dot{m}_4 \tag{3.31}$$

For pump

$$w_{pump} = h_2 - h_1 \tag{3.32}$$

$$\dot{W}_{pump} = \dot{m}_1.(h_2 - h_1) \tag{3.33}$$

The energy associated with the heat flowing out of the system should be equal to the energy flowing into the system:

$$\dot{E}_{in} = \dot{Q}_{HG} + \dot{Q}_{Evap} \tag{3.34}$$

$$\dot{E}_{out} = \dot{Q}_{Cond} + \dot{Q}_{Abs} + \dot{W}_{pump} \tag{3.35}$$

An overall energy balance of the system requires that the sum of the heat transfer of the generator, evaporator, condenser, and absorber be zero:

$$\dot{E}_{tot} = \dot{E}_{out} - \dot{E}_{in} \tag{3.36}$$

Energetic coefficient of performance:

$$COP_{en} = \frac{\dot{Q}_{Evap}}{\dot{Q}_{HG} + \dot{W}_{pump}} \tag{3.37}$$

Thermal exergy of the evaporator [93]:

$$\dot{X}_{Evap,th} = \left[\frac{T_o}{T_{Evap}} - 1\right] \cdot \dot{Q}_{Evap} \tag{3.38}$$

Thermal exergy of the HTG [93]:

$$\dot{X}_{HG,th} = \left[1 - \frac{T_o}{T_{HG}}\right] \cdot \dot{Q}_{HG} \tag{3.39}$$

Exergetic coefficient of performance [93]:

$$COP_{ex} = \frac{\dot{X}_{Evap,th}}{\dot{X}_{HG,th} + \dot{W}_{pump}} \tag{3.40}$$

Exergy rate at each state

$$\dot{X}_i = \dot{m}_i \cdot \left[\left(h_i - h_o\right) - T_o \cdot \left(s_i - s_o\right)\right] \tag{3.41}$$

3.1.2 Triple Effect Absorption System (TEAS).

The design and operating parameters of the triple effect absorption cooling system are listed in Table 3.2.

Table 3.2 Design and operating parameters of TEAS.

Parameter	Symbol	Unit	Value
Mass flow rate of refrigerant	$\dot{m}$	kg/s	1.8 [90]
Absorber temperature	T_A	$°C$	42 [90]
Temperature of HTG	T_{HG}	$°C$	180[40],[94]
Temperature of MTG	T_{MG}	$°C$	145 [90]
Temperature of LTG	T_{LG}	$°C$	95 [90]
Condenser temperature	T_C	$°C$	40 [90]
Evaporator temperature	T_E	$°C$	4 [90]
Effectiveness of HHEX	ε_{HHEX}	$-$	0.85 [96]
Effectiveness of MHEX	ε_{MHEX}	$-$	0.9 [92]
Effectiveness of LHEX	ε_{LHEX}	$-$	0.9 [91]
Solution distribution ratio	Dr	$-$	0.5 [92]
Temperature difference in HHEX	ΔT_{HHEX}	$°C$	75 [96]
Temperature difference in MHEX	ΔT_{MHEX}	$°C$	65 [92]
Dead state temperature	T_o	$°C$	25
Dead state pressure	P_o	kPa	101.325

For High Temperature Generator (HTG)

$$\dot{m}_{12} + \dot{m}_{15} = \dot{m}_{11} \tag{3.42}$$

$$\dot{m}_{12} \cdot x_{12} + \dot{m}_{15} \cdot x_{15} = \dot{m}_{11} \cdot x_{11} \tag{3.43}$$

$$\dot{m}_{12} \cdot h_{12} + \dot{m}_{15} \cdot h_{15} = \dot{m}_{11} \cdot h_{11} + \dot{Q}_{HG} \tag{3.44}$$

$$\dot{S}_{gen,HG} = \dot{m}_{12} \cdot s_{12} + \dot{m}_{15} \cdot s_{15} - \dot{m}_{11} \cdot s_{11} - \left[\frac{\dot{Q}_{HG}}{T_{HG}} \right] \tag{3.45}$$

$$\dot{X}_{dest,HG} = T_o \cdot \dot{S}_{gen,HG} \tag{3.46}$$

For Medium Temperature Generator (MTG)

$$\dot{m}_{12} + \dot{m}_{15} = \dot{m}_{11} \tag{3.47}$$

$$\dot{m}_{12} \cdot x_{12} + \dot{m}_{15} \cdot x_{15} = \dot{m}_{11} \cdot x_{11} \tag{3.48}$$

$$\dot{m}_{12} \cdot h_{12} + \dot{m}_{15} \cdot h_{15} = \dot{m}_{11} \cdot h_{11} + \dot{Q}_{MG} \tag{3.49}$$

$$\dot{S}_{gen,MG} = \dot{m}_{12} \cdot s_{12} + \dot{m}_{15} \cdot s_{15} - \dot{m}_{11} \cdot s_{11} - \left[\frac{\dot{Q}_{MG}}{T_{MG}} \right] \tag{3.50}$$

$$\dot{X}_{dest,MG} = T_o \cdot \dot{S}_{gen,MG} \tag{3.51}$$

For Low Temperature Generator (LTG)

$$\dot{m}_{14} + \dot{m}_{15} = \dot{m}_{7} + \dot{m}_{16} + \dot{m}_{18} \tag{3.52}$$

$$\dot{m}_{14} \cdot x_{14} + \dot{m}_{15} \cdot x_{15} = \dot{m}_{7} \cdot x_{7} + \dot{m}_{16} \cdot x_{16} + \dot{m}_{18} \cdot x_{18} \tag{3.53}$$

$$\dot{m}_{14} \cdot h_{14} + \dot{m}_{15} \cdot h_{15} = \dot{m}_{7} \cdot h_{7} + \dot{m}_{16} \cdot h_{16} + \dot{m}_{18} \cdot h_{18} \tag{3.54}$$

$$\dot{S}_{gen,LG} = \dot{m}_{7} \cdot s_{7} + \dot{m}_{16} \cdot s_{16} + \dot{m}_{18} \cdot s_{18} - \dot{m}_{14} \cdot s_{14} - \dot{m}_{15} \cdot s_{15} - \left[\frac{\dot{Q}_{LG}}{T_{LG}} \right] \tag{3.55}$$

$$\dot{X}_{dest,LG} = T_o \cdot \dot{S}_{gen,LG} \tag{3.56}$$

For High Heat Exchanger (HHEX)

$$\dot{Q}_{HHEX} = \dot{m}_{23} \cdot \left(h_{11} - h_{23} \right) \tag{3.57}$$

$$\dot{Q}_{HHEX} = \dot{m}_{26} \cdot \left(h_{12} - h_{26} \right) \tag{3.58}$$

For Medium Heat Exchanger (MHEX)

$$\dot{Q}_{MHEX} = \dot{m}_{19} \cdot \left(h_{22} - h_{19} \right) \tag{3.59}$$

$$\dot{Q}_{MHEX} = \dot{m}_{13} \cdot \left(h_{29} - h_{13} \right) \tag{3.60}$$

For Low Heat Exchanger (LHEX)

$$\dot{Q}_{LHEX} = \dot{m}_5 \cdot (h_4 - h_5) \tag{3.61}$$

$$\dot{Q}_{LHEX} = \dot{m}_2 \cdot (h_3 - h_2) \tag{3.62}$$

For absorber

$$\dot{m}_1 = \dot{m}_6 + \dot{m}_{10} \tag{3.63}$$

$$\dot{m}_1 \cdot x_1 = \dot{m}_6 \cdot x_6 + \dot{m}_{10} \cdot x_{10} \tag{3.64}$$

$$\dot{m}_1 \cdot h_1 + \dot{Q}_{Abs} = \dot{m}_6 \cdot h_6 + \dot{m}_{10} \cdot h_{10} \tag{3.65}$$

$$\dot{S}_{gen,Abs} = \dot{m}_{10} \cdot s_{10} + \dot{m}_6 \cdot s_6 - \dot{m}_1 \cdot s_1 - \left[\frac{\dot{Q}_{Abs}}{T_{Abs}} \right] \tag{3.66}$$

$$\dot{X}_{dest,Abs} = T_o \cdot \dot{S}_{gen,Abs} \tag{3.67}$$

For evaporator

$$\dot{m}_{10} = \dot{m}_9 \tag{3.68}$$

$$\dot{m}_{10} \cdot x_{10} = \dot{m}_9 \cdot x_9 \tag{3.69}$$

$$\dot{m}_{10} \cdot h_{10} = \dot{m}_9 \cdot h_9 + \dot{Q}_{Evap} \tag{3.70}$$

$$\dot{S}_{gen,Evap} = \dot{m}_{10} \cdot s_{10} - \dot{m}_9 \cdot s_9 - \left[\frac{\dot{Q}_{Evap}}{T_{Evap}} \right] \tag{3.71}$$

$$\dot{X}_{dest,Evap} = T_o \cdot \dot{S}_{gen,Evap} \tag{3.72}$$

For condenser

$$\dot{m}_8 = \dot{m}_7 + \dot{m}_{17} \tag{3.73}$$

$$\dot{m}_8 \cdot x_8 = \dot{m}_7 \cdot x_7 + \dot{m}_{17} \cdot x_{17} \tag{3.74}$$

$$\dot{m}_8 \cdot h_8 + \dot{Q}_{Cond} = \dot{m}_7 \cdot h_7 + \dot{m}_{17} \cdot h_{17} \quad (3.75)$$

$$\dot{S}_{gen,Cond} = \dot{m}_{17} \cdot s_{17} + \dot{m}_7 \cdot s_7 - \dot{m}_8 \cdot s_8 - \left[\frac{\dot{Q}_{Cond}}{T_{Cond}} \right] \quad (3.76)$$

$$\dot{X}_{dest,Cond} = T_o \cdot \dot{S}_{gen,Cond} \quad (3.77)$$

Separation point 1 (S1)

$$\dot{m}_3 = \dot{m}_{19} + \dot{m}_{20} \quad (3.78)$$

Separation point 2 (S2)

$$\dot{m}_{22} = \dot{m}_{23} + \dot{m}_{24} \quad (3.79)$$

Mixing point 1 (M1)

$$\dot{m}_{21} + \dot{m}_{18} = \dot{m}_4 \quad (3.80)$$

Mixing point 2 (M2)

$$\dot{m}_{27} + \dot{m}_{28} = \dot{m}_{29} \quad (3.81)$$

For pump

$$w_{pump} = h_2 - h_1 \quad (3.82)$$

$$\dot{W}_{pump} = \dot{m}_1 . (h_2 - h_1) \quad (3.83)$$

The energy associated with the heat flowing out of the system should be equal to the energy flowing into the system.

$$\dot{E}_{in} = \dot{Q}_{HG} + \dot{Q}_{Evap} \quad (3.84)$$

$$\dot{E}_{out} = \dot{Q}_{Cond} + \dot{Q}_{Abs} + \dot{W}_{pump} \quad (3.85)$$

An overall energy balance of the system requires that the sum of the heat transfer of the generator, evaporator, condenser, and absorber be zero

$$\dot{E}_{tot} = \dot{E}_{out} - \dot{E}_{in} \tag{3.86}$$

Energetic coefficient of performance

$$COP_{en} = \frac{\dot{Q}_{Evap}}{\dot{Q}_{HG} + \dot{W}_{pump}} \tag{3.87}$$

Thermal exergy of the evaporator

$$\dot{X}_{Evap,th} = \left[\frac{T_o}{T_E} - 1\right] \cdot \dot{Q}_{Evap} \tag{3.88}$$

Thermal exergy of the HTG

$$\dot{X}_{HG,th} = \left[1 - \frac{T_o}{T_{HG}}\right] \cdot \dot{Q}_{HG} \tag{3.89}$$

Exergetic coefficient of performance

$$COP_{ex} = \frac{\dot{X}_{Evap,th}}{\dot{X}_{HG,th} + \dot{W}_{pump}} \tag{3.90}$$

Exergy rate at each state

$$\dot{X}_i = \dot{m}_i \cdot \left[\left(h_i - h_o\right) - T_o \cdot \left(s_i - s_o\right)\right] \tag{3.91}$$

3.2 PEMFC-Based HVAC-Cooling System

Mass, energy and exergy analyses of the PEMFC are provided in this section. Fig. 3.1 shows the flows of mass, energy, and exergy into and out of the PEMFC. The reactants are the oxygen and hydrogen and the products are water along with the depleted oxygen and hydrogen. The exergy transfer in and out of the system is associated with mass, heat and work. The input data used in this model is given in Table 3.3.

In order to develop the electrochemical and thermodynamic models of the PEMFC for the sake of investigating the effect of various operating conditions on the overall performance of the cell, the following assumptions are made:

a. PEMFC operates under steady state conditions.
b. All gases are treated as ideal gases.
c. Kinetic and potential exergies are neglected.
d. All overpotentials, activations, ohmics, and concentrations are considered.

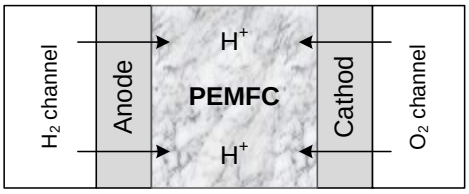

(a)

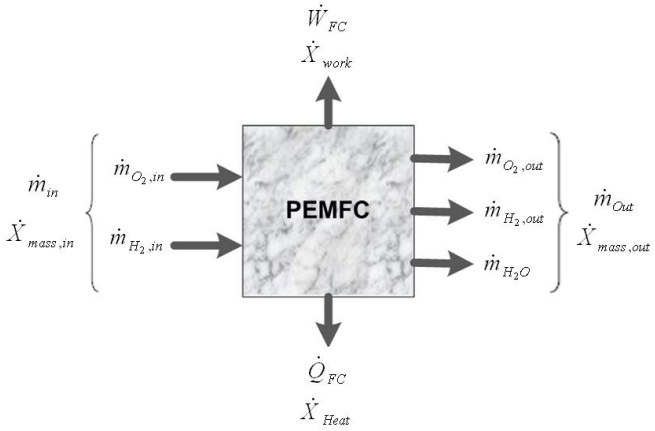

(b)

Fig. 3.1 Illustration of a PEMFC: (a) PEMFC unit. (b) Flows of mass, energy, and exergy in the PEMFC (modified from [97]).

Table 3.3 Design and operating parameters of PEMFC.

Parameter	**Symbol**	**Unit**	**Value**
Cell temperature	T_{cell}	K	300-360
Cell pressure	P_{cell}	bar	3, 4
Dead state temperature	T_o	K	298.15
Dead state pressure	P_o	bar	1
Anode pressure	P_A	bar	1.3[97]
Cathode pressure	P_C	bar	1.1 [97]
Gibbs free energy	ΔG	$J/mole$	249000
Change in Entropy	ΔS	$J/mole \cdot K$	164.05
Faraday's constant	F	$C/mole$	96485
Universal gas constant	R	$J/mole \cdot K$	8.314
Specific heat ratio for air and hydrogen	k	-	1.4
Average specific heat of air	Cp_{air}	$kJ/kg \cdot K$	1.005
Average specific heat of hydrogen	Cp_{H_2}	$kJ/kg \cdot K$	14.3
Transfer coefficient	α	-	0.1668 [97]
Anode (H_2) stoichiometry	ζ_A	-	1.1 [97]
Cathode(O_2) stoichiometry	ζ_C	-	2.5 [97]
Air stoichiometry	ζ_{air}	-	3
Anode dry gas mole fraction	x_A	-	0[98]
Cathode dry gas mole fraction	x_C	-	3.76 [98]
Anode transfer coefficient	α_A	-	0.5 [98]
Cathode transfer coefficient	α_C	-	1 [98]
Heat loss ratio	r_{HL}	-	0.2 [97]
Cell area	A_{cell}	cm^2	640
Molecular weight of hydrogen	M_{H_2}	g/mol	2.016
Molecular weight of oxygen	M_{O_2}	g/mol	15.999
Molecular weight of water	M_{H_2O}	g/mol	18.015
Higher heating value of hydrogen	HHV_{H_2}	kJ/kg	121100
Number of electrons involved	n	-	2
Number of fuel cells	n_{fc}	-	60
Current density	i	A/cm^2	0-2
Maximum current density	i_{max}	A/cm^2	0.1
Membrane thickness	t_{mem}	cm	0.016, 0.018, 0.02

The overall electrochemical reactions for a PEMFC fed with a hydrogen-containing anode gas and an oxygen-containing cathode gas are given as follows:

Anode : $2H_2 \leftrightarrow 4H+ +4e-$

Cathode : $O_2 +4H+ +4e- \leftrightarrow 2H_2O$

Overall : $2H_2 +O_2 \leftrightarrow 2H_2O$ + electrical power+ waste heat

The total voltage of the PEMFC is the difference between the reversible voltage and the irreversible voltage

$$V_{tot} = V_{rev} - V_{irrev} \tag{3.92}$$

Reversible cell voltage for a single PEMFC is ideally described by the Nernst equation as follows [98]:

$$V_{rev} = \frac{\Delta G}{2F} + \frac{\Delta S}{2F}(T_{cell} - T_o) + \frac{RT_{cell}}{2F}\left[\ln\left(p_{H_2}\right) + \frac{1}{2}\ln\left(p_{O_2}\right) - \ln\left(p_{H_2O}\right)\right] \tag{3.93}$$

Where ΔS is the change in entropy (ΔS*=164.05 kJ/kg.K*)

Irreversible voltage is the sum of activation, ohmic, and concentration overpotential losses [98].

$$V_{irrev} = \upsilon_{act} + \upsilon_{ohmic} + \upsilon_{conc} \tag{3.94}$$

Activation overpotential can exist at both the cathode and the anode and is calculated using the following formula [98]:

$$\upsilon_{act} = \frac{\alpha_A + \alpha_C}{\alpha_A . \alpha_C}\frac{RT_{cell}}{nF}\ln\left(\frac{i}{i_o}\right) \tag{3.95}$$

where i *(A/cm^2)* is the current density and i_o is the exchange current density *(A/cm^2)* which is in the form [99]:

$$i_o = 1.08 \times 10^{-21} \exp\left(0.086 T_{cell}\right) \tag{3.96}$$

The ohmic overpotential is mainly due to resistance in the electrolyte and is defined as follows:

$$\upsilon_{ohmic} = R_{ohmic}.i \tag{3.97}$$

where R_{ohmic} is the cell resistance ($\Omega\ cm^2$) and is in the form [100]:

$$R_{ohmic} = \frac{t_{mem}}{\sigma_{mem}} \tag{3.98}$$

The membrane conductivity is determined as a function of the membrane water content and fuel cell temperature [100]:

$$\sigma_{mem} = (0.005139\,\lambda_{mem} - 0.00326)\exp\left[1268\left(\frac{1}{303} - \frac{1}{T_{cell}}\right)\right] \tag{3.99}$$

Membrane water content is determined from the membrane water activity, *a*, using the following equation [97]:

$$\lambda_{mem} = \begin{cases} 0.043 + 17.81a - 39.85a^2 + 39.85a^3, & 0 < a = x_{H_2O}\dfrac{P}{P_{sat}} \le 1 \\ 14 + 1.4(a-1), & 1 < a = x_{H_2O}\dfrac{P}{P_{sat}} \le 3 \end{cases} \tag{3.100}$$

where x_{H_2O} is the water mole fraction and P_{sat} is the saturation pressure at T_{cell}.

The concentration overpotential results from the increased loss at high current density. It is given by [97]:

$$\upsilon_{conc} = i\left(\beta_1 \frac{i}{i_{\max}}\right)^{\beta_2} \tag{3.101}$$

where B_1, B_2 and i_{max} are constants that depend on temperature and reactant partial pressure and can be determined empirically. $B_2$is taken as 2 and i_{max} as 2 A/cm^2while B_1 is defined as [97]:

$$\beta_1 = \begin{cases} (7.16\times10^{-4}\,T_{cell} - 0.622)\left(\dfrac{p_{O_2}}{0.1173} + P_{sat}\right) + (-1.45\times10^{-3}\,T_{cell} + 1.68), & for\ \dfrac{p_{O_2}}{0.1173} + P_{sat} < 2\,atm \\ (8.66\times10^{-5}\,T_{cell} - 0.068)\left(\dfrac{p_{O_2}}{0.1173} + P_{sat}\right) + (-1.6\times10^{-4}\,T_{cell} + 0.54), & for\ \dfrac{p_{O_2}}{0.1173} + P_{sat} \ge 2\,atm \end{cases} \tag{3.102}$$

Where the partial pressure of oxygen is calculated from the molar fraction of oxygen and cathode pressure. The molar fraction of oxygen is calculated using air

stoichiometry at the cathode, the cathode dry gas molar fraction, and the molar fraction of water which is the ratio of saturation pressure at fuel cell temperature and cathode or anode pressures as follows [98]:

$$p_{O_2} = x_{O_2}.P_C \tag{3.103}$$

$$x_{H_2O,C} = \frac{P_{sat}}{P_C} \tag{3.104}$$

$$x_{O_2} = \frac{1 - x_{H_2O,C}}{1 + \frac{x_C}{2}\left[1 + \frac{\zeta_C}{\zeta_C - 1}\right]} \tag{3.105}$$

The same concept is used in the calculation of partial pressure of hydrogen but considering the anode side [98]:

$$p_{H_2} = x_{H_2}.P_A \tag{3.106}$$

$$x_{H_2O,A} = \frac{P_{sat}}{P_A} \tag{3.107}$$

$$x_{H_2} = \frac{1 - x_{H_2O,A}}{1 + \frac{x_A}{2}\left[1 + \frac{\zeta_A}{\zeta_A - 1}\right]} \tag{3.108}$$

Finally, the total voltage of the fuel cell can be calculated in volts from Eq. (3.92) and plotted versus the current density.

The power of a fuel cell is found by multiplying the total voltage by the current density and fuel cell area:

$$\dot{W}_{PEM} = V_{tot}\, i\, A_{cell} \tag{3.109}$$

Mass flow rate of inlet and outlet air, inlet and outlet hydrogen, oxygen and hydrogen consumption rates and water production rate are calculated using the following formulas [101]:

$$\dot{m}_{O_2,in} = \zeta_C \frac{M_{O_2}}{X_{O_2}} i \frac{A_{cell}}{2\,F} \times 10^{-3} \tag{3.110}$$

$$\dot{m}_{H_2,in} = \zeta_A M_{H_2} i \frac{A_{cell}}{2\,F} \times 10^{-3} \tag{3.111}$$

$$\dot{m}_{O_2,react} = M_{O_2} i \frac{A_{cell}}{2\,F} \times 10^{-3} \tag{3.112}$$

$$\dot{m}_{H_{2,react}} = M_{H_2} i \frac{A_{cell}}{2\,F} \times 10^{-3} \tag{3.113}$$

$$\dot{m}_{O_{2,out}} = \dot{m}_{O_{2in}} + \dot{m}_{O_{2react}} \tag{3.114}$$

$$\dot{m}_{H_{2,out}} = \dot{m}_{H_{2in}} + \dot{m}_{H_{2react}} \tag{3.115}$$

$$\dot{m}_{H_2O} = M_{H_2O} i \frac{A_{cell}}{2\,F} \times 10^{-3} \tag{3.116}$$

The energy efficiency of the PEMFC system is then calculated using the following formula:

$$\eta_{PEM,en} = \frac{\dot{W}}{\dot{m}_{H_{2in}} HHV_{H_2}} \tag{3.117}$$

The total exergy consists of physical exergy and chemical exergy. Physical exergy is associated with the temperature and pressure of the matter while chemical exergy is associated with the departure of the chemical composition of a system from the environment.

Physical exergy for the reactants, oxygen and hydrogen, is determined using the following formulas [102]:

$$e^{PH}_{O_{2in}} = Cp_{O_2} T_o \left[\frac{T_{cell}}{T_o} - \left(1 - ln\frac{T_{cell}}{T_o}\right) + \left(ln\left(k - \frac{1}{k}\right)\left(\frac{P_{cell}}{P_o}\right)\right)\right] \tag{3.118}$$

$$e^{PH}_{H_{2in}} = Cp_{H_2} T_o \left[\frac{T_{cell}}{T_o} - \left(1 - ln\frac{T_{cell}}{T_o}\right) + \left(ln\left(k - \frac{1}{k}\right)\left(\frac{P_{cell}}{P_o}\right)\right)\right] \tag{3.119}$$

Exergy transfer by mass for i^{th} component, exergy transfer by inlet mass, and exergy transfer by exit mass are determined as follows:

$$\dot{X}_{i,mass} = \dot{m}_i (e^{PH}_i + e^{CH}_i) \tag{3.120}$$

$$\dot{X}_{mass,in} = \dot{X}_{H_{2,in}} + \dot{X}_{O_{2,in}} \tag{3.121}$$

$$\dot{X}_{mass,out} = \dot{X}_{H_{2,out}} + \dot{X}_{O_{2,out}} + \dot{X}_{H_2O} \tag{3.122}$$

Exergy transfer by work is equal to the power produced by the PEM fuel cell, that is:

$$\dot{X}_{work} = \dot{W}_{PEM} \tag{3.123}$$

Exergy transfer by heat and irreversibility of the PEMFC system are given by the following equations [97]:

$$\dot{X}_{heat} = \left(1 - \frac{T_o}{T_{cell}}\right) r_{HL} \dot{Q}_{PEM} \tag{3.124}$$

$$\dot{I}_{cell} = \dot{X}_{heat} - \dot{W} + \dot{X}_{mass_{in}} - \dot{X}_{mass_{out}} \tag{3.125}$$

The useful heat generated by the PEMFC system throughout the cell operation is given by [97]:

$$\dot{Q}_{PEM} = \left[T_o \left(\dot{m}_{O_{2,out}} s_{O_2} + \dot{m}_{H_2 out} s_{H_2} + \dot{m}_{H_2 O}\, s_w\right) - \left(\dot{m}_{O_{2,in}} s_{O_2} + \dot{m}_{H_2 in} s_{H_2}\right) + \dot{W}_{PEM} + \dot{X}_{mass_{out}} - \dot{X}_{mass_{in}}\right] \left[r_{HL} + (1 - r_{HL}) \frac{T_o}{T_{cell}}\right]^{-1} \tag{3.126}$$

The exergetic efficiency of a fuel cell system defined as the ratio of the irreversibility to the exergy of the reactants (air and hydrogen) as shown in the following formula:

$$\eta_{PEM,ex} = 1 - \frac{\dot{I}_{cell}}{\dot{X}_{mass_{in}}} \tag{3.127}$$

The heat generated by the PEMFC is used as heat input to the HTG to drive the DEAS. Thus:

$$\dot{Q}_{HTG} = \dot{Q}_{PEM} + \dot{W}_{PEM} - \dot{W}_{Pump} \tag{3.128}$$

The overall energetic and exergetic efficiencies of the PEMFC-based HVAC cooling system are:

$$\eta_{sys,en} = \left(\frac{\dot{Q}_{Evap}}{\dot{m}_{H_2} \times HHV_{H_2}}\right) \tag{3.129}$$

$$\eta_{sys,ex} = \left(\frac{\dot{X}_{Evap,th}}{\dot{X}_{H_2,in}}\right) \tag{3.130}$$

3.3 FPSC-Based HVAC-Cooling System

The model of the FPSC system based on energy and exergy analyses is provided in this section. The various relations required to determine the useful energy and the performance of the FPSC are presented. Fig. 3.2 shows an isometric view of the FPSC and its components and provides the geometric details of the absorber plate of the FPSC. The FPSC unit consists of an insulated metal box with a glass cover which serves as a heat trap, a dark-colored absorber plate used to heat liquid water, and a tube array used as the working fluid passage.

The input data used in this model is given in Table 3.4. The thermodynamic analysis is based on the following assumptions:

a. The working fluid is water.
b. The energy transfer rate is steady.
c. Properties of materials are independent of temperature.
d. No solar energy is absorbed by the cover.
e. The same ambient temperature exists at the front and back of the collector.
f. The temperature of the surrounding fluid is uniform.
g. The overall loss heat transfer coefficient is the same all over the plate surfaces.
h. The hot water is stored in an insulated wall tank.

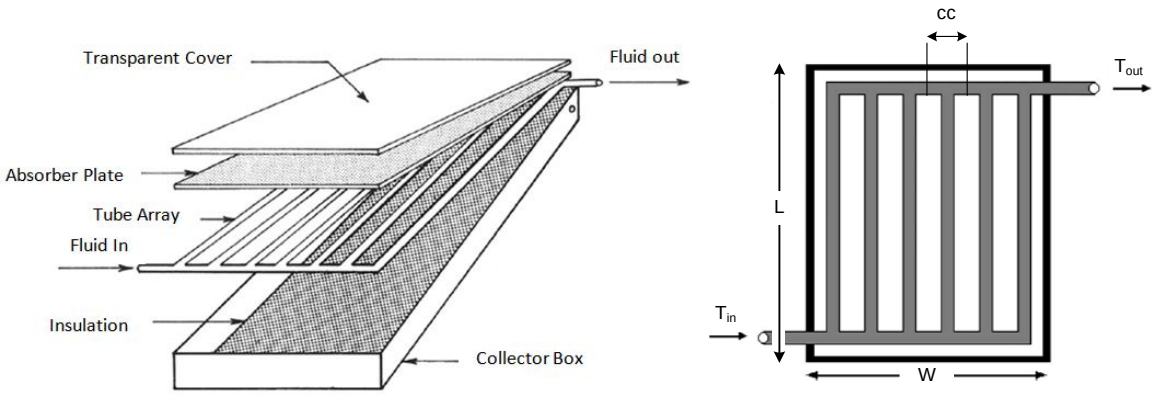

(a) (b)

Fig. 3.2 Illustration of the FPSC: (a) Isometric view of the flat plate collector including components. (b) Geometrical details of the absorber plate of the FPSC (Adapted from [103] and [104]).

Table 3.4 Design and operating parameters of FPSC.

Parameter	Symbol	Unit	Value
Constants and assumptions			
Stephen-Boltzman constant	σ	$W/m^2 . K^4$	5.67×10^{-8}
Wind velocity	v	m/s	2.5 [105]
Collector tilt angle	β	deg	35
Bond conductance	C_b	$m. K/W$	0.03 [105]
Fluid			
Specific heat of water	C_{p_w}	$J/kg \cdot K$	4185
Water density	ρ_w	Kg/cm^3	1000
Inlet temperature	T_{in}	K	313 [106]
Outlet temperature	T_{out}	K	318
Water speed in the tube	v_w	m/s	0.1 [105]
Ambient			
Ambient air temperature	T_{amb}	K	308
Temperature of the sun	T_s	K	5770
Pressure of ambient air	P_o	kPa	101.325
Glazing			
Solar transmittance of glazing	τ_g	-	0.85[105]
Emissivity of glass cover	ε_g	-	0.88 [105]
Number of glass cover	N	-	1
Absorber plate			
Solar absorbtance of collector plate	α_p	-	0.9 [105]
Emissivity of absorber plate	ε_p	-	0.1 [105]
Thermal conductivity of plate (copper)	kt_p	$W/m. K$	385 [105]
Temperature of the absorber plate	T_p	K	353
Plate thickness	δ_p	m	0.0005
Bottom			
Thermal conductivity of bottom insulator (polyurethane)	kt_b	$W/m. K$	0.034[106]
Bottom insulation thickness	δ_b	m	0.05
Convection heat loss coefficient from bottom to ambient	$h_{c,ba}$	$W/m^2 . K$	0.5 [107]
Edge			
Thermal conductivity of edge insulator	kt_e	$W/m. K$	0.045[106]
Edge insulation thickness	δ_e	m	0.05
Convection heat loss coefficient from edge to ambient	$h_{c,ea}$	$W/m^2 . K$	1.7 [107]
Tubes			
Tube external diameter	D_{out}	m	0.015
Tube internal diameter	D_{in}	m	0.01
Distance between the centers of two neighboring tubes	cc	m	0.12
Collector box			
Collector length	L	m	1
Collector width	w	m	0.5

The prediction of collector performance requires information on the solar energy absorbed by the collector absorber plate. The solar energy incident on a tilted surface has three special components: beam, diffused, and ground-reflected radiation. The absorbed radiation by the absorber plate is found by multiplying the direct incident solar radiation by the transmittance of the glass cover and the absorptance of the absorber plate property as follows[105]:

$$I = (\tau_g \alpha_p)\, I_D \tag{3.131}$$

Under steady state conditions, the rate of useful energy delivered by the FPSC is equal to the rate of energy absorbed by the heat transfer fluid minus the direct or indirect heat losses from the surface to the surroundings. The useful energy collected from the FPSC can be obtained from the following formula [105]:

$$\dot{Q}_u = F_R A_{FP}\left[(\tau_g \alpha_p)\, I_D - U_L(T_{in} - T_{amb})\right] \tag{3.132}$$

whereA_{FP} is the area of the collector which is a simple rectangular form of width W and length L,T_{amb} is the ambient temperature provided from the meteorological data, and T_{in} is a design parameter and represents the temperature of the inlet fluid (water) and depends on the characteristics of the complete solar heating system and the hot water demand or heat demand of the building.

The heat removal factor $F_R$represents the ratio of the actual heat delivered to that delivered if the collector plate is at uniform temperature equal to that of the entering fluid. $F_R$is affected only by the solar collector characteristics, the fluid types, and the fluid flow rate through the collector. F_R can be obtained from [108]:

$$F_R = \frac{\dot{m}_w C_{p_w}}{A_{FP} U_L}\left[1 - exp\left(-\frac{A_{FP} U_L F'}{\dot{m}_w C_{p_w}}\right)\right] \tag{3.133}$$

where $C_{p_w}$and $\dot{m}_w$are the specific heat and mass flow rate of the working fluid (water).

The mass flow rate depends on the geometry of the tube and the collector as well as the properties of the working fluid as illustrated in the following equations:

$$\dot{m}_{tube} = \rho_w \cdot v_w \cdot \pi \cdot \frac{D_{in}^2}{4} \tag{3.134}$$

Thus, the total mass flow rate on the collection area and the number of tubes give the mass flow rate of water in the collector:

$$\dot{m}_{tot} = \dot{m}_{tube} \cdot n \tag{3.135}$$

$$n = \frac{w}{cc} \tag{3.136}$$

$$\dot{m}_w = \frac{\dot{m}_{tot}}{A_{FP}} \tag{3.137}$$

The collector efficiency factor F' represents the ratio of the actual useful energy gain to the useful energy gain that would result if the collector absorbing surface had been at the local fluid temperature and is given by [108]:

$$F' = \frac{1/U_L}{1/U_o} = \frac{U_o}{U_L} \tag{3.138}$$

The overall heat loss coefficient is a complicated function of the collector construction and its operating conditions. U_L represents the heat transfer resistance from the absorber plate to the ambient air and is given by [109]:

$$U_L = U_t + U_b + U_e \tag{3.139}$$

The top loss coefficient U_t is given by the following empirical relation for the glazed solar collector [109], [21]:

$$U_t = \left[\frac{N}{\left(\frac{C}{T_{out}} \cdot \left(\frac{T_p - T_{amb}}{N+f}\right)^d\right) + \frac{1}{h_{conv}}}\right]^{-1} + \frac{\sigma\left(T_p + T_{amb}\right)\left({T_p}^2 + {T_{amb}}^2\right)}{\frac{1}{\varepsilon_p + \left(0.0425\, N\left(1-\varepsilon_p\right)\right)} + \frac{2\,N+(f-1)}{\varepsilon_g} - N} \tag{3.140}$$

where:

$$C = 365.9 \times (1 - 0.00883\beta + 0.0001298\beta^2) \tag{3.141}$$

$$h_{conv} = 5.7 + 3.8\, v \tag{3.142}$$

$$f = \left(1 - 0.04 h_{conv} + 0.0005\, {h_{conv}}^2\right)(1 + 0.091\, N) \tag{3.143}$$

$$d = 0.43\left[1 - \frac{100}{T_{out}}\right] \tag{3.144}$$

The bottom heat loss coefficient U_b represents the energy loss from the bottom of the collector and is given by [21]:

$$U_b = \frac{1}{\frac{\delta_b}{kt_b} + \frac{1}{h_{c,ba}}} \tag{3.145}$$

Similarly, the edge heat loss coefficient is given by [21]:

$$U_e = \frac{1}{\frac{\delta_e}{kt_e} + \frac{1}{h_{c,ea}}} \tag{3.146}$$

In equation (3.138), $1/U_o$ is the heat transfer resistance from the fluid to the ambient airwhere $U_o$is given by [21]:

$$U_o = \frac{1}{cc\left[\frac{1}{U_L\cdot\left(D_{out}+(cc-D_{out})\cdot F_{fi}\right)} + \frac{1}{C_b} + \frac{1}{\pi D_{in} h_{fi}}\right]} \tag{3.147}$$

where C_b is the bond conductance which is a function of the bond thermal conductivity, thickness and width. Here C_b has been set as a constant. The heat transfer coefficient between the working fluid and tube wall $h_{fi}$is evaluated using the following empirical formula [109]:

$$h_{f_i} = \left(1430 + 23.3T_{f_m} - 0.048{T_{f_m}}^2\right)v_w^{0.8} D_{in}^{-0.2} 3 \tag{3.148}$$

where T_{f_m} is the average working fluid temperature inside the tube in °C:

$$T_{f_m} = \frac{T_{in}+T_{out}}{2} \tag{3.149}$$

In Equation (3.147), F_{fi} is the standard fin efficiency for straight fins with rectangular profiles and is determined from [109]:

$$F_{fi} = \frac{tanh\left[m\left(\frac{cc-D_{out}}{2}\right)\right]}{m\left(\frac{cc-D_{out}}{2}\right)} \tag{3.150}$$

where m is a variable given by [109]:

$$m = \left[\frac{U_L}{kt_p\cdot\delta_p}\right]^{-0.5} \tag{3.151}$$

Finally, the thermal efficiency of the FPSC can be obtained by dividing the useful heat gain by $(A_{FP}I_t)$. Therefore:

$$\eta_{FP_{en}} = \frac{\dot{Q}_u}{A_{FP}I} \tag{3.152}$$

For incident angles below about 35°, the product ($\tau_g \alpha_p$) is essentially constant so that the useful heat gain and thermal efficiency formulas are linear with respect to the parameter $\frac{T_{in}-T_{amb}}{I}$ as long as U_L remains constant.

$$\eta_{FP_{en}} = F_R \left(\tau_g \alpha_p - U_L \frac{T_{in}-T_{amb}}{I} \right) \tag{3.153}$$

The exergy efficiency of the solar collector is defined as the ratio of the exergy stored by the fluid that passes through the stream tube, that is, the useful exergy delivered to the exergy of the solar radiation absorbed by the FPSC [110]:

$$\eta_{FP_{ex}} = \frac{\dot{X}_u}{\dot{X}_{FP}} \tag{3.154}$$

Where:

$$\dot{X}_u = \dot{m}_w [(h_{out} - h_{in}) - T_{amb}(s_{out} - s_{in})] \tag{3.155}$$

or

$$\dot{X}_u = \dot{m}_w C_{p_w} \left[(T_{out} - T_{in}) - T_{amb} \left(ln \frac{T_{out}}{T_{in}} \right) \right] \tag{3.156}$$

and

$$\dot{X}_{FP} = A_{FP} I \left[1 + \frac{1}{3} \left(\frac{T_{amb}}{T_{sun}} \right)^4 - \frac{4}{3} \frac{T_{amb}}{T_{sun}} \right] \tag{3.157}$$

The heat generated by the FPSC is used as a heat input to the HTG of the DEAS. Thus the heat input to the HTG is:

$$\dot{Q}_{HTG} = \dot{Q}_{FP} \tag{3.158}$$

The overall efficiencies of the integrated FPSC-based HVAC cooling system are:

$$\eta_{sys_{en}} = \frac{\dot{Q}_{Evap}}{A_{FP} I} \tag{3.159}$$

$$\eta_{sys_{ex}} = \frac{\dot{X}_{Evap,th}}{\dot{X}_{FP}} \tag{3.160}$$

3.4 PTSC-Based HVAC-Cooling System

This section covers the mathematical model of the PTSC system based on energy and exergy analyses.

Fig. 3.3 shows a cross sectional view of the PTSC. The PTSC unit consists of a metal black tube placed along the focal line of the receiver, covered with a glass tube to reduce heat losses that can take place by radiation and convection in addition to a parabola which serves as a reflective surface where the parallel rays incident on it are reflected onto the receiver tube.

The input data used in this model is given in Table 3.5. For the purpose of analysis, the following assumptions have been made:

a. The integrated system operates at a steady state.
b. The porous medium properties have a cylindrical symmetry.
c. All phases are continuously in thermal, mechanical, and chemical local equilibrium.
d. The glass tube temperature is uniform at any given time.
e. Properties of materials are independent of temperature.
f. The hot water is stored in an insulated wall tank.

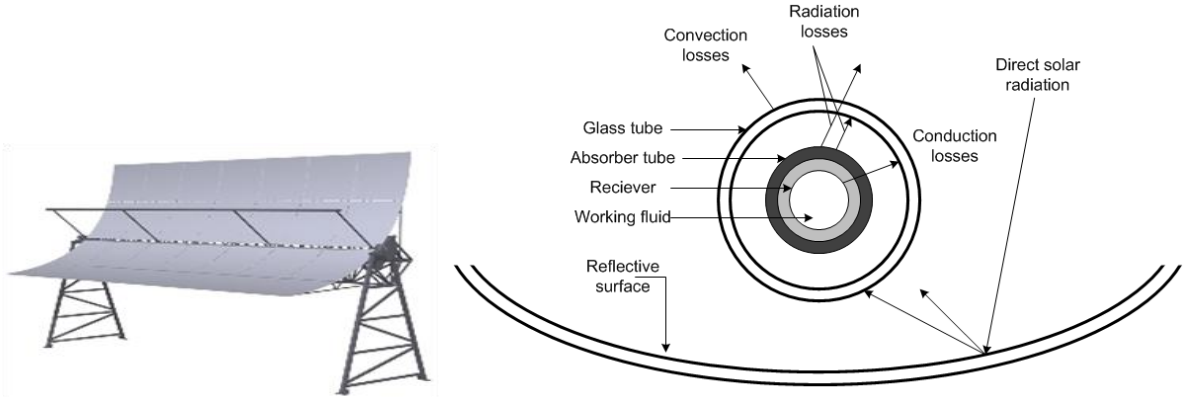

Fig. 3.3 Illustration of PTSC: (a) PTSC unit. (b) Cross sectional view of the PTSC.

Table 3.5 Design and operating parameters of PTSC.

Parameter	Symbol	Unit	Value
Mass flow rate of oil in the receiver	$\dot{m}_{oil}$	kg/s	0.3
Pipe receiver outside diameter	D_{r_o}	m	0.05
Receiver inside diameter	D_{r_i}	m	0.04
Glass cover outer diameter	D_{c_o}	m	0.09
Collector width	w	m	3
Collector length	L	m	20
Receiver temperature of inlet fluid	T_i	$°C$	220
Receiver thermal conductivity	k_r	$W/m.K$	15
Receiver temperature	T_r	$°C$	260
Receiver emissivity	ε_r	-	0.92 [111]
Receiver efficiency	η_r	%	75 [111]
Glass cover emissivity	ε_c	-	0.87 [111]
Stefan-Boltzmann constant	σ	$W/m^2.K^4$	5.67×10^{-8}
Glass cover temperature	T_c	$°C$	64
Sun temperature	T_s	K	5770
Ambient temperature	T_{amb}	$°C$	25
Atmospheric pressure	P_{atm}	kPa	101.325
Wind velocity	v	m/s	5 [111]

Under steady state conditions, the rate of useful energy delivered by the PTSC is equal to the rate of energy absorbed by the heat transfer fluid minus the direct or indirect heat losses from the surface to the surroundings. The useful energy collected from PTSC can be obtained from the following formula [21]:

$$\dot{Q}_{u,PT} = F_R[I_B A_a - A_r U_L(T_i - T_{amb})] \tag{3.161}$$

where A_a and A_r are the aperture and receiver area of the collector, respectively. They are defined as:

$$A_a = (w - D_{c_o})L \tag{3.162}$$

$$A_r = \pi\, D_{r_o} L \tag{3.163}$$

Hence, the concentration ratio, which is defined as the ratio of the aperture area to the receiver area, is then calculated [21]:

$$C = \frac{A_a}{A_r} \tag{3.164}$$

Concentrating collectors can utilize only beam radiation instead of the total radiation. The beam radiation is the portion of direct radiation absorbed by the receiver and depends on the receiver efficiency as follows [21]:

$$I_B = I_D \eta_r \tag{3.165}$$

The heat removal factor F_R represents the ratio of the actual heat delivered to that delivered if the collector plate were at uniform temperature equal to that of the entering fluid. $F_R$is affected only by the solar collector characteristics, the fluid types, and the fluid flow rate through the collector. $F_R$can be obtained from [21]:

$$F_R = \dot{m}_{oil} \cdot \frac{Cp_{oil}}{A_r U_L}\left[1 - e\left(-\frac{A_r U_L F'}{\dot{m}_{oil} Cp_{oil}}\right)\right] \tag{3.166}$$

where Cp_{oil} is the heat capacity of circulating fluid-Therminol 66 in $\mathrm{kJ/kg \cdot K}$ and is calculated as a function of the receiver temperature of the inlet fluid (oil) [86]:

$$Cp_{oil} = 0.003313\, T_i\,(°C) + 8.970785 \times 10^{-7} {T_i}^2 (°C) + 1.496005 \tag{3.167}$$

The collector efficiency factor F'represents the ratio of the actual useful energy gain to the useful energy gain that would result if the collector absorbing surface had been at the local fluid temperature. F' is given by [21]:

$$F' = \frac{U_o}{U_L} \tag{3.168}$$

The overall heat loss coefficient is a complicated function of the collector construction and its operating conditions. The solar collector heat loss coefficient between ambient and receiver is defined as [21]:

$$U_L = \left(\frac{A_r}{(h_{c_{ca}} + h_{r_{ca}}) A_c} + \frac{1}{h_{r_{cr}}}\right)^{-1} \tag{3.169}$$

Where A_c is the glass cover area of the PTSC which is simply represented by the perimeter of a pipe:

$$A_c = \pi\, D_{c_o} L \tag{3.170}$$

$h_{c_{ca}}$ is the convection heat transfer coefficient between the glass cover and ambient [111]:

$$h_{c_{ca}} = \frac{Nus_{ca}\, k_{air}}{D_{c_o}} \tag{3.171}$$

where $\mathrm{Nus_{ca}}$ is the Nusselt number and is given by [111]:

$$Nus_{ca} = 0.3\ (Re)_{ca}^{0.6} \text{For } 0.1 < Re < 2300$$
$$Nus_{ca} = 0.4 + 0.54\ (Re)_{ca}^{0.6} \text{For } Re > 4000 \tag{3.172}$$

where Re is the Reynolds number and is calculated from the general formula:

$$Re_{ca} = \rho_{air}\, v\, \frac{D_{c_o}}{\mu_{air}} \tag{3.173}$$

where ρ_{air}, μ_{air} and k_{air} are determined for the air at the mean temperature and atmospheric pressure.The mean temperature is the average temperature on the glass cover:

$$T_m = \frac{T_{amb} + T_c}{2} \tag{3.174}$$

The radiation heat transfer coefficient between the glass cover and ambient is defined as [111]:

$$h_{r_{ca}} = \varepsilon_c\, \sigma\, (T_c + T_{amb})({T_c}^2 + {T_{amb}}^2) \tag{3.175}$$

The radiation heat transfer coefficient between the glass cover and receiver is given by [112]:

$$h_{r_{cr}} = \frac{\sigma\,(T_c+T_r)({T_c}^2+{T_r}^2)}{\left(\frac{1}{\varepsilon_r}+\frac{A_r}{A_c}\right)\left(\frac{1}{\varepsilon_c}-1\right)} \tag{3.176}$$

The estimation of the overall heat coefficient includes the tube wall because the heat flux in a concentrating collector is high. Based on the outside tube diameter, this is given by [113]:

$$U_o = \left[\left(\frac{1}{U_L}+\frac{D_{r_o}}{h_{c_{r_{in}}} D_{r_i}}+\frac{D_{r_o}}{2k_r}\right) ln\left(\frac{D_{r_o}}{D_{r_i}}\right)\right]^{-1} \tag{3.177}$$

where $h_{cr_{in}}$is the convention heat transfer coefficient inside the receiver tube. It is calculated using the general formula:

$$h_{cr_{in}} = \frac{Nus_r k_r}{D_{r_i}} \tag{3.178}$$

The Nusselt number in the overall heat coefficient formula is given by:

$$Nus_r = 0.023\ {Re_r}^{0.8} {Pr_r}^{0.4} \quad \text{For turbulent flow } (Re > 4000)$$
$$Nus_r = constant = 4.364 \quad \text{For laminar flow } (Re < 2300) \tag{3.179}$$

The Prandtl number is calculated using the following formula:

$$Pr_r = Cp_{oil}\frac{\mu_{oil}}{k_{oil}} \tag{3.180}$$

where:

The kinematic viscosity of oil-Therminol 66 in $(\mathrm{mm}^2/\mathrm{s})$ is given by [86]:

$$v_{oil} = e\left(\frac{586.375}{T_i\,(°C)+62.5} - 2.2809\right) \tag{3.181}$$

The density of circulating fluid-Therminol 66 in$(\mathrm{kg/m^3})$ is given by [86]:

$$\rho_{oil} = -0.614254\, T_i(°C) - 0.000321\, {T_i}^2(°C) + 1020.62 \tag{3.182}$$

The dynamic viscosity $(\mathrm{Pa \cdot s})$ is:

$$\mu_{oil} = \upsilon_{oil}\rho_{oil} \times 10^{-6} \tag{3.183}$$

The thermal conductivity of circulating fluid-Therminol 66 in $(\mathrm{W/m \cdot K})$ is given by [86]:

$$k_{oil} = -0.000033\, T_i(°C) - 1.5 \times 10^{-7} {T_i}^2(°C) + 0.118294 \tag{3.184}$$

The Reynolds number is:

$$Re_r = \frac{v\, D_{r_i}}{\upsilon_{oil}} \tag{3.185}$$

The cover average temperature can be calculated to recheck the assumed value using the following equation [114]:

$$T_c = \frac{h_{r_{cr}} T_r + \left(\frac{A_c}{A_r} T_{amb}\left(h_{c_{ca}} + h_{r_{ca}}\right)\right)}{h_{r_{cr}} + \left(\frac{A_c}{A_r}\left(h_{c_{ca}} + h_{r_{cr}}\right)\right)} \tag{3.186}$$

The outlet temperature of the flowing fluid is calculated using the inlet temperature, the useful heat gain, and the capacity of the flowing fluid:

$$T_o = T_i + \frac{\dot{Q}_{u,PT}}{\dot{m}_{oil} Cp_{oil}} \tag{3.187}$$

As the useful energy delivered from the collector can now be determined, energy efficiency of the PTSC is:

$$\eta_{en} = \frac{\dot{Q}_{u,PT}}{A_a I_B} \tag{3.188}$$

The exergetic efficiency is simply the ratio of the output exergy to the input exergy. For a PTSC, it is the ratio of the exergy stored by the fluid that passes through the stream tube to the exergy of the solar radiation absorbed by the PTSC:

$$\eta_{ex} = \frac{\dot{X}_{out,PT}}{\dot{X}_{in,PT}} \tag{3.189}$$

where $\dot{X}_{in,PT}$ and $\dot{X}_{out,PT}$ are given as follows [115]:

$$\dot{X}_{in,PT} = A_a I_B \left[1 + \frac{1}{3}\left(\frac{T_{amb}}{T_s}\right)^4 - \frac{4}{3}\left(\frac{T_{amb}}{T_s}\right)\right] \tag{3.190}$$

$$\dot{X}_{out,PT} = \dot{Q}_{u,PT}\left(1 - \frac{T_{amb}}{T_r}\right) \tag{3.191}$$

Hence, exergy destruction and entropy generation can be calculated. The exergy destruction is simply the difference between input and output exergy:

$$\dot{X}_{des} = \dot{X}_{in,PT} - \dot{X}_{out,PT} \tag{3.192}$$

$$\dot{S}_{gen} = \frac{X_{des}}{T_{amb}} \tag{3.193}$$

The useful energy delivered from the PTSC is fed into the HTG to drive the absorption system. So:

$$\dot{Q}_{HTG} = \dot{Q}_{u,PT} \tag{3.194}$$

The overall efficiencies of the integrated system PTSC-based HVAC cooling system are:

$$\eta_{sys,en} = \frac{\dot{Q}_{Evap}}{I_B A_a} \tag{3.195}$$

$$\eta_{sys,ex} = \frac{\dot{X}_{Evap,th}}{\dot{X}_{in,PT}} \tag{3.196}$$

3.5 PV/T Based-HVAC-Cooling System

A mathematical model of a glass-to-glass PV/T system with a parallel flat plate provided below the glass base of a solar cell is developed. Energy and exergy analyses are conducted to examine the performance of the system and study the variation of operating conditions and PV/T characteristics on the overall performance of the PV/T collector. Fig. 3.4 shows a cross sectional view of the glass-to-glass PV/T collector. The PV/T collector consists of a glass cover and solar cells where the solar radiation is passed through a duct composed of parallel flat plates provided below the glass base of the solar cells to regulate the passage of the working fluid. The collector also has a black surface to absorb the solar radiation.

The input data used in this model is given in Table 3.6. The following assumptions have been made in order to write the energy balance equations:

g. The heat conduction is one dimensional.
h. The system is in a quasi steady state.
i. The glass cover is at uniform temperature.
j. There flow of air through the duct is uniform.
k. The temperature variation along the thickness is negligible.

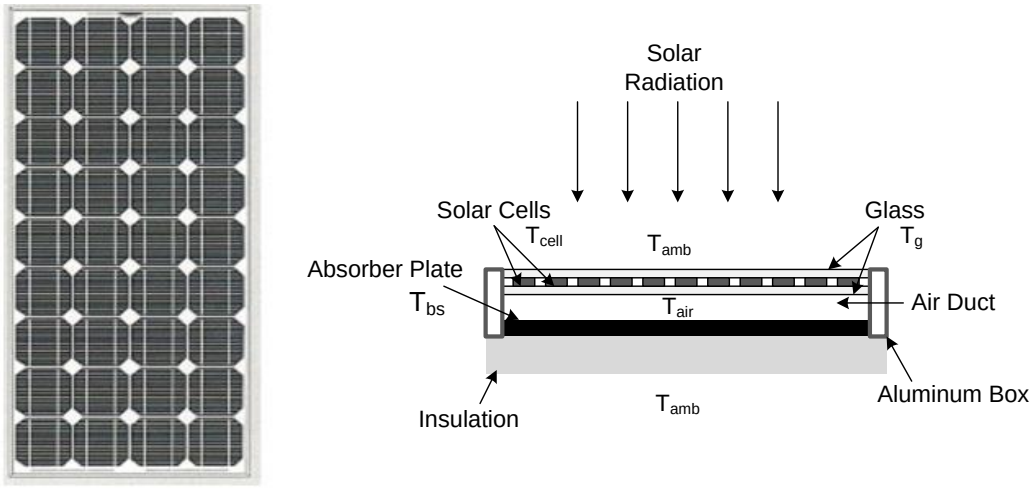

(a) (b)

Fig. 3.4 Glass-to-glass PV/T collector: (a) Top view. (b) Side view (Adapted from [116]).

Table 3.6 Design and operating parameters of PV/T.

Parameter	Symbol	Unit	Value
Mass flow rate of air	$\dot{m}_{air}$	kg/s	0.06
Specific heat capacity of air	$C_{p,air}$	kJ/kg.K	1.005
Conversion factor of the thermal power plant	C_f	-	0.36 [116]
Transimitivity of glass cover	τ_g	-	0.95 [117]
Packing factor of solar cell	β_c	-	0.83 [116]
Absorbitivity of black surface	α_b	-	0.95 [117]
Absorbitivity of absorber plate	α_c	-	0.9[117]
Overall heat loss coefficient from the PV/T air collector to the environment	U_L	W/m^2.K	4.56 [117]
Overall heat transfer coefficient from bottom to ambient	U_b	W/m^2.K	0.62 [117]
Overall heat transfer coefficient from glass to black surface through solar cell	U_{tb}	W/m^2.K	23.5 [117]
Overall heat transfer coefficient from solar cell to ambient though glass cover	U_t	W/m^2.K	2.8[117]
Penalty factor due to the presence of solar cell material and glass	h_{p1}	-	0.978 [116]
Penalty factor due to the presence of interface between glass and working fluid though absorber plate	h_{p2}	-	0.189 [116]
Heat transfer coefficient from black surface to air	h_{ba}	W/m^2.K	100[117]
Heat transfer coefficient from back surface to air through glass	h_t	W/m^2.K	125 [117]
Electrical efficiency at reference conditions	η_c	%	12 [118]
Width of PV/T air collector	W	m	0.45
Length of air duct	L	m	1.2
Area of collector	A_c	m^2	0.605
Number of collectors	N_c	-	1
Ambient temperature at reference conditions	$T_{amb,ref}$	°C	25
Sun temperature	T_s	K	5770
Ambient temperature	T_{amb}	°C	38

The rate of useful thermal energy obtained from the PV/T air collector is the overall heat gain minus the overall heat loss from the collector [116]:

$$\dot{Q}_{u,PVT} = \frac{\dot{m}_{air} \cdot C_{p,air}}{U_L}\left(h_{p_2} \cdot P_{eff,\alpha,\tau} \cdot I - U_L \cdot (T_{air,in} - T_{amb})\right) \cdot \left[1 - \exp\left(\frac{-W \cdot U_L \cdot L}{\dot{m}_{air} \cdot C_{p,air}}\right)\right] \tag{3.197}$$

where I and $T_{air,in}$ are the solar irradiance in (W/m^2)and the temperature of the inlet fluid in °C, respectively, which are varying from month to month. The effective parameter $P_{eff,\alpha,\tau}$ is defined as [119]:

$$P_{eff,\alpha,\tau} = \alpha_b \tau_g^{\,2}(1-\beta_c) + h_{p1}\tau_g \beta_c (\alpha_c - \eta_c) \tag{3.198}$$

The instantaneous thermal efficiency of the PV/T air collector can be defined as the rate of useful thermal energy divided by the intensity of solar radiation absorbed by the collector area:

$$\eta_{th,PVT} = \frac{\dot{Q}_{u,PVT}}{W \cdot L \cdot I} \tag{3.199}$$

The average temperature of flowing air above the black surface over the length of air duct below the PV module, black surface temperature, solar cell temperature, and outlet air temperature of the flowing air inside the air duct are given by [117]:

$$\overline{T}_{air} = \left[T_{amb} + \frac{h_{p2} \cdot P_{eff,\alpha,\tau} \cdot I}{U_L}\right] \cdot \left[1 - \left(\frac{\left[1 - \exp\left(\frac{-W \cdot U_L \cdot L}{\dot{m}_{air} \cdot C_{p,air}}\right)\right]}{\frac{W \cdot U_L \cdot L}{\dot{m}_{air} \cdot C_{p,air}}}\right)\right] + T_{air,in} \cdot \left(\frac{\left[1 - \exp\left(\frac{-W \cdot U_L \cdot L}{\dot{m}_{air} \cdot C_{p,air}}\right)\right]}{\frac{W \cdot U_L \cdot L}{\dot{m}_{air} \cdot C_{p,air}}}\right) \tag{3.200}$$

$$T_{bs} = \frac{P_{eff,\alpha,\tau} \cdot I + (U_b + U_{tb}) \cdot T_{amb} + h_{ba} + h_t \cdot \overline{T}_{air}}{U_b + U_{tb} + h_{ba}} \tag{3.201}$$

$$T_{cell} = \frac{\tau_g \cdot \beta_c \cdot I \cdot [\alpha_c - \eta_c] + U_t \cdot T_{amb} + h_t \cdot T_{bs}}{U_t + h_t} \tag{3.202}$$

$$T_{air,out} = \left[T_{amb} + \frac{h_{p_2} \cdot P_{eff,\alpha,\tau} \cdot I}{U_L} \right] \cdot \left[1 - \exp\left(\frac{-W \cdot U_L \cdot L}{\dot{m}_{air} \cdot C_{p,air}} \right) \right] + T_{air,in} \cdot \exp\left(\frac{-W \cdot U_L \cdot L}{\dot{m}_{air} \cdot C_{p,air}} \right) \quad (3.203)$$

The electrical efficiency of the PV module is calculated using the following equation[118]:

$$\eta_{el,PVT} = \eta_c \cdot \left(1 - 0.0045 \cdot \left(T_{cell} - T_{amb,ref}\right)\right) \quad (3.204)$$

Conversion of electrical efficiency to the thermal efficiency equivalent is done through the following equation[118]:

$$\eta_{el,PVT,eq} = \frac{\eta_{el,PVT}}{C_f} \quad (3.205)$$

The overall energy efficiency of the PV/T air collector is the sum of the thermal and thermal equivalent of electrical efficiency:

$$\eta_{en,ov,PVT} = \eta_{th,PVT} + \eta_{el,PVT,eq} \quad (3.206)$$

The power produced by the PV module is the product of the electrical efficiency at reference conditions and solar intensity absorbed by the PV module for a number of collectors:

$$\dot{W}_{PV} = \eta_c \cdot A_c \cdot N_c \cdot I \quad (3.207)$$

The rate of exergy input to the system is equal to the exergy rate of the sun while the thermal exergy rate is the rate of exergy associated with useful heat gain from the collector and the electrical exergy rate is equal to the power produced by the PV module as illustrated in the following formulas [117]:

$$\dot{X}_{in,PVT} = A_c \cdot N_c \cdot I \cdot \left[1 - \frac{3}{4}\left(\frac{T_{amb}}{T_s} \right) + \frac{1}{3}\left(\frac{T_{amb}}{T_s} \right)^4 \right] \quad (3.208)$$

$$\dot{X}_{th} = \dot{Q}_{u,PVT} \cdot \left[1 - \left(\frac{T_{amb}}{T_{air,out}} \right) \right] \quad (3.209)$$

$$\dot{X}_{el} = \dot{W}_{PV} \quad (3.210)$$

So, the exergy output rate from the system is the sum of the thermal and electrical rates of exergy:

$$\dot{X}_{out,PVT} = \dot{X}_{th} + \dot{X}_{el} \tag{3.211}$$

Thus, the rate of exergy destructed from the system and the exergetic efficiency of the PV/T air collector are calculated by:

$$\dot{X}_{des} = \dot{X}_{in,PVT} + \dot{X}_{out,PVT} \tag{3.212}$$

$$\eta_{ex,PVT} = \left[1 - \frac{\dot{X}_{des}}{\dot{X}_{in,PVT}}\right] \tag{3.213}$$

The useful energy delivered from the PTSC is fed into the HTG to drive the absorption system:

$$\dot{Q}_{HG} = \dot{Q}_{u,PVT} + \dot{W}_{PV} - \dot{W}_{pump} \tag{3.214}$$

The overall energetic and exergetic efficiencies of the PTSC-based HVAC cooling system are given by:

$$\eta_{sys,en} = \frac{\dot{Q}_{Evap}}{I\,W\,L} \tag{3.215}$$

$$\eta_{sys,ex} = \frac{\dot{X}_{Evap,th}}{\dot{X}_{in,PVT}} \tag{3.216}$$

3.6 Hybrid PEMFC-PTSC-PV/T-Based HVAC-Cooling System

The hybrid system uses the same analysis illustrated in the previous sections except that the energy fed into the HTG to drive the absorption system is the sum of the useful energy delivered from the PEMFC-PTSC-PV/T:

$$\dot{Q}_{HTG} = (\dot{Q}_{PEM} + \dot{W}_{PEM} - \dot{W}_{pump})_{PEM} + \dot{Q}_{u,PT} + (\dot{Q}_{u,PVT} + \dot{W}_{PV} - \dot{W}_{pump})_{PVT} \tag{3.217}$$

Also, the overall energetic and exergetic efficiencies of the integrated system are:

$$\eta_{sys,en} = \frac{\dot{Q}_{Evap}}{(\dot{m}_{H_2} \times HHV_{H_2}) + (I_B\,A_a) + (I\,W\,L)} \tag{3.218}$$

$$\eta_{sys,ex} = \frac{\dot{X}_{Evap,th}}{\dot{X}_{H_2,in} + \dot{X}_{in,PT} + \dot{X}_{in,PVT}} \tag{3.219}$$

Chapter 4 Results and Discussion

In this chapter, the stated objectives are met by using the detailed analysis in the preceding chapter. Input parameters related to the system characteristics and operating conditions are listed. The efficiency and the rate of the output energy of the subsystems and the performance as well as the efficiency of the integrated systems are investigated based on the energy and exergy analyses conducted for each system. Moreover, a parametric study is carried out to examine the effect of the variation in the operating conditions and system characteristics on the overall performance of the system.

4.1 PEMFC-Based HVAC-Cooling System

In this section, the results obtained from the electrical and thermodynamic models of the PEMFC system are presented to study the behavior of the PEMFC unit. In order to examine the effect of the operating conditions on the performance of the PEMFC system, a parametric study is conducted so that the effect of varying the operating temperature, current density, and membrane thickness on the PEMFC's performance and power output can be examined. In addition, the effect of these operating conditions on the overall performance of the integrated system is studied.

First of all, a comparison of the model of the PEMFC unit with that provided by the literature is shown in Fig. 4.1. It is noted that there is a small variation in the behavior of the PEMFC's exergetic efficiency with respect to the current density. The deviation in the present model as compared to the model developed by Midilli and Dincer [102] is attributed mainly to the difference in the assumptions made and constants used in the calculation of the overpotential voltages. However, the behavior of the two models is in good agreement.

Fig. 4.2 and Fig. 4.3 present the electrical model of the PEMFC unit. Fig. 4.2 shows how the irreversible voltage and overpotential losses vary with the current density ranging from 0.0 to 1.0 A/cm^2. It is noted that losses due to the ohmic overpotential are greatly influenced by the variation in the current density while the activation and concentration overpotential losses are less affected by varying the current density. This is due to the direct relation between the ohmic losses and the current density in comparison

to the activation and concentration losses which are not directly proportional to the current density. As a result, the irreversible voltage increases with increasing the current density as it is the sum of these three overpotential losses which are all increasing with increasing the current density.

Fig. 4.3 shows the behavior of the total voltage of the system. It can be noticed that the total voltage is inversely proportional to the current density since it is defined as the difference between the reversible and irreversible voltages. As the reversible voltage does not change with varying the current density and the irreversible voltage increases with increasing the current density, the difference between the reversible and irreversible voltages decreases causing the total voltage to be decreased.

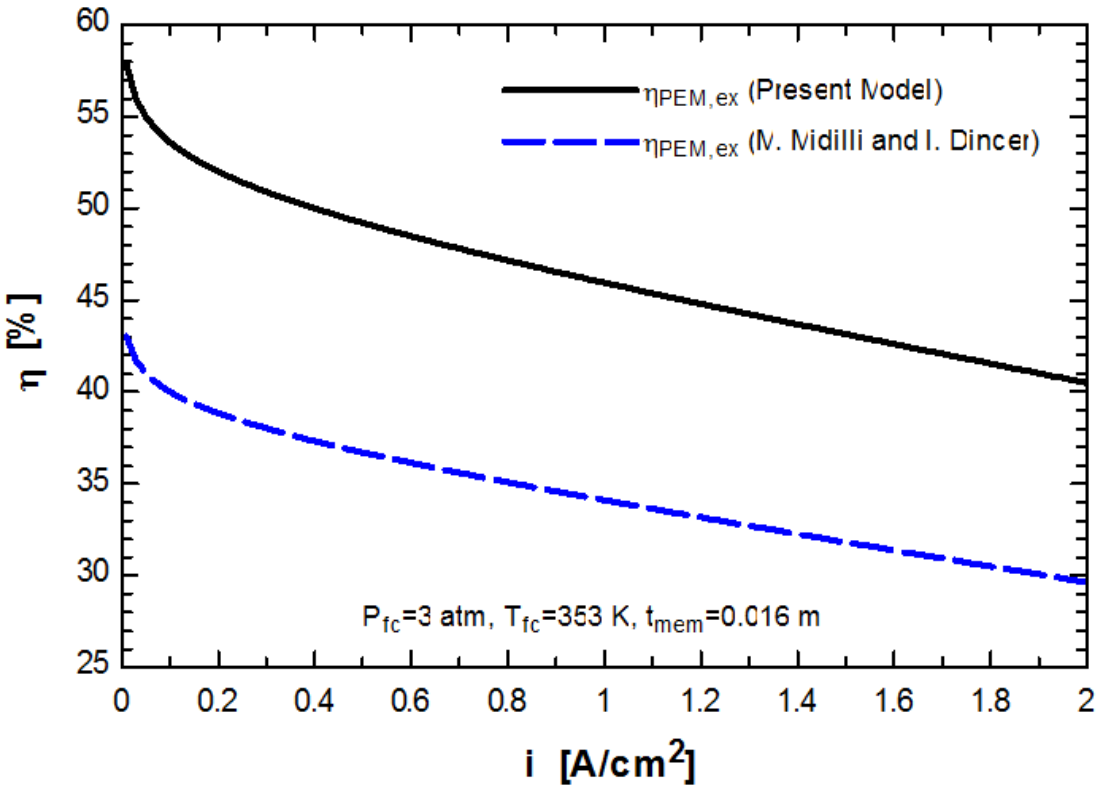

Fig. 4.1 Comparison of the current PEMFC model with the model presented by Midilli and Dincer [102].

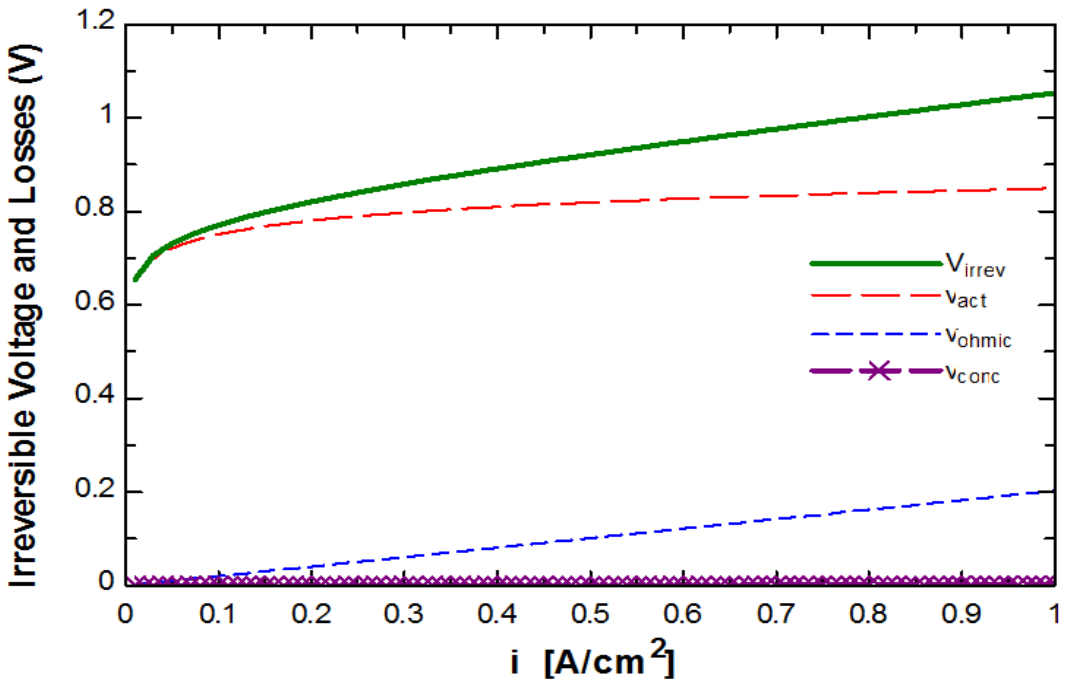

Fig. 4.2 Variation of irreversible voltage, activation, ohmic, and concentration losses with the current density in the PEMFC unit.

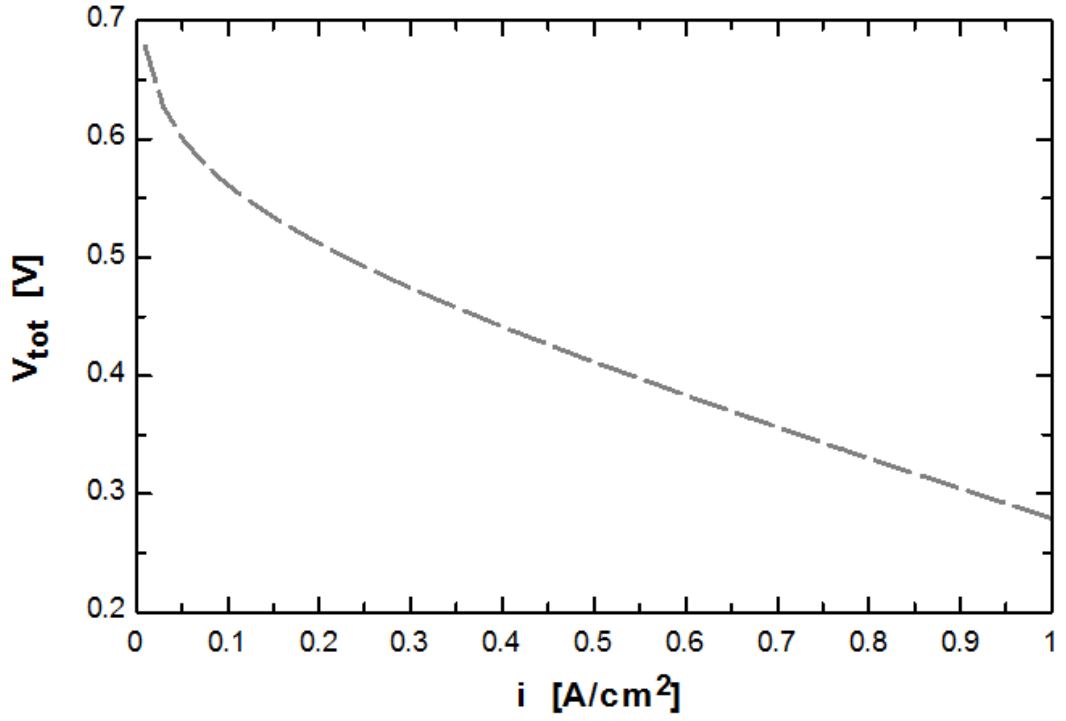

Fig. 4.3 Total voltage of PEMFC unit.

The variation of the system's energy and exergy efficiencies with the current density at constant operating conditions (3 atm, 353 K, and membrane thickness of 0.016 cm) is shown in Fig. 4.4. The maximum system energy and exergy efficiencies obtained are 63.62% and 57.88%, respectively at a current density of 0.01 A/cm^2. As seen from the figure, both energy and exergy efficiencies decrease with the increase in the current density which is due to the increase in the molar consumption of the fuel.

Fig. 4.5 shows how the rate of heat generation of the PEMFC varies with the current density. For current densities ranging from 0.0 to 2.0 A/cm^2, the rate of heat generation ranges from 0.26 to 68.8 kW. It increases linearly with increasing the current density as it is a function of the mass flow rate of the reactants and products which are directly proportional to the current density.

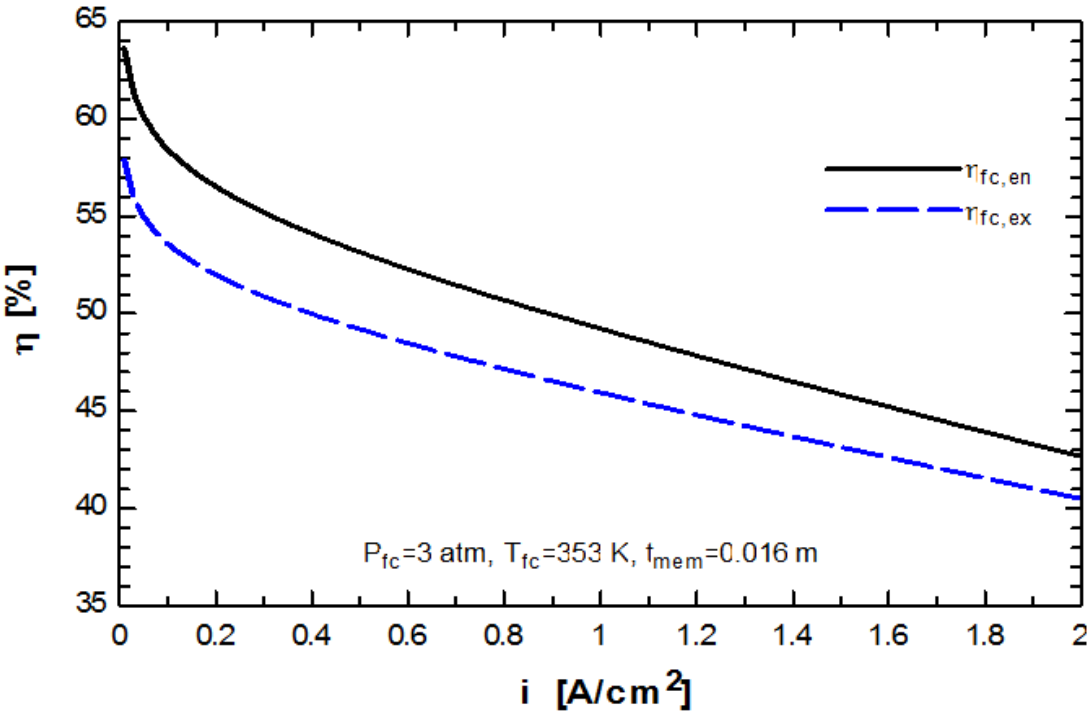

Fig. 4.4 Variation of energy and exergy efficiencies of the PEMFC unit with current density at constant operating conditions.

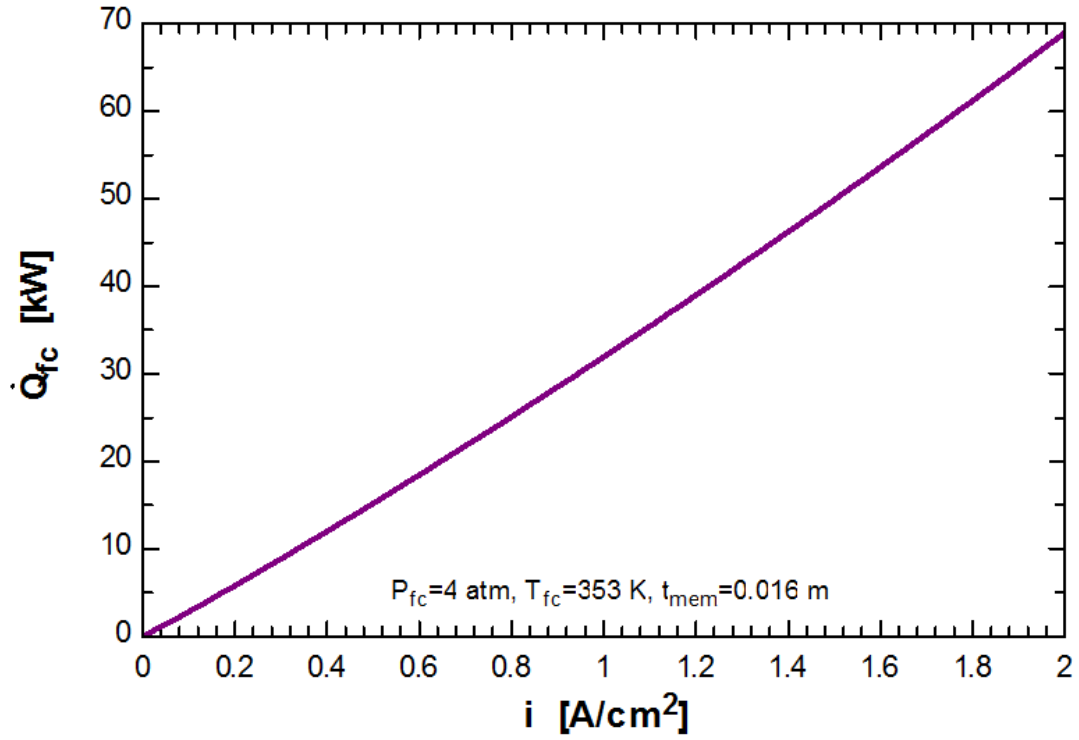

Fig. 4.5 Rate of heat generation of PEMFC at the operating conditions.

Fig. 4.6 shows the calculated energetic efficiency and power output at different current density values and constant temperature and pressure. It can be noticed that the energetic efficiency decreases while the power output of the PEMFC increases with increasing the current density. This is due to the fact that the power depends mainly on the available current in the cell. For the current density ranging from 0.0 to 2.0 A/cm^2, the energetic efficiency decreases from 63.6 to 42.6% and the power output increases from 0.1 to 9.1 kW.

Besides, increasing the membrane thickness results in decreasing the energetic efficiency as well as the net power production. As the membrane thickness increases, the ohmic overpotential increases causing the irreversible voltage to be increased which results in decreasing the total voltage of the system, the power output, and the energetic efficiency of the PEMFC unit accordingly. For example, for membrane thickness of 0.016, 0.018, and 0.02 cm at a current density of 1.0 A/cm^2, the power output is 6.9, 6.7, and 6.5 kW, respectively.

The effect of variation in the current density on the exergetic efficiency and thermodynamic irreversibility of the PEMFC is shown in Fig. 4.7 for different membrane thicknesses at constant cell pressure and temperature. As the current density increases, the exergetic efficiency decreases while the irreversibility increases at constant cell pressure and temperature for a certain membrane thickness. Increasing the current density results in increasing the mass flow rate of the reactants and products leading to an increase in the exergy associated with mass, heat, and work which in turn causes the irreversibly to be increased and the exergetic efficiency to be decreased.

Also, it is observed that increasing membrane thickness results in increasing the PEMFC's irreversibility while decreasing its exergetic efficiency since increasing the membrane thickness results in decreasing the exergy transfer by work which contributes negatively to the system's irreversibility. For example, at 3 atm, 333 K, and 1.0 A/cm^2 and for membrane thicknesses of 0.016, 0.018 and 0.02 cm, the exergetic efficiency is 43.11, 42.33, and 41.84% and the irreversibility is 3.77, 3.79 and 3.82 kW, respectively. So, low membrane thickness and low current density result in high PEMFC efficiency.

The energetic and exergetic COP of the integrated system versus the current density is shown in Fig. 4.8. Both energetic and exergetic COPs are decreasing with increasing the current density. Increasing the current density causes the mass flow rate of the reactants and products as well as the power produced by the PEMFC to be increased leading to an increase in the useful heat generated by the PEMFC throughout the cell operation. This results in a decrease in the energetic and exergetic COPs of the integrated system for a certain cooling capacity. The highest energetic and exergetic COPs are obtained at 0.5 A/cm^2 with values of 2.7 and 2.3, respectively and the lowest values are 0.67 and 0.35 obtained at a current density of 2.0 A/cm^2.

From Fig. 4.9, it can be observed how the energetic and exergetic efficiencies of the integrated system are decreasing with increasing the current density. The inverse relationship is attributed to the mass flow rate of the input hydrogen which is directly proportional to the current density and inversely proportional to the overall energetic and exergetic efficiencies of the integrated system. As the current density ranges from 0.5 to 2.0 A/cm^2, the energetic efficiency ranges from 63.41 to 45.9% and the exergetic efficiency ranges from 53.6 to 37.2%.

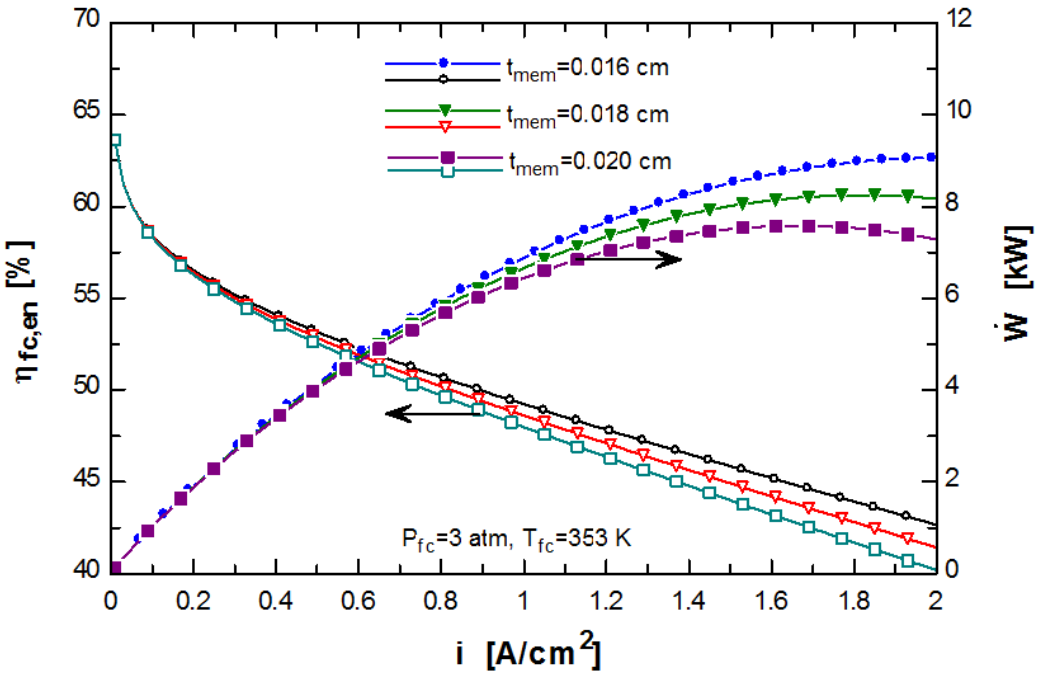

Fig. 4.6 Variation of energy efficiency and power output of the PEMFC unit with current density for different membrane thicknesses.

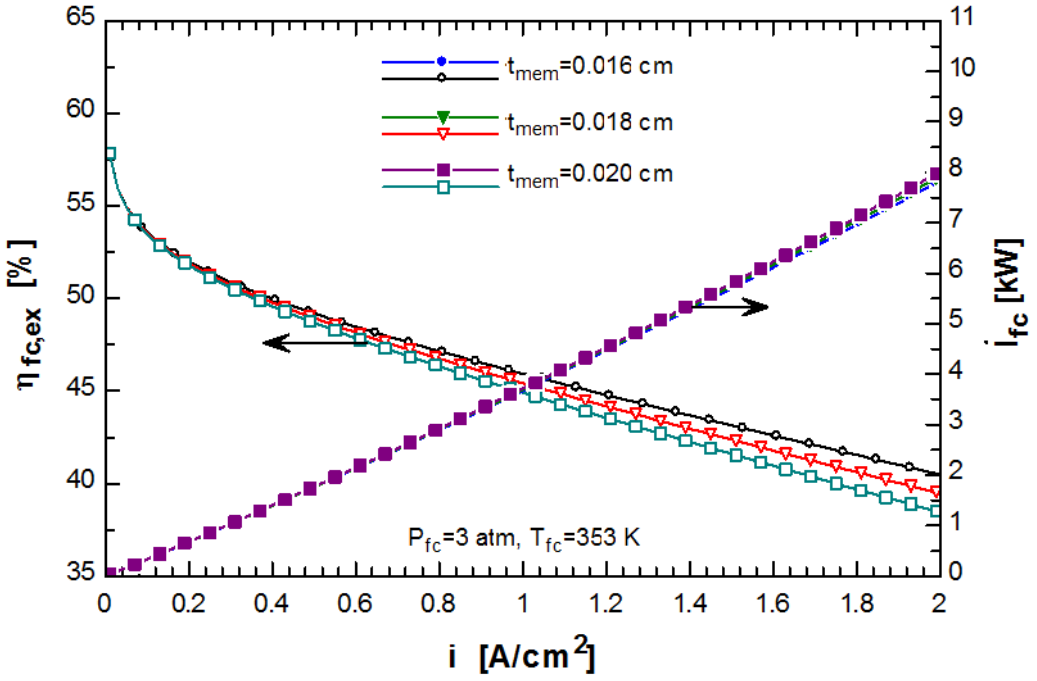

Fig. 4.7 Variation of exergy efficiency and thermodynamic irreversibility of PEMFC unit versus current density for different membrane thicknesses.

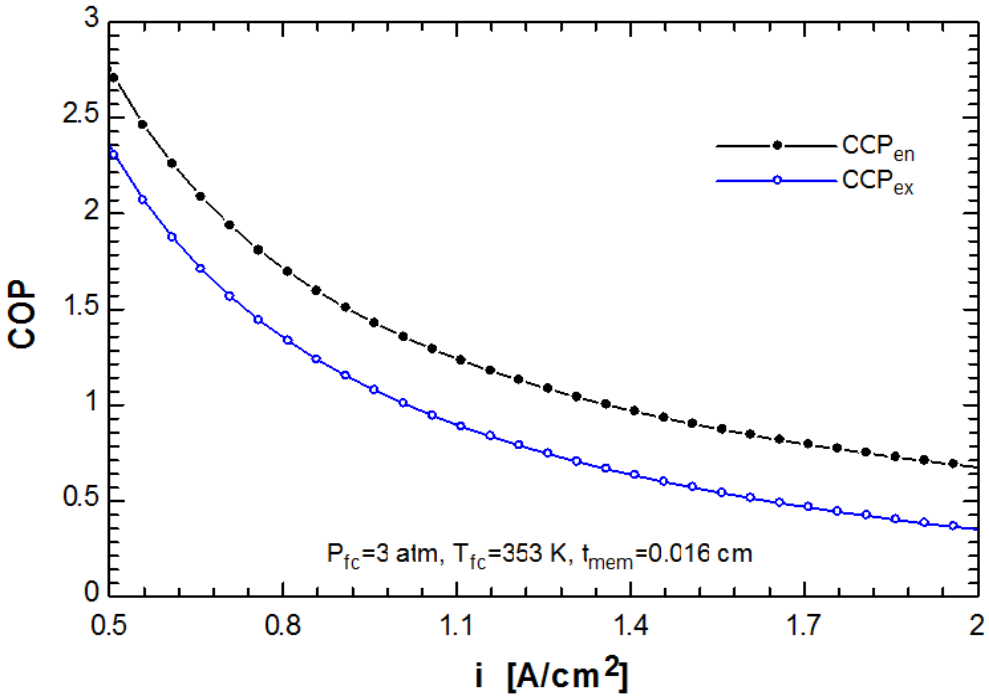

Fig. 4.8 Energetic and exergetic COP of the integrated PEMFC-based HVAC system versus current density.

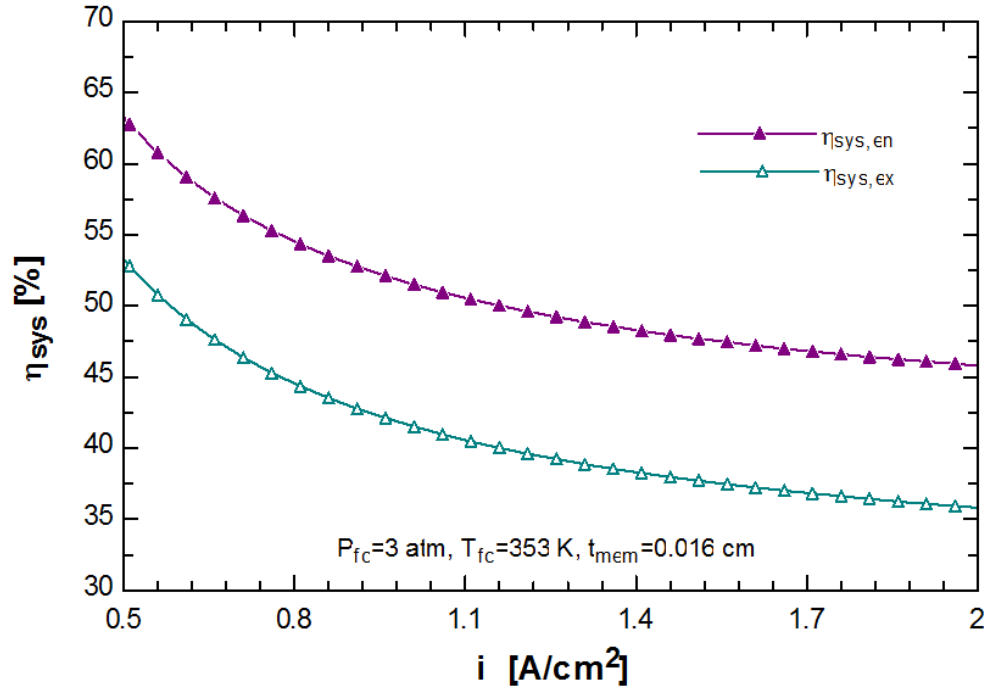

Fig. 4.9 Energetic and exergetic efficiencies of the integrated PEMFC-based HVAC system for constant pressure, temperature, and membrane thickness.

Fig. 4.10 shows the variation of the energy efficiency and power output of the PEMFC with the operating temperature of the fuel cell for different membrane thickness values at constant cell pressure (3 atm) and current density (1.0 A/cm^2). As the temperature increases, the energy efficiency is increased while increasing the membrane thickness causes the efficiency to be decreased. For example, for a membrane thickness of 0.018 cm, the energy efficiency is found to be 39% and 49% at a cell operating temperature of 300 and 360 K, respectively. This is due to the fact that mass transport limitations are reduced at higher temperatures. Also, increasing the operating temperature of the PEMFC from 300 to 360 K causes the power output to be increased from 3.5 to 7 kW, respectively, as increasing the operating temperature results in decreasing the ohmic resistance of the electrolyte and accelerates the kinetics of the electrode reactions.

So, the operating temperature of the PEMFC has a significant influence on its performance. This leads to the conclusion that the cell performance can be improved through increasing the operating temperature and decreasing the membrane thickness. However, this is limited by the vapor pressure of water in the ion exchange membrane due to the membrane's susceptibility to dehydration and the subsequent loss of ionic conductivity.

The effect of variation in the operating temperature on exergy efficiency and thermodynamic irreversibility of the PEMFC is shown in Fig. 4.11 for different membrane thicknesses at constant cell pressure (3 atm) and constant current density (1.0 A/cm^2). As the operating temperature increases, the exergy efficiency increases while the irreversibility decreases at constant cell pressure and current density for a certain membrane thickness. The reason is that increasing the operating temperature causes the total voltage and the power output to be increased resulting in decreasing the irreversibility and increasing the exergy efficiency. For operating temperature ranges between 300 and360 K, the PEMFC irreversibility decreases from 3.94 to 3.64 kW and the exergetic efficiency increases from 40 to 47%.

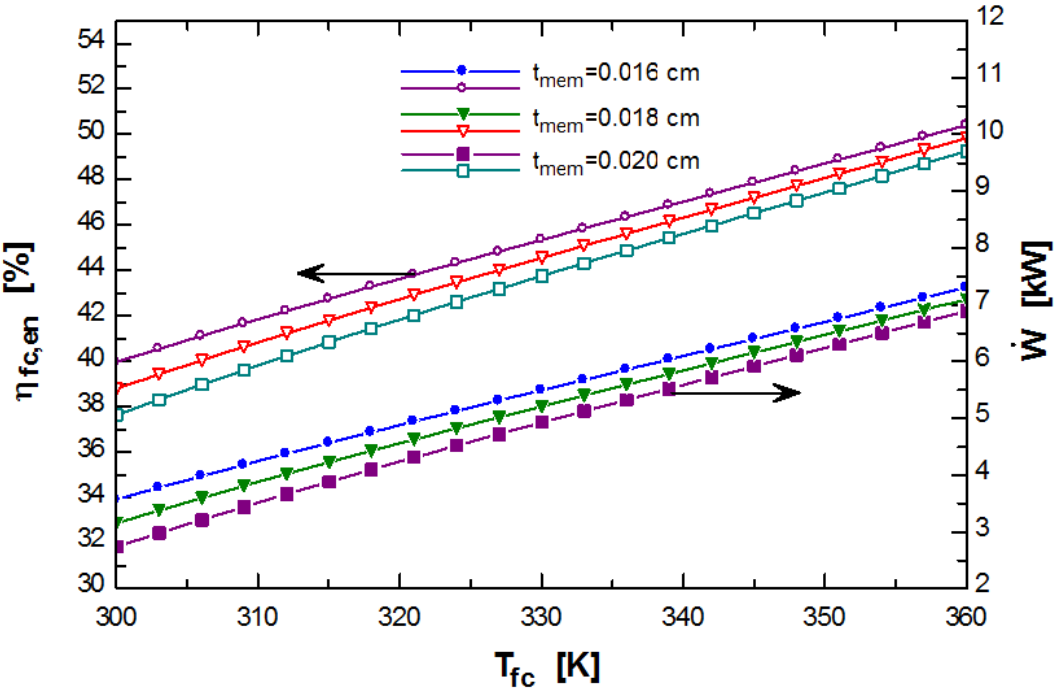

Fig. 4.10 Variation of energy efficiency and power output of PEMFC versus fuel cell temperature at constant cell pressure (3 atm) and constant current density (1.0 A/cm^2) for different membrane thicknesses.

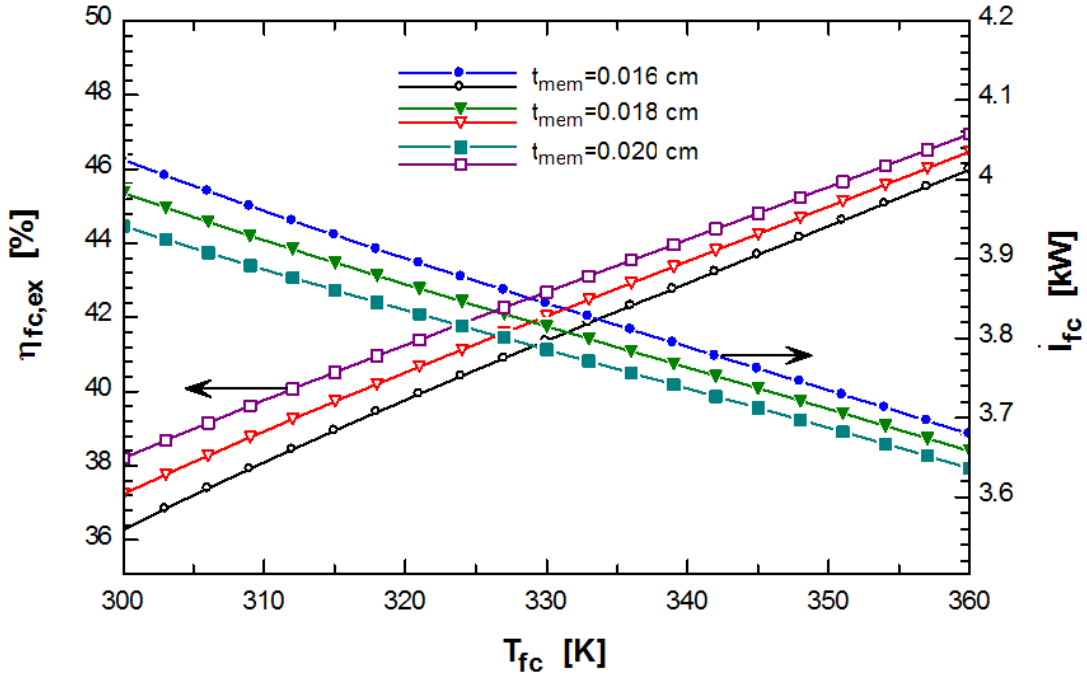

Fig. 4.11 Effect of variation in operating temperature on exergy efficiency and thermodynamic irreversibility of the PEMFC unit at constant cell pressure (3 atm) and constant current density (1.0 A/cm^2) for different membrane thicknesses.

Fig. 4.12 presents the effect of variation in operating temperature on energetic and exergetic COP of the integrated system at constant cell pressure and constant membrane thickness. As the operating temperature of the PEMFC increases, both COPs decrease. This is due to the fact that increasing the operating temperature causes the total voltage of the PEMFC to be increased leading to an increase in the power produced by the cell and hence the amount of energy needed to power the absorption system, causing the COP to be decreased. However, for fuel cell temperatures ranging from 300 to 360 K, the rate of decrease is small in comparison to the rate of increase in the temperature.

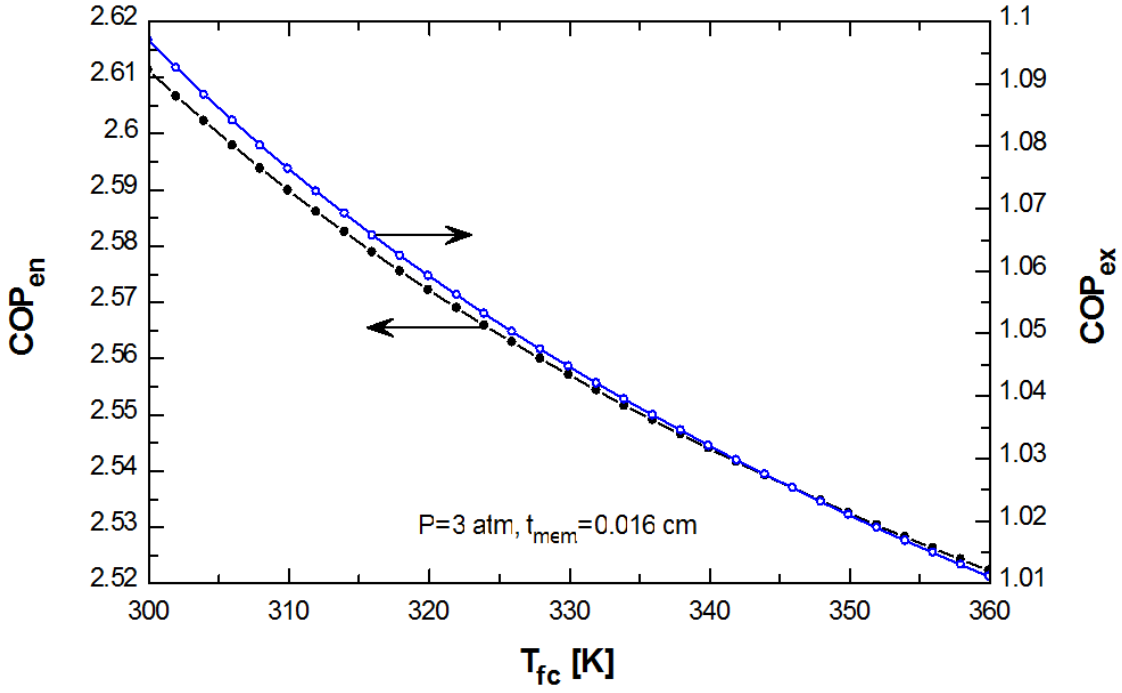

Fig. 4.12 Effect of variation in operating temperature on energy and exergy COP of the integrated PEMFC based HVAC system at constant cell pressure and membrane thickness.

4.2 FPSC-Based HVAC-Cooling System

In this section, the results of energy and exergy modeling of the HVAC cooling system using flat plate solar collectors are presented and discussed. The effect of solar irradiance, ambient temperature, mass flow rate of inlet fluid, and solar collector area is examined.

Fig. 4.13 and Fig. 4.14 provide meteorological data for UAE that is used to conduct the analysis of the FPSC-based HVAC cooling system. The data covers the solar irradiance and the water inlet temperatures. The water inlet temperature is higher than the ambient temperature by 5 °C. These data are used to examine the effect of different operating conditions of FPSC on the performance of the integrated system on a monthly basis. Also, the comparison of the FPSC model with the present models in the literature is shown in Fig. 4.15. The figure represents the variation of the FPSC efficiency with respect to the parameter $\Delta T/I$. The deviation in the present model as compared to the model developed by Rojas et al. [105] is attributed to the difference in the assumptions made for heat transfer loss coefficients.

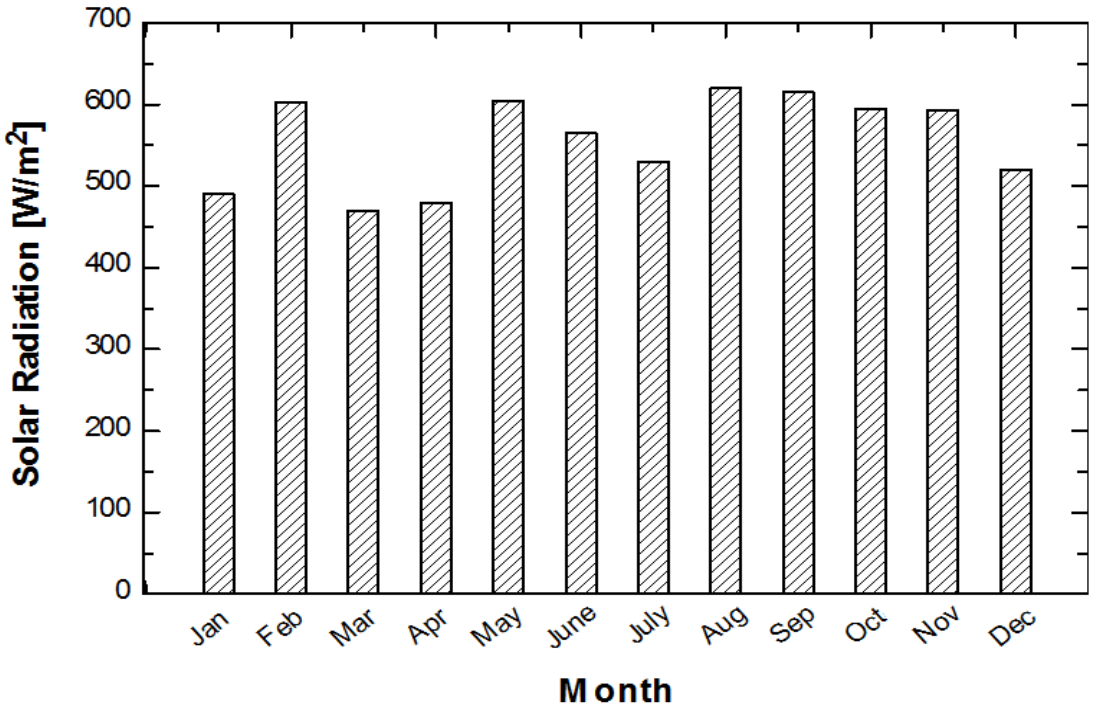

Fig. 4.13 Monthly average solar irradiance of the UAE.

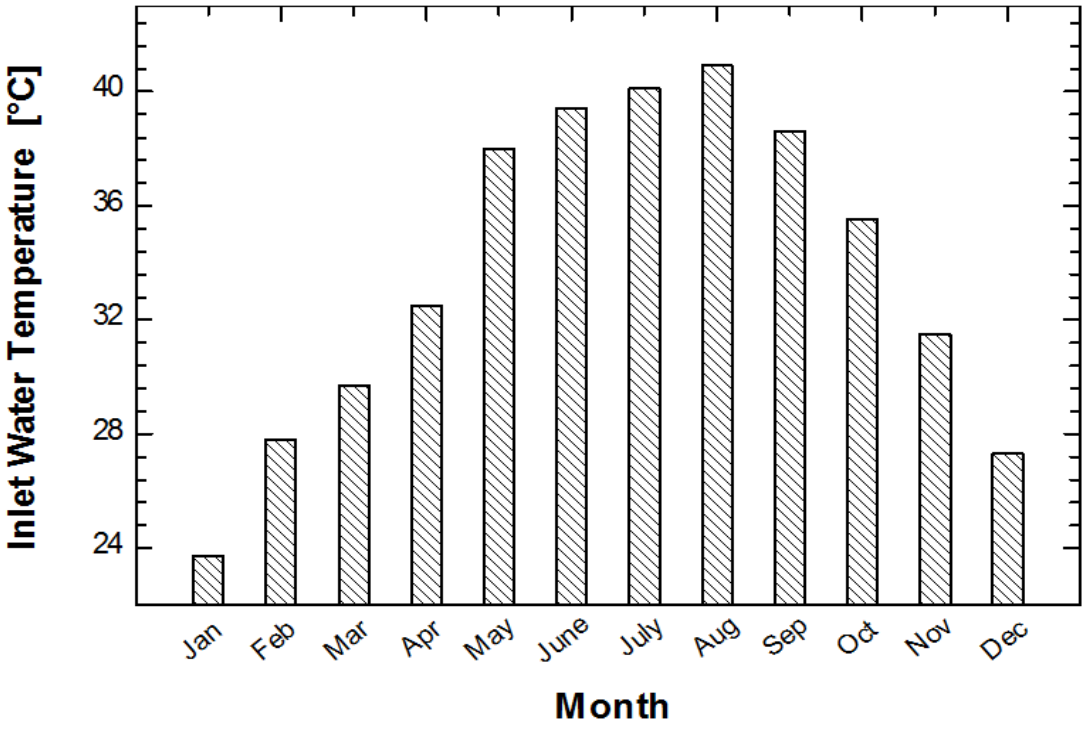

Fig. 4.14 Monthly average inlet water temperature of the UAE.

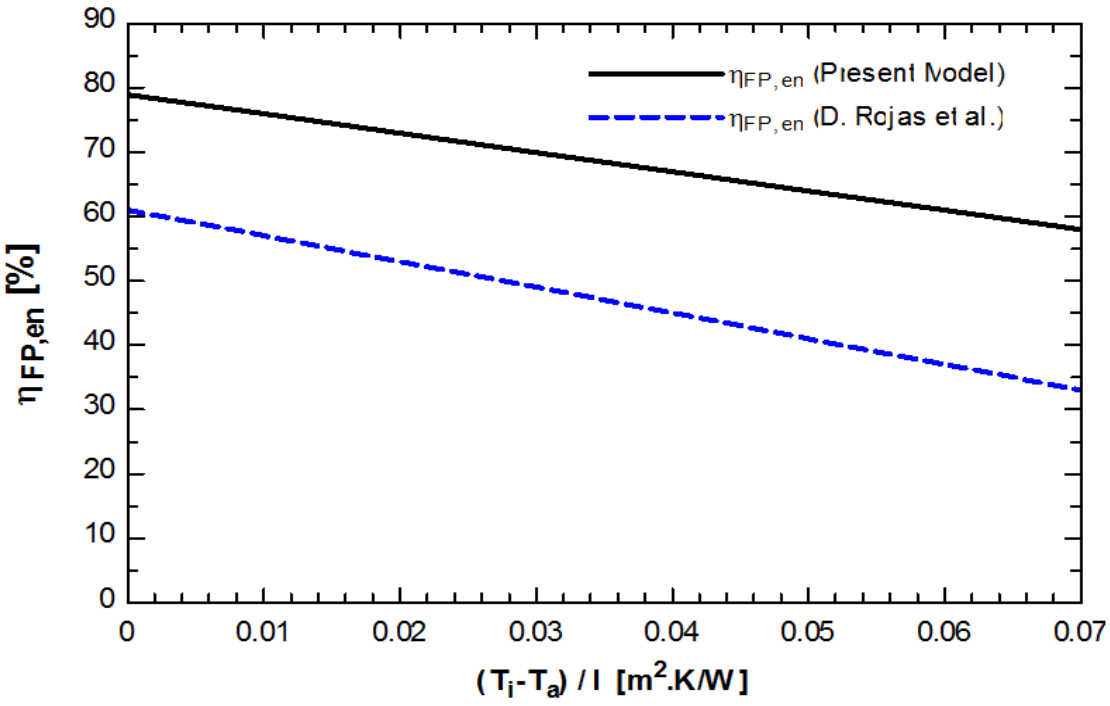

Fig. 4.15 Comparison of the current FPSC model with the model presented by Rojas et al.[105].

Monthly variation of the rate of heat generated by the FPSC is shown in Fig. 4.16 for constant mass flow rate of water. It is observed that the highest rate of heat generation occurs in August followed by September. This is due to the high solar irradiance available in these two months so that higher irradiance is absorbed by the heat transfer fluid flowing in the absorber plate. Also, increasing the ambient temperature causes the rate of heat generated to be increased as the difference between the ambient and the inlet water temperatures is decreased resulting in decreasing the heat losses from the surface to the surroundings.

As a result, the thermal efficiency of the FPSC is increased with increasing the solar irradiance absorbed by the absorber plate and with increasing the inlet water temperature as the efficiency is inversely proportional to the irradiance and directly proportional to the difference between the ambient and inlet water temperatures. In other words, as the thermal efficiency is the ratio of the useful energy gain from the FPSC to the energy incident on the collector surface. Increasing the solar irradiance causes the useful heat generated to be increased so that the efficiency is increased although it is inversely proportional to the irradiance as the increase in the heat gain is higher than that of the solar irradiance falls on the FPSC from month to month. Regarding the exergetic efficiency of the FPSC, it is noted that the exergetic efficiency is low compared with the energetic efficiency as in all solar systems. The figure shows how the increase in the inlet water temperature causes the exergetic efficiency to be decreased. This decrease is attributed to the fact that the exergetic efficiency is the ratio of the useful exergy to the exergy of the solar radiation absorbed by the FPSC which are both functions of the inlet water temperature in addition to the fact that the temperature difference between the sun and the fluid temperature in the collectors is large. This is shown in Fig. 4.17.

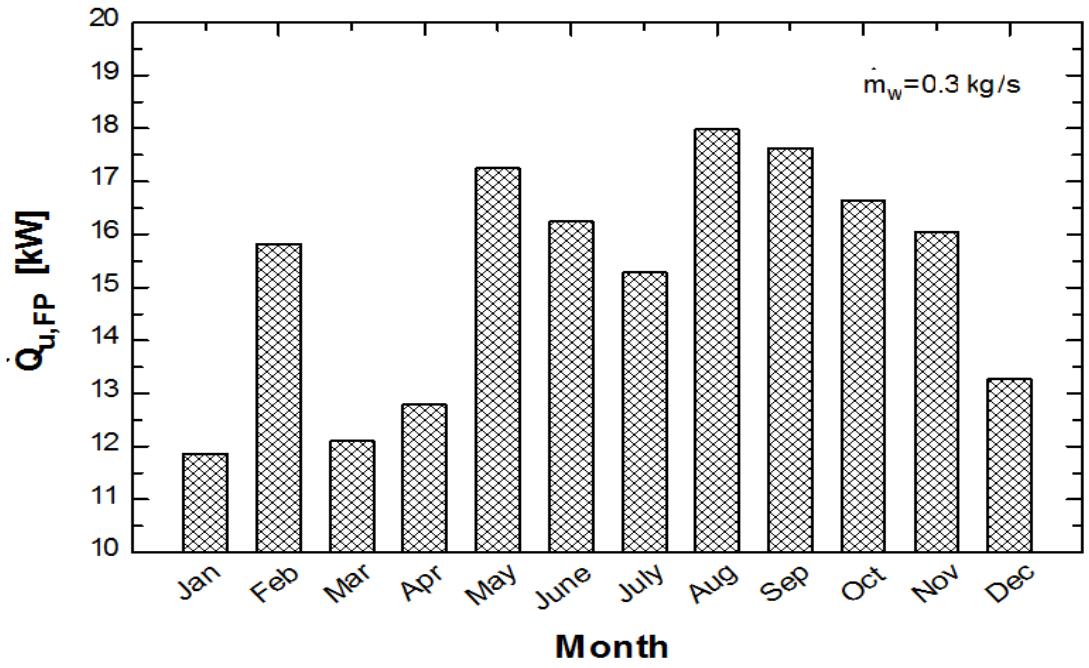

Fig. 4.16 Monthly rate of heat generated by the FPSC.

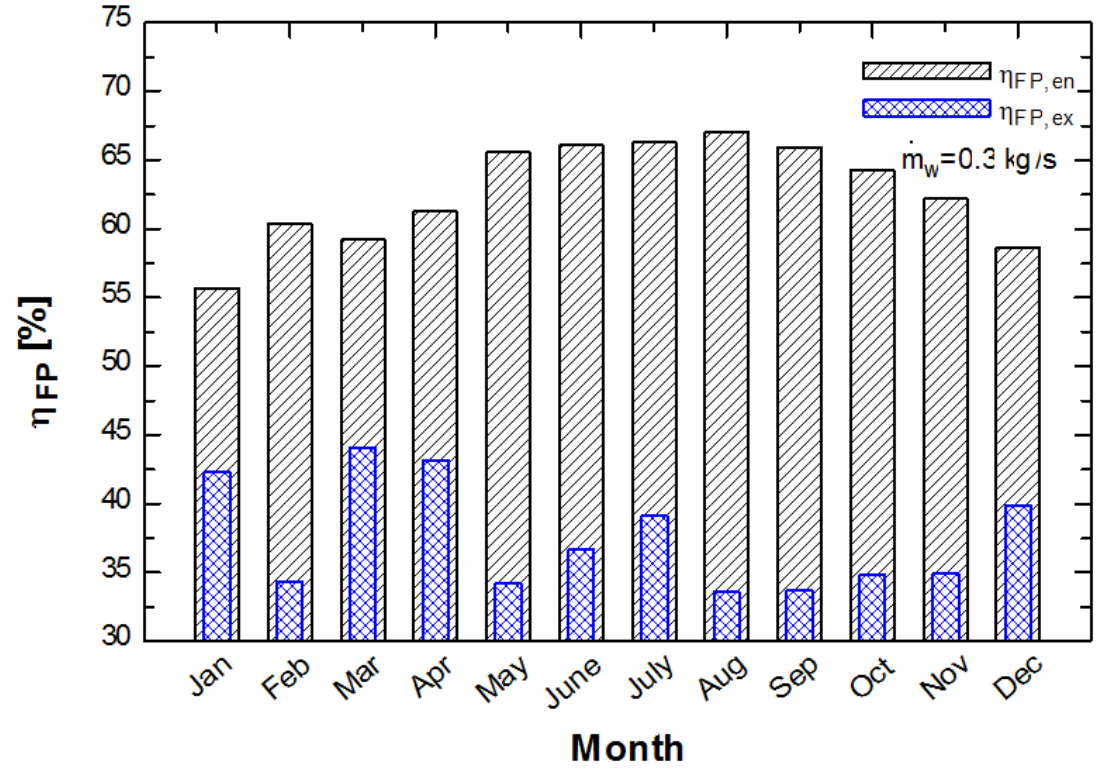

Fig. 4.17 Monthly energetic and exergetic efficiencies of the FPSC unit.

The effect of variation in the mass flow rate of the inlet water on the rate of useful heat gain by the FPSC for constant collector area for the month of August is shown in Fig. 4.18. The range of mass flow rate has been taken from 0.01 to 1.6 kg/s with an interval of 0.05 kg/s. It is noted that the rate of heat generated increases more rapidly in the range from 0.01 to 0.2 kg/s of the mass flow rate. For example, the rate of heat generated at 0.01 kg/s is 17.61 kW and at 0.2 kg/s it is found to be 17.91 kW for a difference of 0.3 kW for the rate of heat generated and 0.2 kg/s for the mass flow rate. Similarly, the rate of heat generated at 0.4 kg/s is 18.01 kW, which accounts for a difference of 0.1 kW. At 1 kg/s, the rate of heat generated is 18.18 kW results in an increase of 0.17 kW that is only a 0.94% increase in the rate of heat generated for a 0.6 kg/s increase in the mass flow rate of the inlet water (60%). So one can conclude that increasing the mass flow rate of the inlet water has a insignificant effect on the rate of heat generated such that it is not worthwhile to increase the mass flow rate by 60% for the purpose of increasing the rate of heat generated by 0.94%. This effect is shown in Fig. 4.18.

Fig. 4.19 shows the effect of increasing the mass flow rate of the inlet water on the rate of heat generated by the FPSC for different collector areas. The increase in the rate of heat generated by the FPSC when the collector area is increased is due to the increase in the amount of solar irradiance absorbed by the collector. For 0.5 and 1 m^2 of collector area, it is noted that doubling the area causes the rate of heat generated to be increased by 16 to 19%. However, this affects the cost of the solar system so that one should account for both the performance and the cost of system in the selection of the optimum design to provide the required heat while keeping the cost of the system within acceptable ranges.

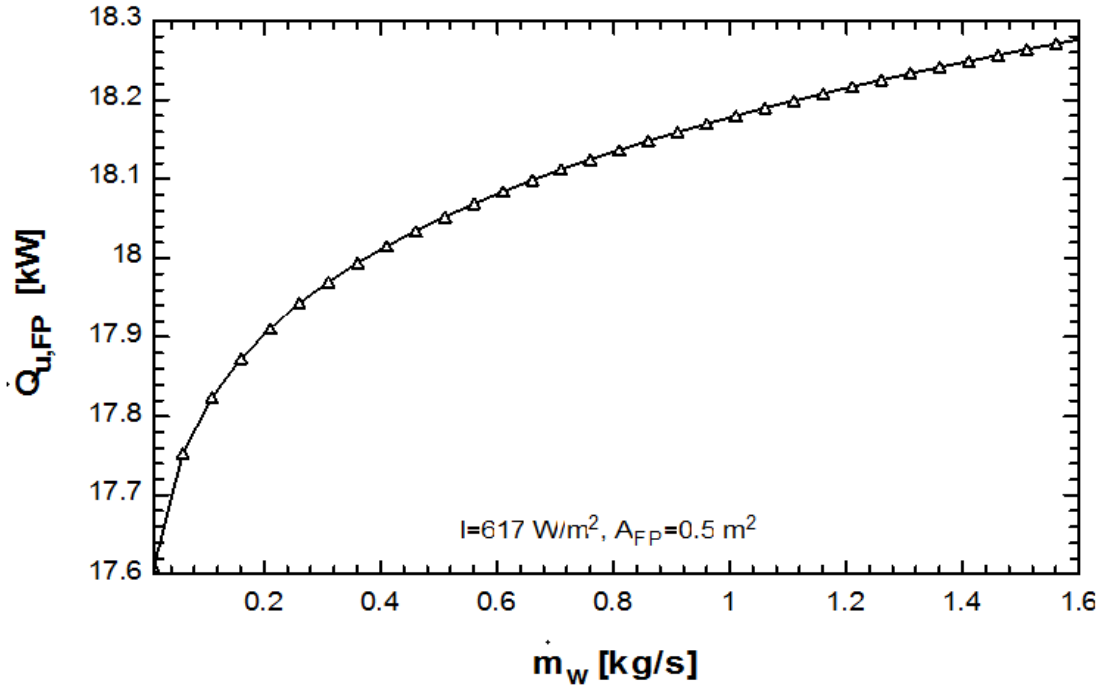

Fig. 4.18 The effect of increasing the mass flow rate of the inlet water on the rate of heat gain by the FPSC for constant collector area for the month of August.

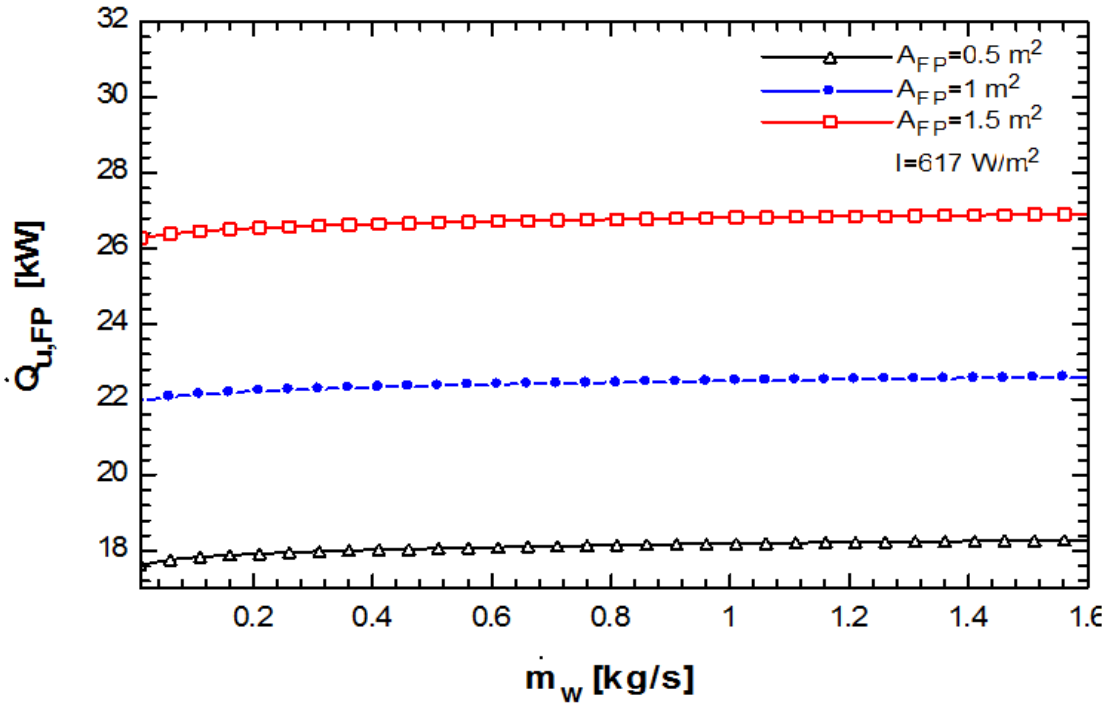

Fig. 4.19 The effect of increasing the mass flow rate of the inlet water on the rate of heat gain by the FPSC for different collector areas.

Fig. 4.20 presents the energetic efficiency versus the mass flow rate of the inlet fluid at a constant collector area for the month of August. An aspect that is highlighted from Fig. 4.20 is that increasing the flow rate causes the energetic efficiency to be increased. At 0.01 kg/s, the energetic efficiency is 65.61% and at 0.21 kg/s it is 66.73% for an increase of 1.68. At 0.4 kg/s, the energetic efficiency is 67.12% accounting for a 0.58 increase. At 1 kg/s, the energetic efficiency is 67.73% resulting in an increase of 1.48 for a 0.8 kg/s increase in the mass flow rate. As is the case in the rate of heat generated by the FPSC, increasing the mass flow rate of the inlet fluid at higher rates does not have significant influence on the thermal efficiency of the solar system.

The effect of increasing the mass flow rate of the inlet water on the energetic efficiency for different collector areas for the month of August is shown in Fig. 4.21. It is noted that increasing the collector area from 0.5 to 1 m^2 results in decreasing the energetic efficiency by 3.68% and from 1 to 1.5m^2 results in a 2.57% decrease for a mass flow rate of 0.01 kg/s. The decrease in the energetic efficiency is 3.12% when the collector area is increased from 0.5 to 1m^2 and 2.18% when it is increased form 1 to 1.5 m^2 for 0.6 kg/s of mass flow rate. So, increasing the collector area has a negative effect on the thermal efficiency of the solar collector unit. This decrease in the energetic efficiency is attributed to the decrease in the ratio of the rate of heat generated by the collector to the solar irradiance incident on the increased area.

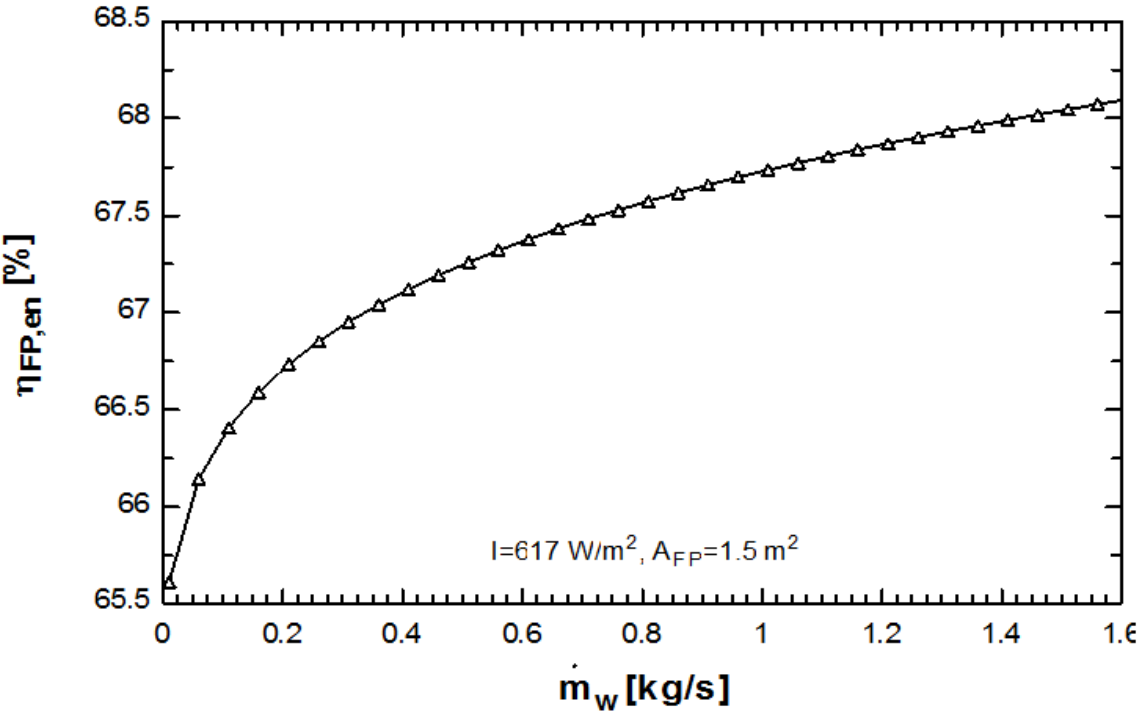

Fig. 4.20 The effect of increasing the mass flow rate of the inlet water on the energetic efficiency of the FPSC unit for a constant collector area for the month of August.

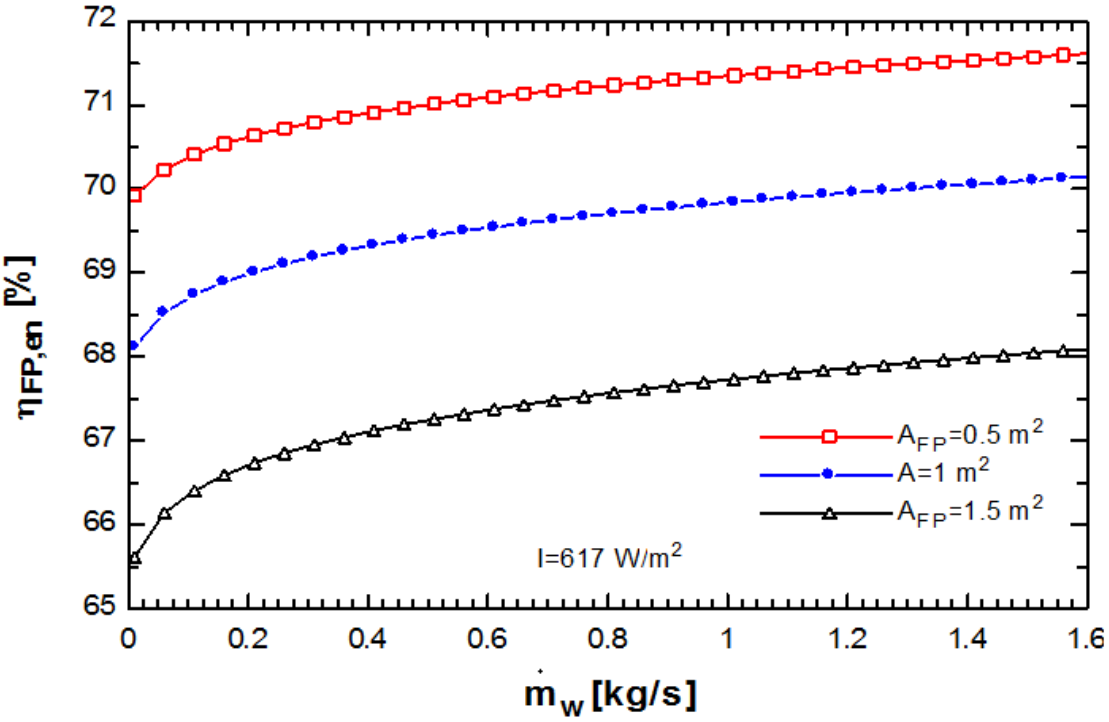

Fig. 4.21 The effect of increasing the mass flow rate of the inlet water on the energetic efficiency of the FPSC unit for different collector areas for the month of August.

Energetic and exergetic COPs of the FPSC integrated with a 10 kW DEAS system for a constant mass flow rate of water and collector area is shown in Fig. 4.22. Both energetic and exergetic COPs are decreasing with increasing the solar irradiance and the inlet water temperature. As the solar irradiance increases, the rate of heat generated by the FPSC is increased due to the higher amount of irradiance absorbed by the absorber plate of the FPSC so that the useful heat fed to the HTG is higher causing the energetic COP to be decreased for constant cooling capacity. The exergetic COP also decreased because of the high exergy of the solar radiation absorbed by the FPSC when the solar irradiance is increased. This is because the exergetic COP is inversely proportional to the exergy of the solar radiation absorbed by the FPSC.

For the month of August where the highest solar irradiance occurs, the energetic COP is at its minimum. In contrast, it is maximum in the month of March when the minimum amount of solar irradiance is collected by the FPSC. The energetic and exergetic COPs obtained in August are 1.417 and 1.366, respectively, while they are 1.878 and 1.809 in March for a mass flow rate of inlet water of 0.3 kg/s and collector area of 1 m^2 producing a cooling capacity of 10 kW.

Fig. 4.23 shows the overall monthly energetic and exergetic efficiencies of the FPCS-based HVAC cooling integrated system for a constant mass flow rate of water and constant collector area. As both energetic and exergetic overall efficiencies are inversely proportional to the solar irradiance for constant cooling capacity, they are decreased with increasing the solar irradiance as illustrated in the figure.

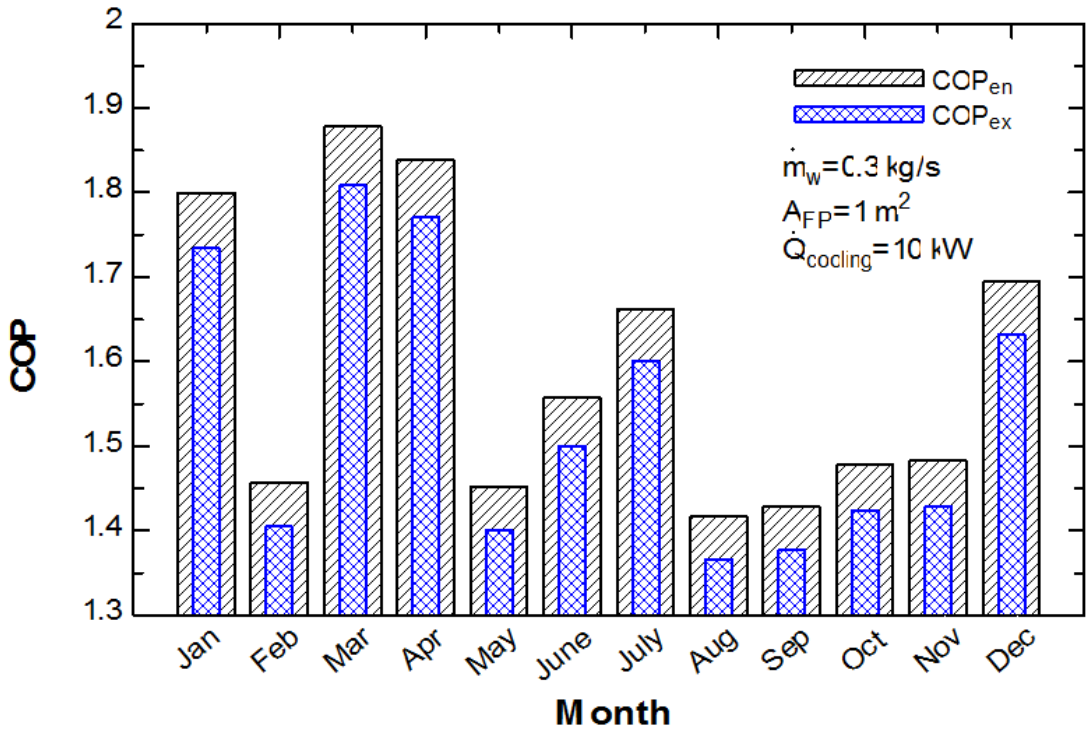

Fig. 4.22 Energy and exergy COPs of the FPSC integrated with a 10 kW DEAS system for a constant mass flow rate of water and collector area.

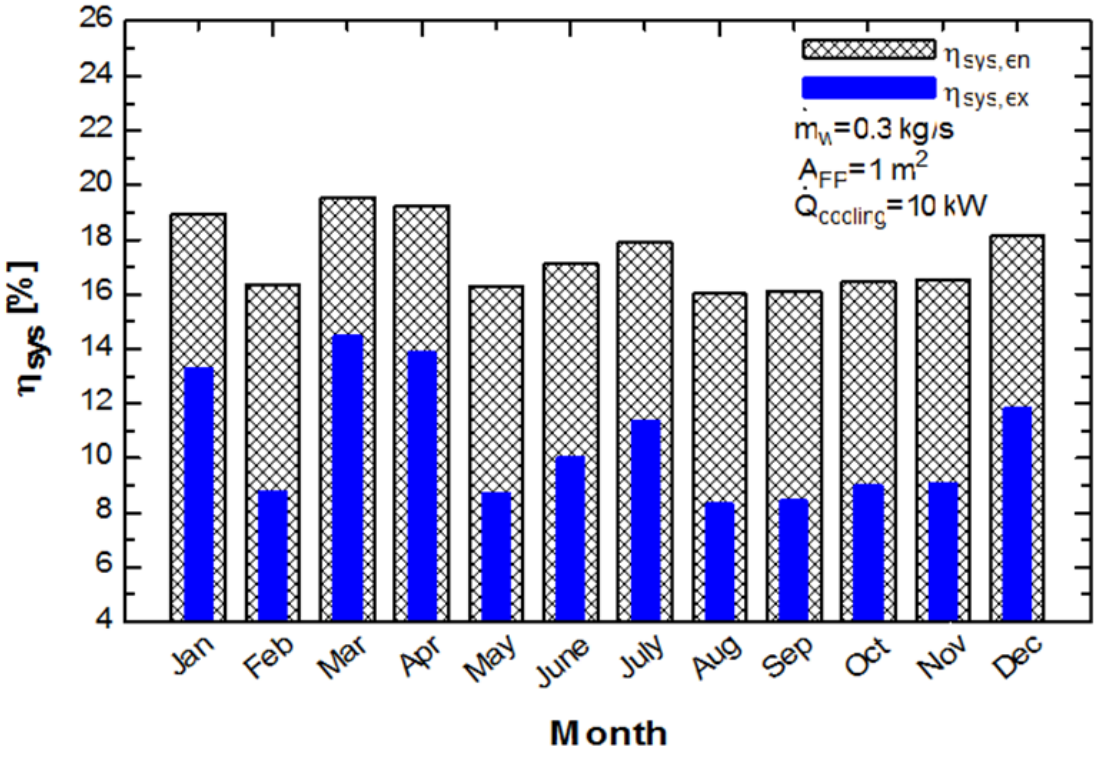

Fig. 4.23 Overall monthly energy and exergy efficiency of the FPSC integrated with a 10 kW DEAS system for a constant mass flow rate of water and collector area.

Fig. 4.24 represents the variation of energetic and exergetic COPs of the integrated system with the mass flow rate of inlet water at a constant collector area for the month of August. As the mass flow rate of the inlet water increases, both COPs decrease. This is because the rate of heat generated by the FPSC is increased with increasing the mass flow rate of water. However, the rate of increase is very small.

For example, at 0.01 kg/s, the energetic and exergetic COPs are 1.44 and 1.388, respectively. At 0.2 kg/s, the energetic COP is 1.426 while the exergetic COP is 1.375. This results in a decrease of 0.972% for the energetic COP and 0.936% for the exergetic COP. At 0.6 kg/s, the energetic and exergetic COPs are 1.418 and 1.367, respectively. This is represented in a decrease of 0.561% in the energetic COP and 0.581% in the exergetic COP for an increase in the mass flow rate of 0.4 kg/s. Again, the mass flow rate has insignificant improvement on the overall performance of the integrated system.

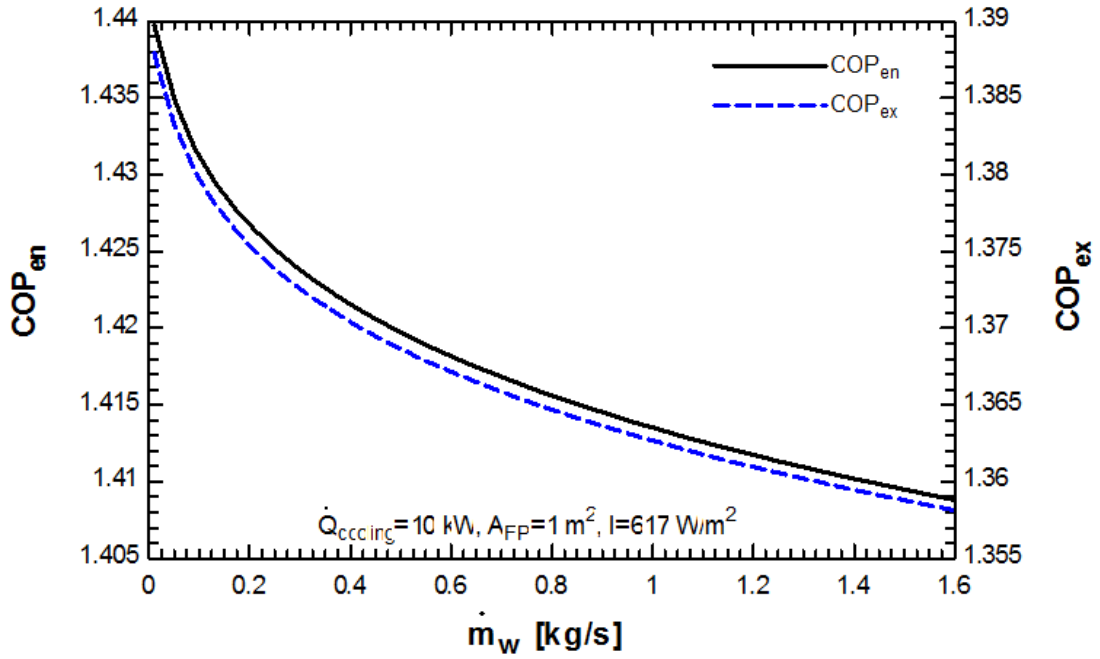

Fig. 4.24 Energy and exergy COPs of the integrated FPSC-based HVAC system for different mass flow rates of water and a constant collector area for the month of August.

4.3 PTSC-Based HVAC-Cooling System

Fig. 4.25 provides data on the solar irradiance available in the UAE on a monthly basis to be used in the analysis of a PTSC-based HVAC cooling system. In PTSCs, only a proportion of the solar irradiance is concentrated and absorbed by the receiver while the remaining is reflected to the surroundings (instantaneous irradiance).Fig. 4.26 shows the comparison of our PTSC model with that presented by Brooks et al. The figure represents the variation of the PTSC efficiency with respect to the parameter $\Delta T/I$. It is noted that there is a small deviation due to the difference in assumptions made in the calculation of the heat removal factor.

Fig. 4.27 shows the monthly heat generated from the PTSC unit for a constant mass flow rate of Therminol-66. It can be observed that the highest rate of heat generation occurs in August followed by September. This is due to the high solar irradiance available in those two months.

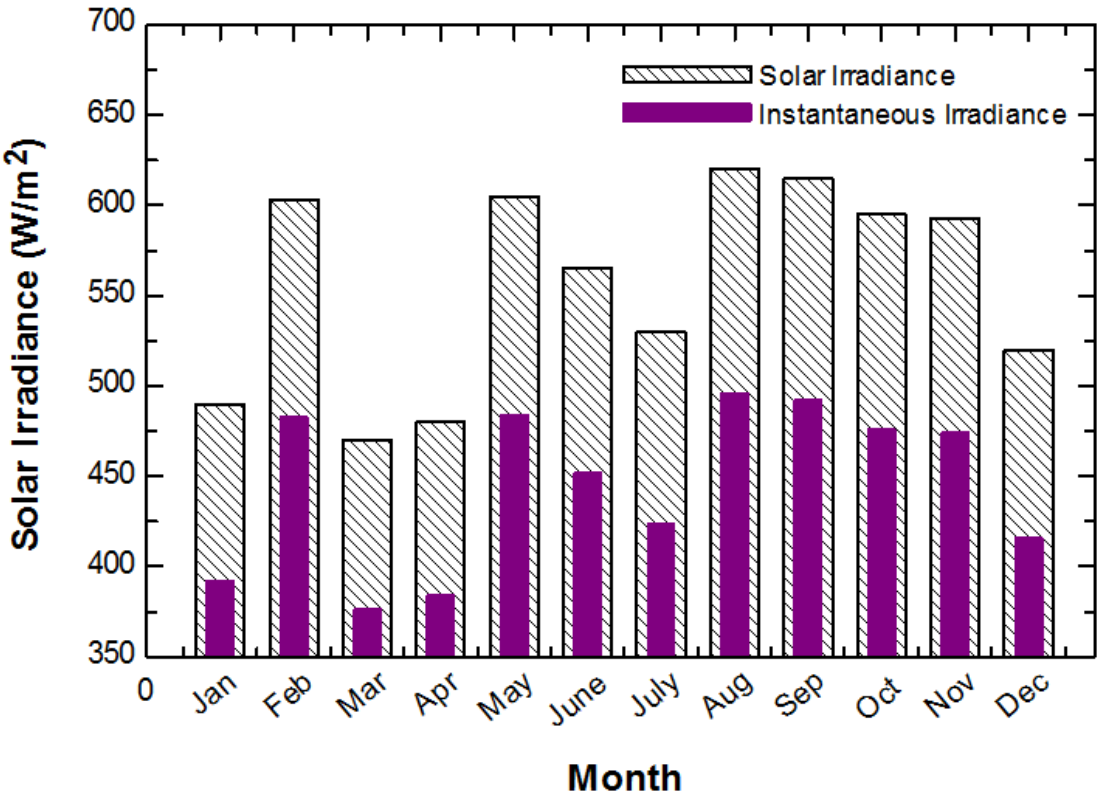

Fig. 4.25 Monthly average solar irradiance for UAE and instantaneous irradiance absorbed by the PTSC.

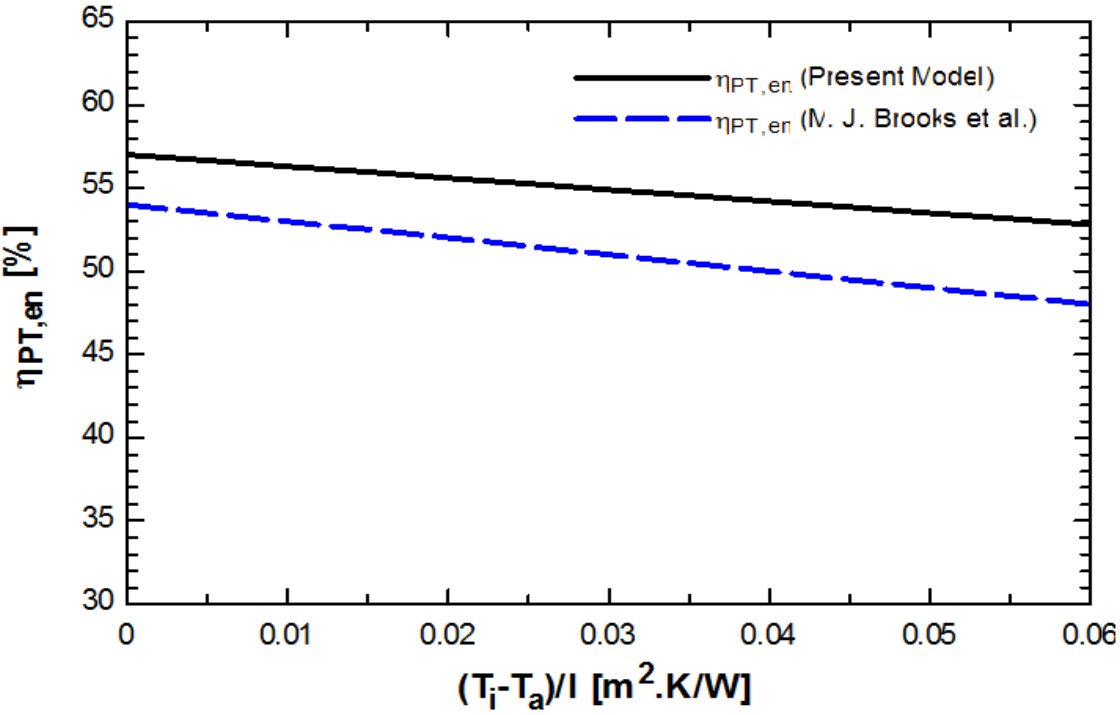

Fig. 4.26 Comparison of the current PTSC model with the model presented by Brooks et al.[115]

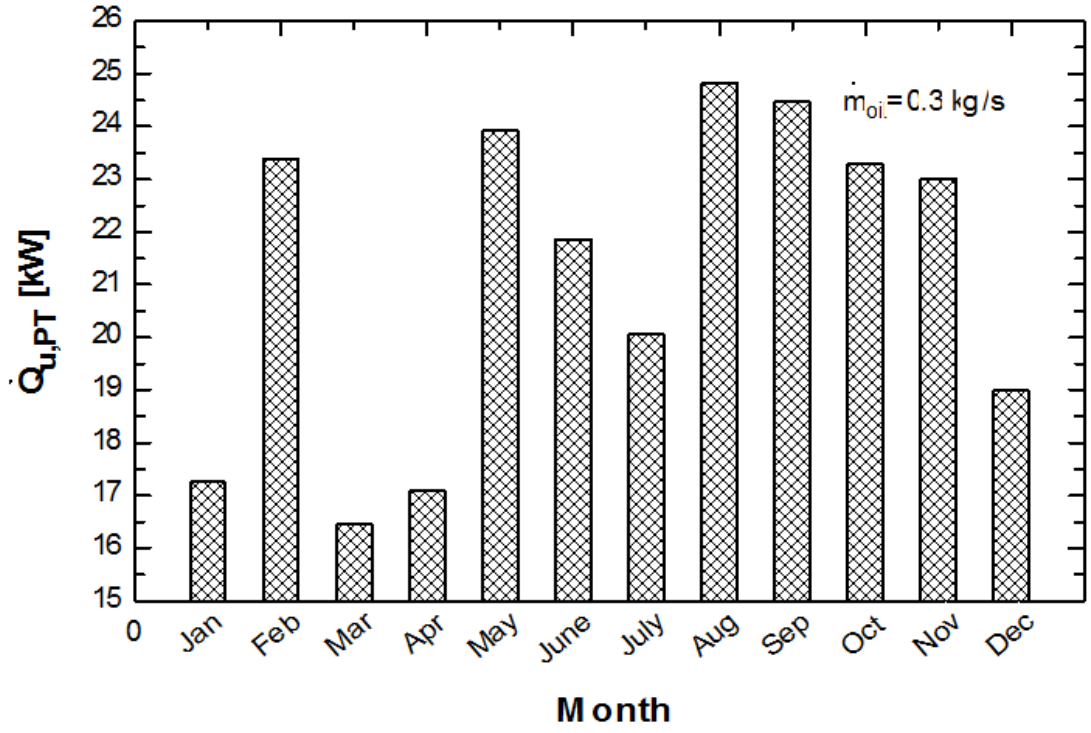

Fig. 4.27 Monthly heat generated by the PTSC unit.

Fig. 4.28 presents the energetic and exergetic efficiencies of the PTSC for every month. Again, due to the high irradiance available in August, this month has the highest energetic and exergetic efficiencies. Energetic and exergetic efficiencies are increased as the heat generated is increased.

Fig. 4.29 shows the rate of heat generated by the PTSC for different mass flow rates of Therminol-66 for the month of August at different concentration ratios. Heat generation rate is increased by increasing the mass flow rate of Therminol-66. Increasing the mass flow rate of the oil from 0.01 to 0.5 kg/s results in increasing the heat generated from 4.73 to 10.58 kW for a concentration ratio= 15. Increasing the concentration ratio has a positive effect on the heat generated. As the concentration ratio increases, the rate of heat generation by the PTSC is increased.

Fig. 4.30 presents energy and exergy efficiencies of PTSC for different mass flow rates of Therminol-66 for the month of August at different concentration ratios. Energy and exergy efficiencies are increased by increasing the mass flow rate of Therminol-66 at constant solar irradiance as the useful energy delivered by the PTSC is increased by supplying higher amounts of oil. Also, increasing the concentration ratio results in increasing both efficiencies. The increase is attributed to the increase in the concentrated area that allows more heat to be produced by the PTSC.

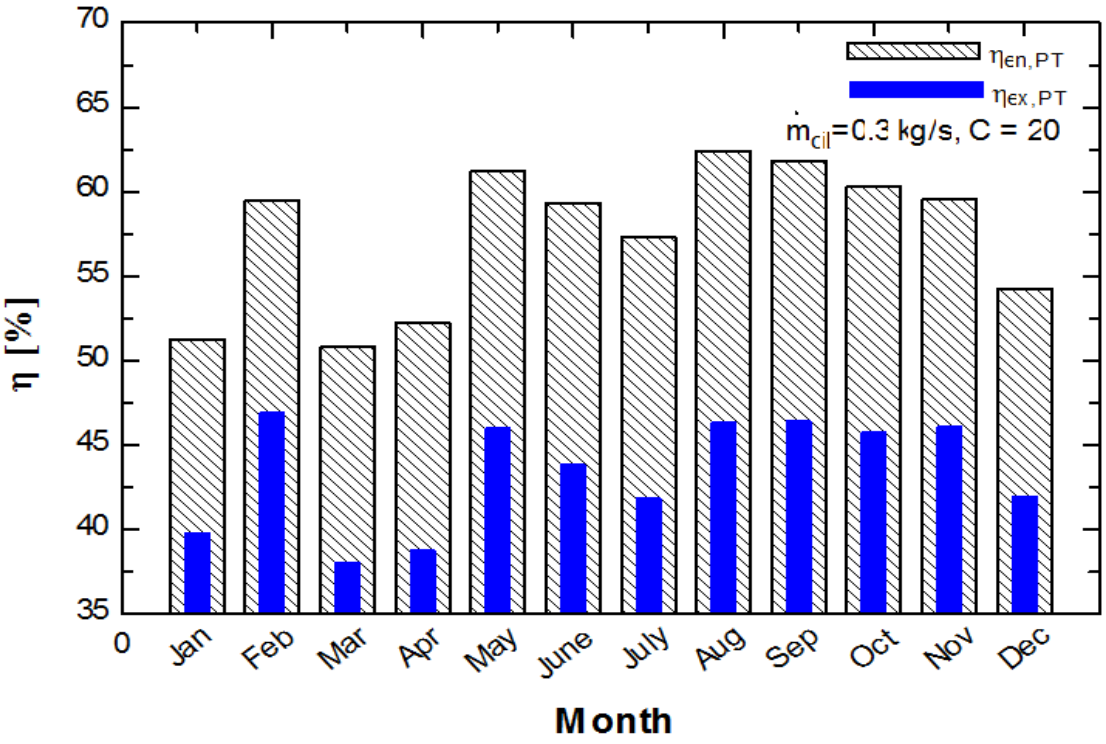

Fig. 4.28 Monthly energetic and exergetic efficiencies obtained by PTSC unit.

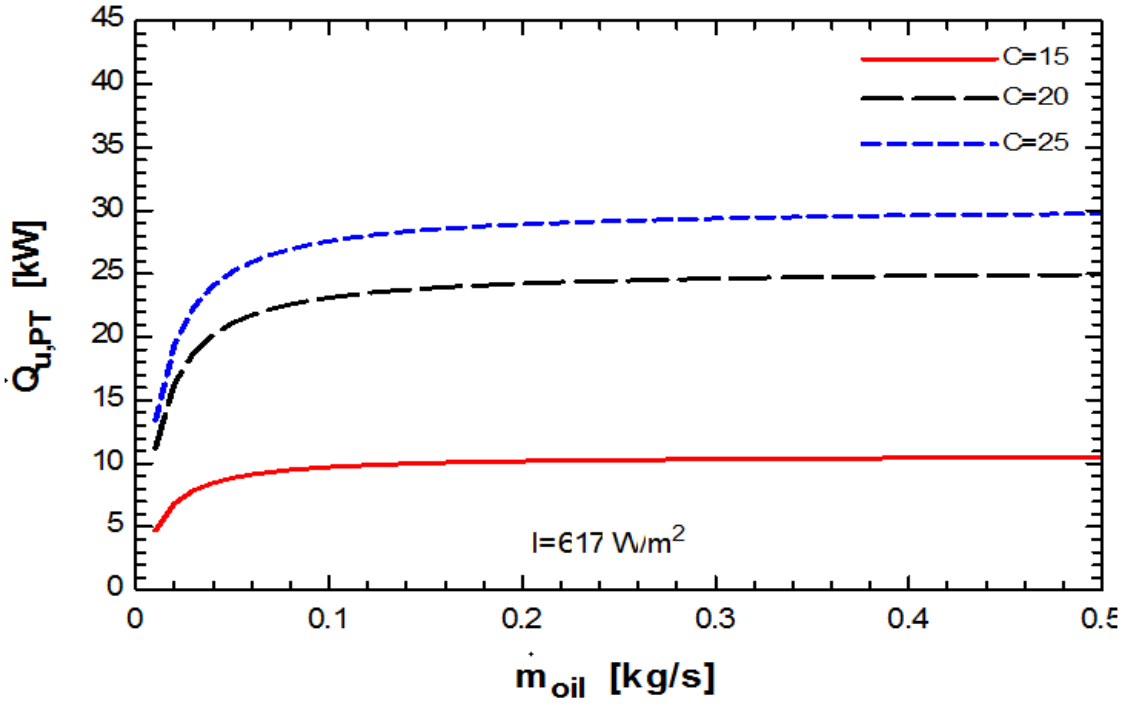

Fig. 4.29 Rate of heat generated by the PTSC unit for different mass flow rates of oil.

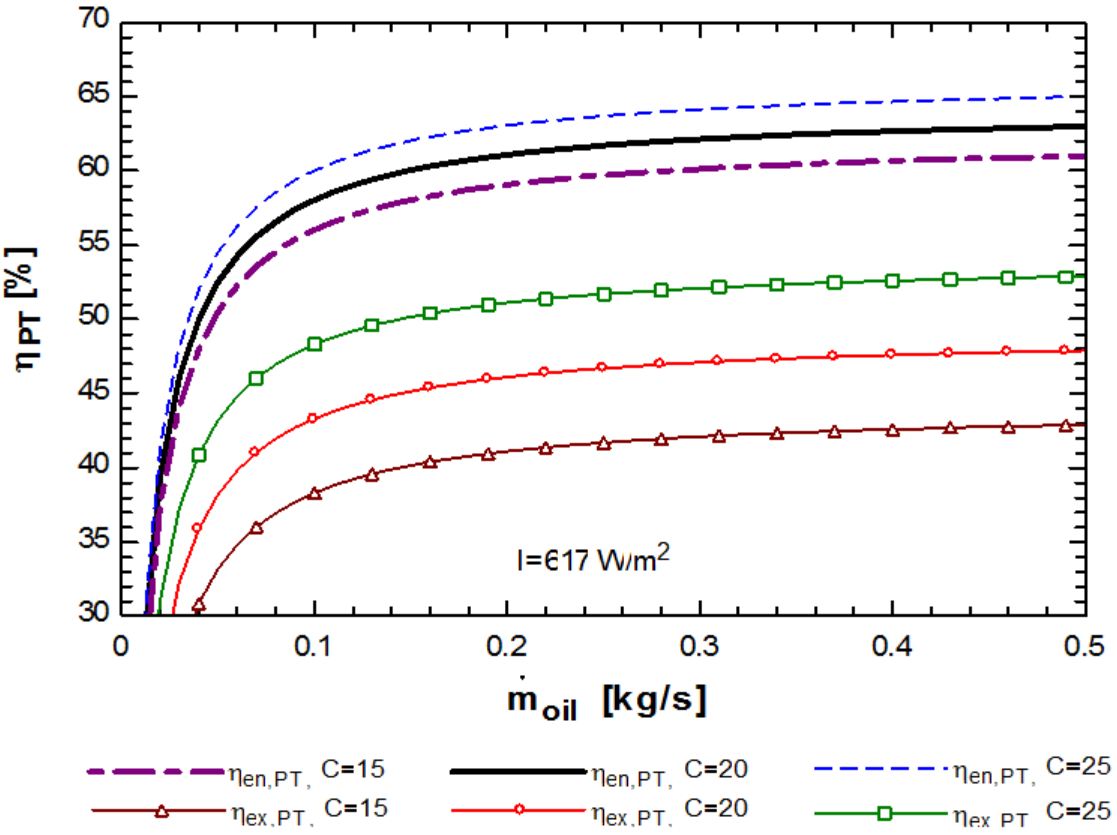

Fig. 4.30 Energy and exergy efficiency of the PTSC unit for different mass flow rates of oil.

Fig. 4.31 shows the variation of the overall efficiency of the integrated system with the solar irradiance. Both energetic and exergetic efficiencies decrease with increasing the solar irradiance at a constant mass flow rate of the oil and constant concentration ratio since increasing solar irradiance while keeping the collector area constant results in higher amounts of solar intensity to be reflected by the collector.

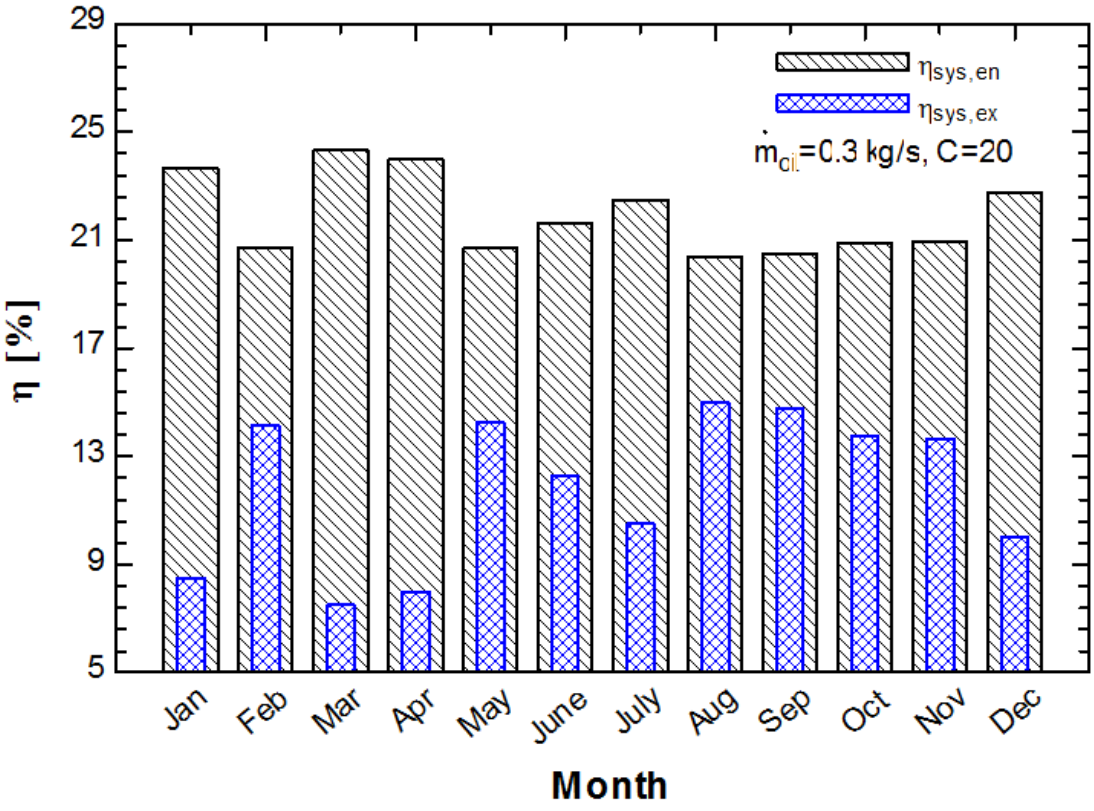

Fig. 4.31 Overall monthly energy and exergy efficiency of the integrated PTSC-based HVAC system for a constant mass flow rate of Therminol-66 and concentration ratio.

Figures 4.32 and 4.33 present the variation of the coefficient of performance of the integrated system with the solar irradiance and mass flow rate of the oil, respectively. It can be noticed that both energetic and exergetic COPs are decreased with increasing the solar irradiance for a constant mass flow rate of oil and constant concentration ratio. Moreover, increasing the mass flow rate of the oil from 0.1 to 0.5 kg/s results in decreasing the energetic COP from 2.15 to 1.98 and the exergetic COP from 2.05 to 1.93. This is due to the fact that increasing the solar irradiance and the mass flow rate of the inlet fluid allow more heat to be generated by the collector so that more power is fed into the absorption system for the same cooling capacity resulting in lowering its performance.

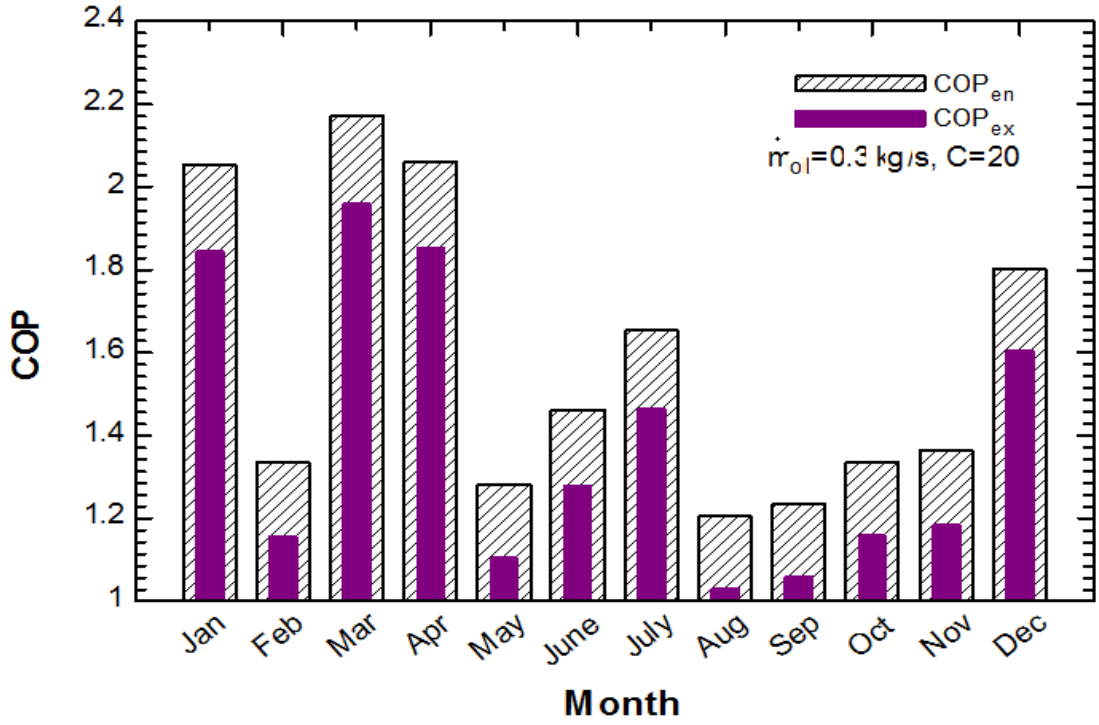

Fig. 4.32 Energy and exergy COP of the integrated PTSC-based HVAC system for a constant mass flow rate of Therminol-66 and concentration ratio.

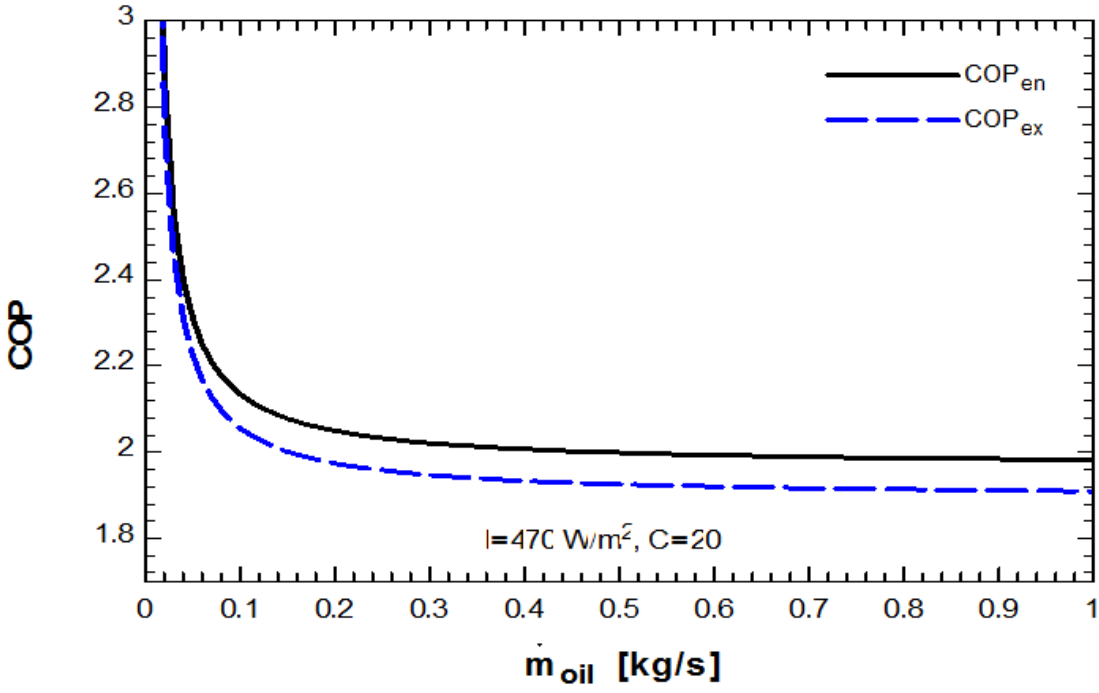

Fig. 4.33 Energy and exergy COP of the integrated PTSC-based HVAC system for different mass flow rates of Therminol-66 and concentration ratios for the month of March.

4.4 PV/T-Based HVAC-Cooling System

Figs. 4.34 and Fig. 4.35 provide weather data for the UAE that is used in conducting the analysis of the PV/T-based HVAC cooling system. The data covers the solar irradiance and the air inlet temperature. The data is used to examine the effect of different operating conditions of the PV/T collector on the performance of the PV/T unit and the integrated system on a monthly basis.

Fig. 4.36 shows the comparison of the present PV/T model with that presented by Joshi [119]. The figure represents the variation of the PV/T overall efficiency with respect to the solar radiation. The small deviation in the present model is due to the different assumptions set for the collector's dimensions and the solar intensity available in the UAE. However, the two models are in good agreement.

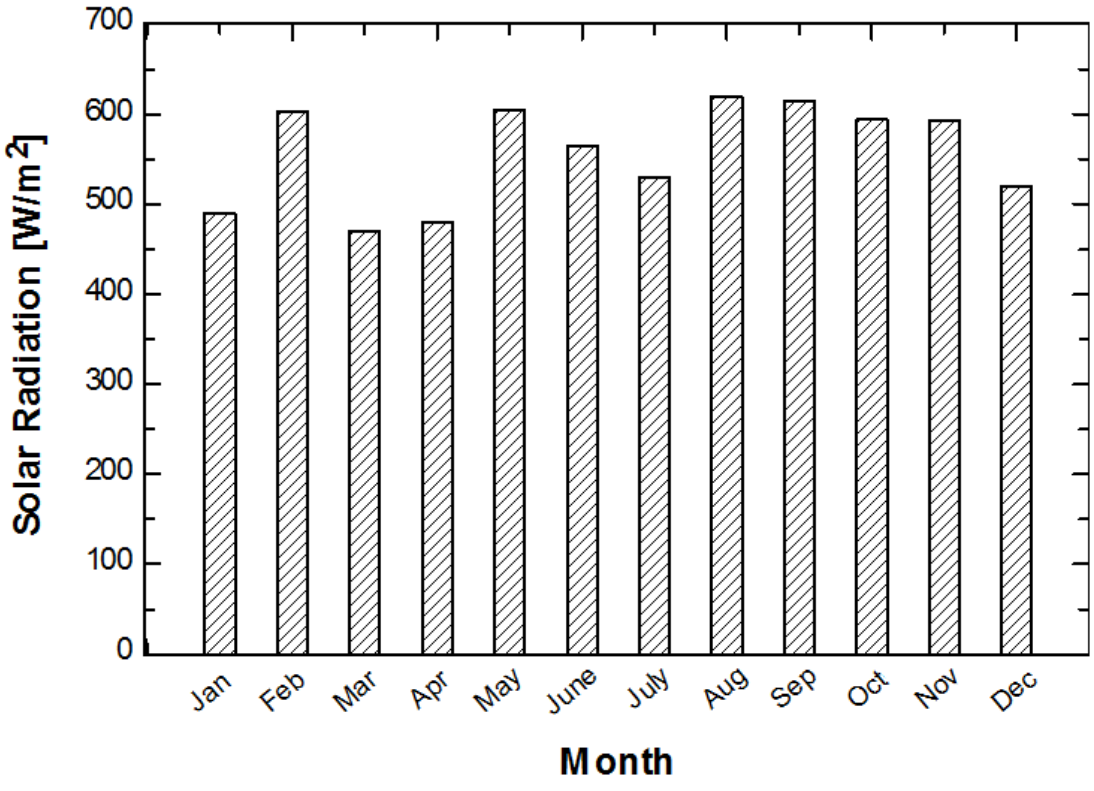

Fig. 4.34 Monthly average solar irradiance for the UAE.

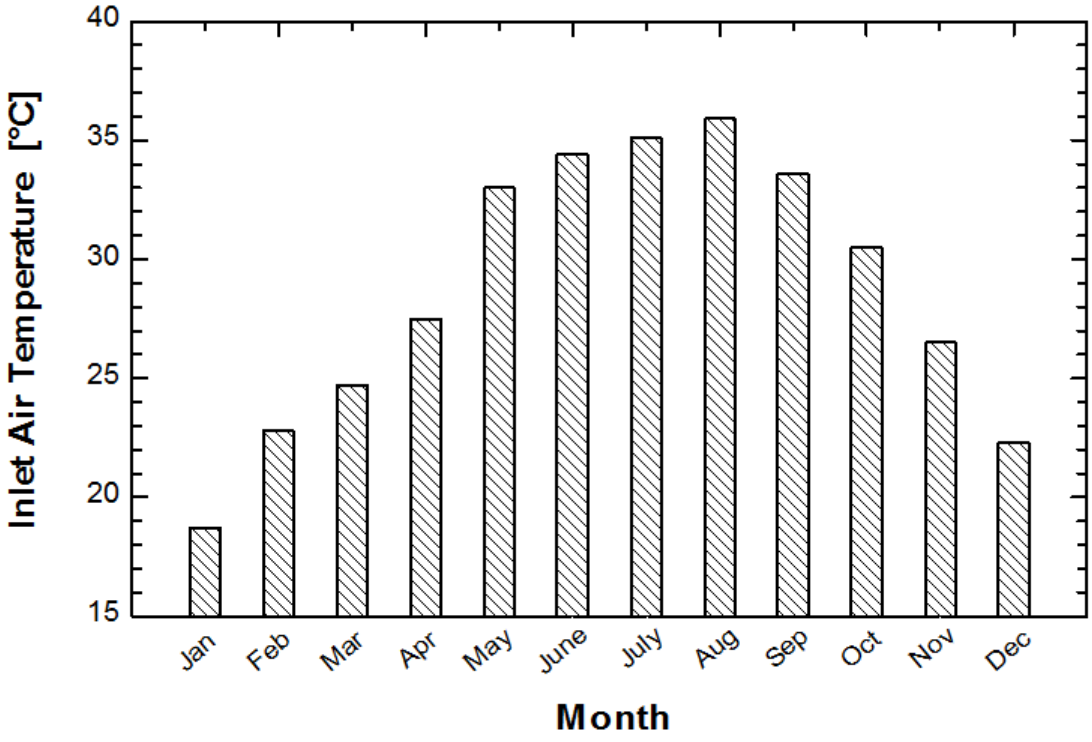

Fig. 4.35 Monthly average inlet air temperature for UAE.

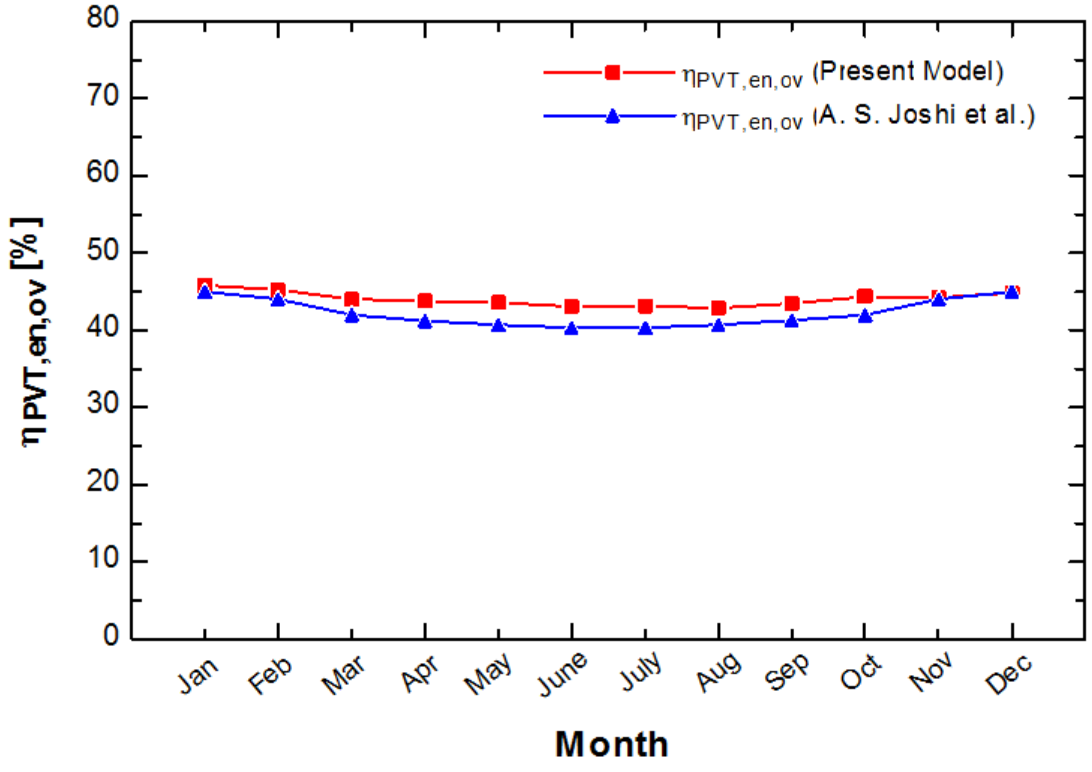

Fig. 4.36 Comparison of the current PV/T model with the model presented by Joshi et al.[119]

Monthly variation of the heat and power generated by the PV/T collector is shown in Fig. 4.37. It is observed that the power output from the PV/T collector increases with increasing solar irradiance and inlet air temperature. This is due to the fact that the electrons flowing within the PV module are excited by the photons available in the solar radiation. So, the more the solar intensity falls on the PV/T, the more the photons excite the electrons into a higher state of energy, allowing them to act as a charge carrier for the electric current. On the other hand, heat generated by the PV/T collector is decreased when the inlet air temperature is increased because of the increase in the difference between inlet air temperature and ambient temperature which causes some of the heat generated to be lost to the surroundings. This is because of the inability of the high temperature air to absorb the generated heat as the flowing air is considered as the heat removal medium.

Monthly average energetic, exergetic and electrical efficiencies of the PV/T collector are provided in Fig. 4.38 and Fig. 4.39. The electrical efficiency of the PV/T collector increases with increasing the solar irradiance, as the greater number of photons available at higher solar irradiance causes more electrons to be excited within the PV module and consequently more current in the PV cells. Energetic efficiency decreases as the solar intensity increases since energetic efficiency measures the capability of the system to generate heat. The heat generated decreases with increasing air inlet temperature. The exergetic efficiency for the PTSC increases with increasing solar irradiance and air inlet temperature. However, the change in exergetic efficiency is small from month to month, although there is significant variation in the solar irradiance and air inlet temperature.

Fig. 4.40 shows how the rate of energy output of the PV/T collector is greatly influenced by the module construction characteristics. One of these characteristics is the collector area. Both, the power output and the heat generated are increased with increasing the collector area as more solar irradiance is absorbed by the collector. So, for higher power and heat production requirements, the PV/T collector can be sized to provide the amount of power and heat needed.

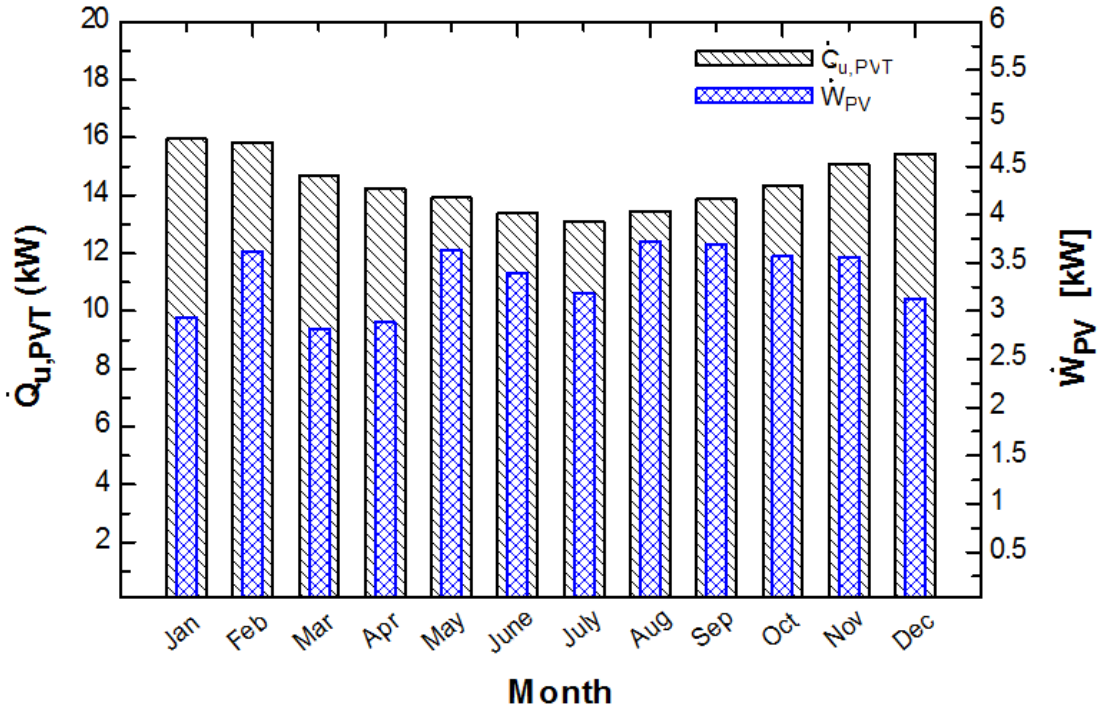

Fig. 4.37 Monthly heat and power generated by the PV/T unit.

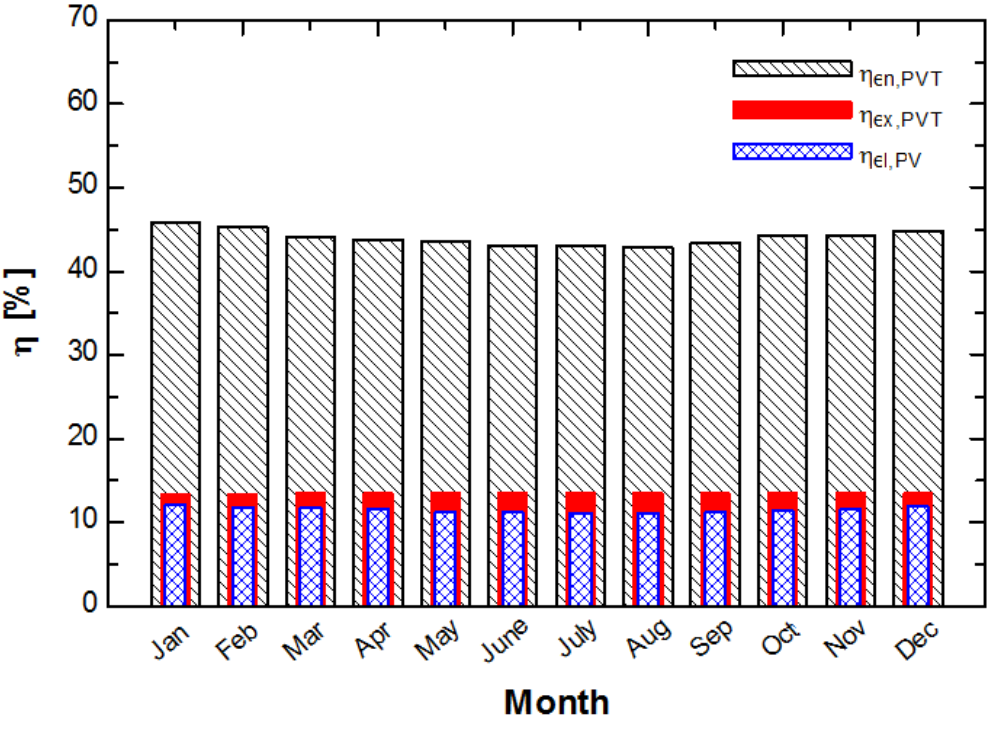

Fig. 4.38 Monthly energetic and exergetic efficiencies obtained by the PV/T unit.

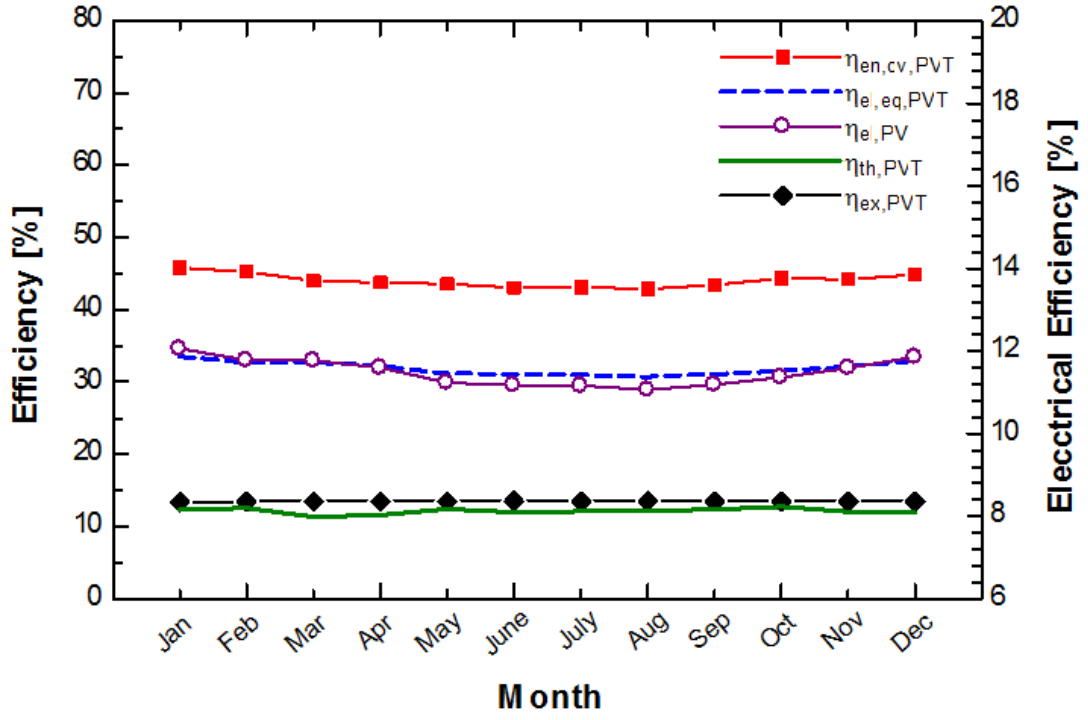

Fig. 4.39 Monthly thermal, energy, exergy, and electrical efficiencies and thermal equivalents of electrical efficiency obtained by the PV/T unit.

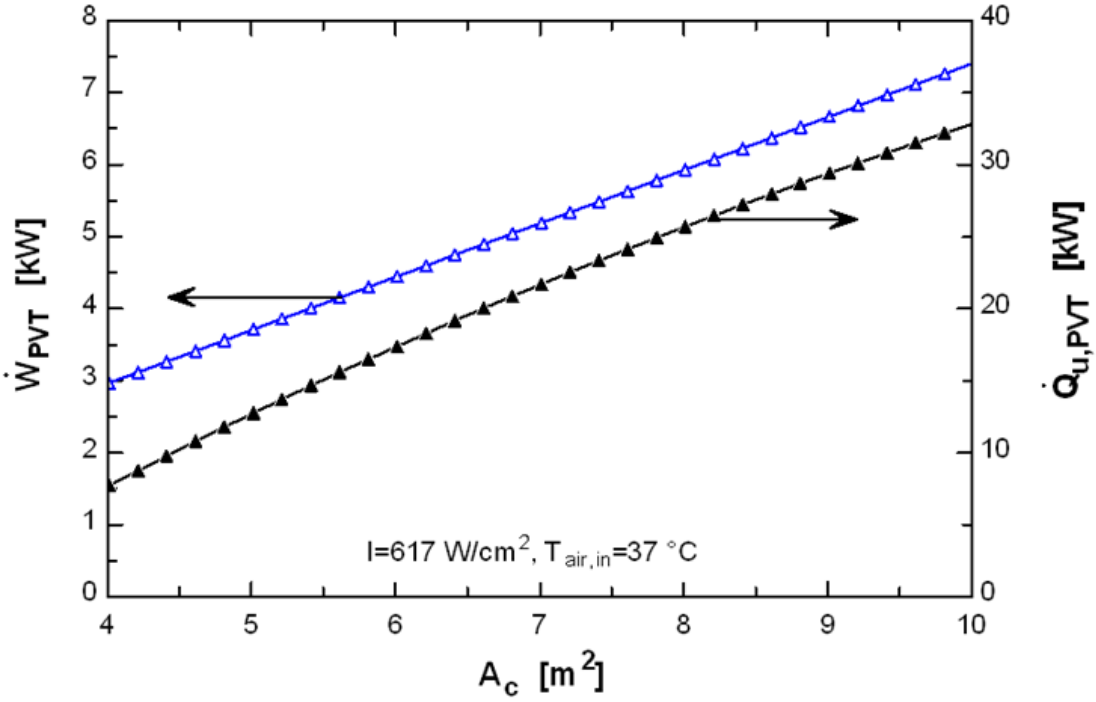

Fig. 4.40 Rate of heat and power generated by the PV/T unit versus collector area.

As the inlet air temperature and solar irradiance increase, the heat generated from the PV/T collector is decreased which causes the heat supplied to the HTG to be decreased. This results in higher energetic and exergetic COPs as shown in Fig. 4.41. The plot is generated for a constant collector area = 5 cm^2 and cooling capacity of 10 kW.

As energetic and exergetic efficiencies of the PV/T collector decrease with increasing the solar irradiance, the overall energetic and exergetic efficiencies of the integrated system are decreased. This is due to high heat dissipation to the surroundings. The effect is shown in Fig. 4.42.

As the inlet air temperature increases, the heat generated from the PV/T collector is decreased. This heat is used to drive the absorption cooling system. Therefore, higher energetic and exergetic COPs are obtained as the inlet air temperature increase as shown in Fig. 4.43 for a constant collector area = 5 cm^2 and cooling capacity of 10 kW. The effect of increasing the collector area on the energetic and exergetic COPs is presented in Fig. 4.44. As the area increases, both COPs are decreased as a result of increasing heat input to the HTG.

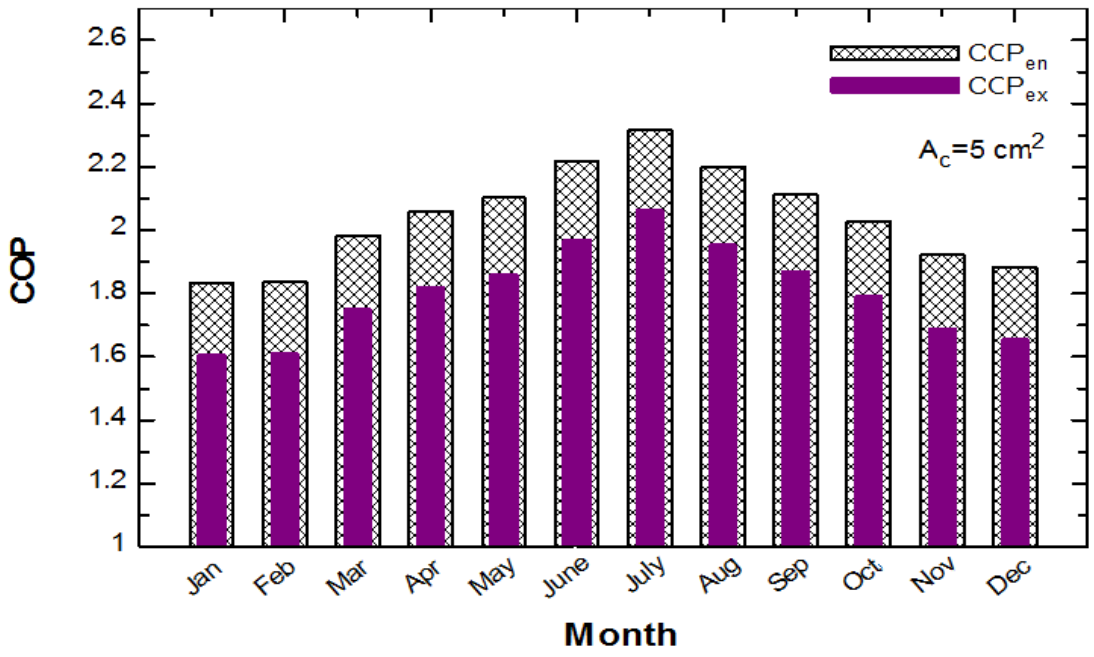

Fig. 4.41 Energy and exergy COP of the integrated PV/T-based HVAC system for collector area = 5 cm^2.

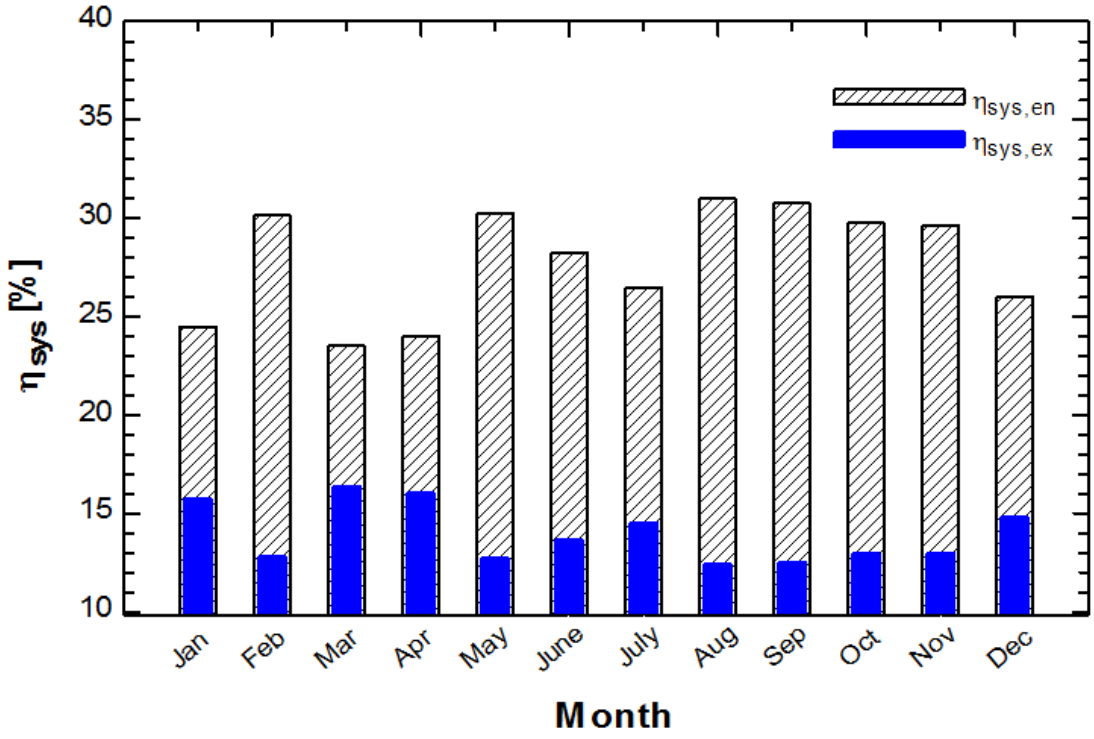

Fig. 4.42 Overall monthly energy and exergy efficiency of the integrated PV/T-based HVAC system for a constant collector area.

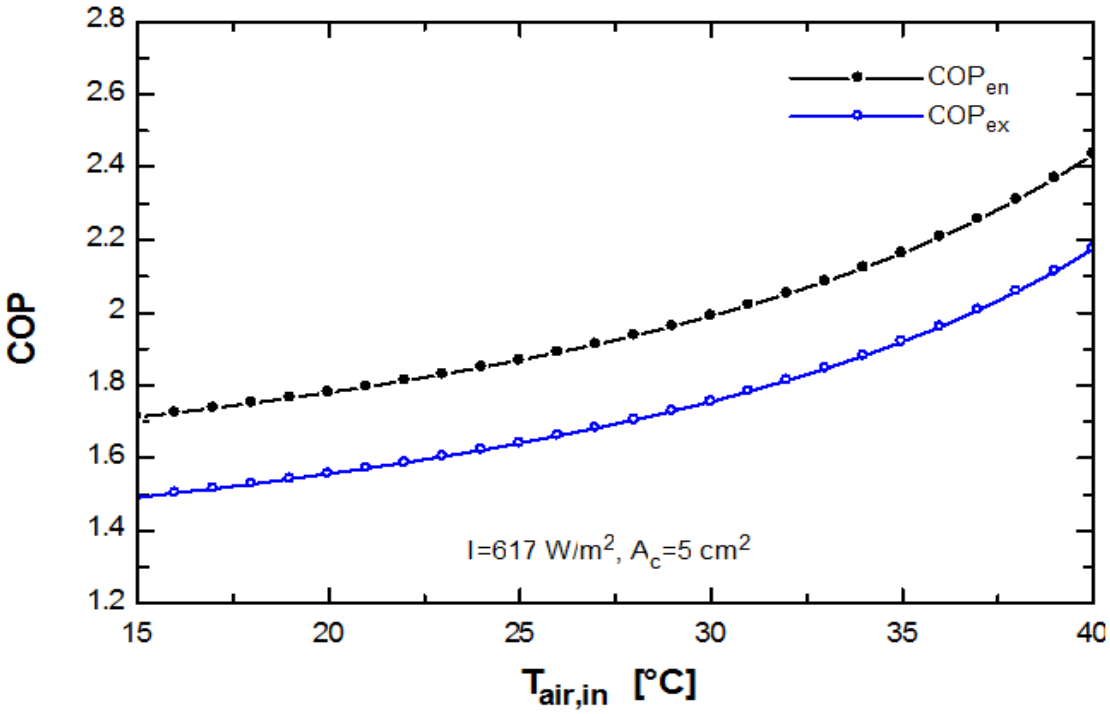

Fig. 4.43 Energy and exergy COP of the integrated PV/T-based HVAC system for different inlet air temperatures and a constant collector area for the month of August.

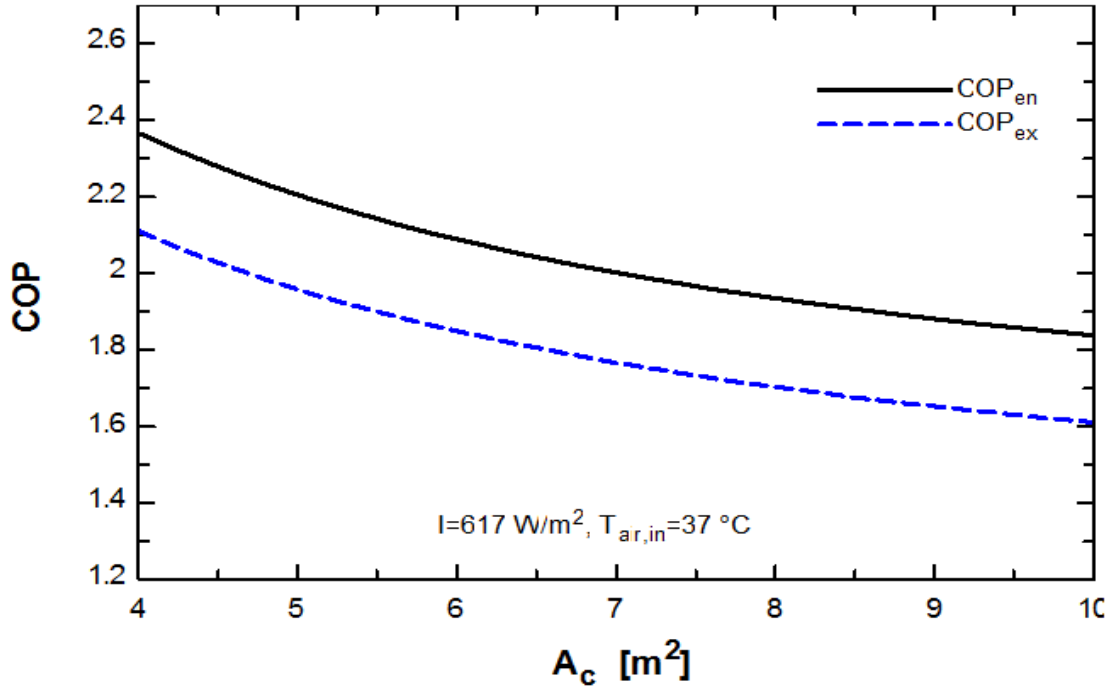

Fig. 4.44 Energy and exergy COP of the integrated PV/T-based HVAC system for different collector areas for the month of August.

4.5 Hybrid PEMFC-PTSC-PV/T-Based HVAC-Cooling System

In this section, optimum design parameters determined from the analyses conducted for the PEMFC-, PTSC- and PV/T-based HVAC cooling systems are used in order to come up with a hybrid system that has the optimum COP and efficiency.

Fig. 4.45 shows the energetic and exergetic COPs of the PEMFC, PTSC and PV/T integrated with a 10 kW DEAS system. The maximum energetic and exergetic COPs attained by the hybrid system are 2.936 and 2.500, respectively, which occur in March where the solar irradiance is minimum. The minimum energetic and exergetic COPs which are 2.239 and 2.137, respectively, correspond to August which characterized by high solar irradiance. This is due to the fact that increasing the solar irradiance allows more heat to be generated by the collector so that more power is fed into the absorption system for the same cooling capacity resulting in lowering its performance.

Fig. 4.46 shows the overall monthly energetic and exergetic efficiencies of the hybrid system. The maximum energetic efficiency 69.13% corresponds to March while the minimum energetic efficiency 64.27 % corresponds to August. The maximum exergetic efficiency attained by the integrated system is 54.64 % and it occurs in March while its minimum value, 52.06%, corresponds to August.

The inverse relation is due to the fact that increasing the solar irradiance while keeping the collector area constant results in a higher amount of solar intensity to be dissipated to the surroundings.

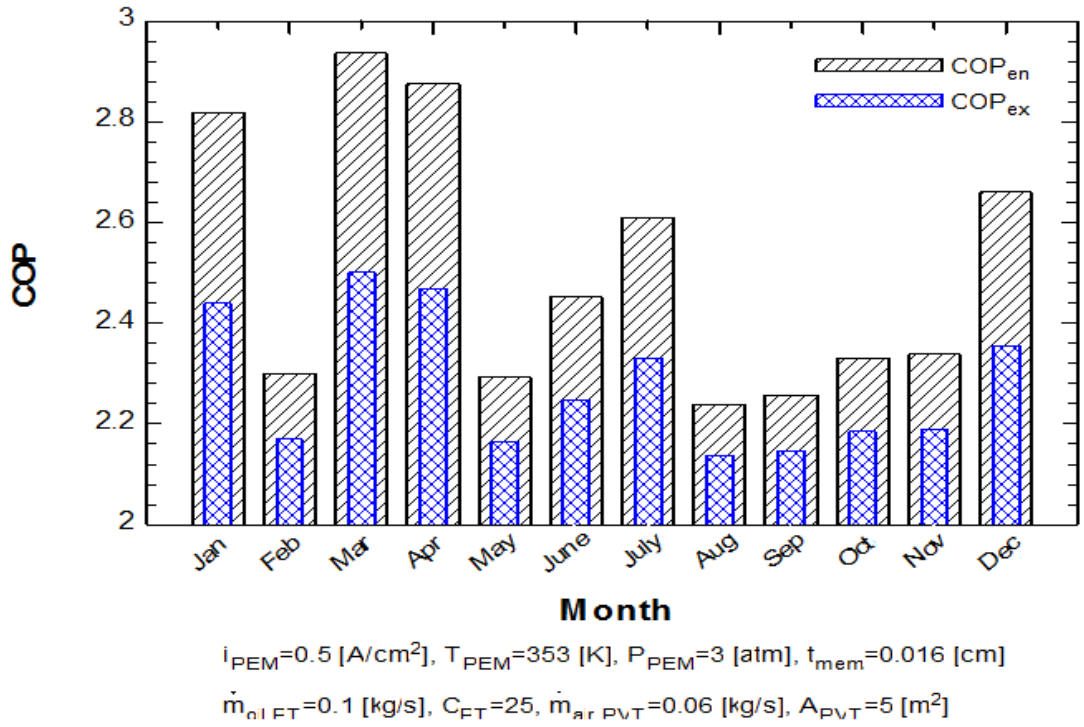

Fig. 4.45 Optimum energetic and exergetic COPs obtained by the hybrid system.

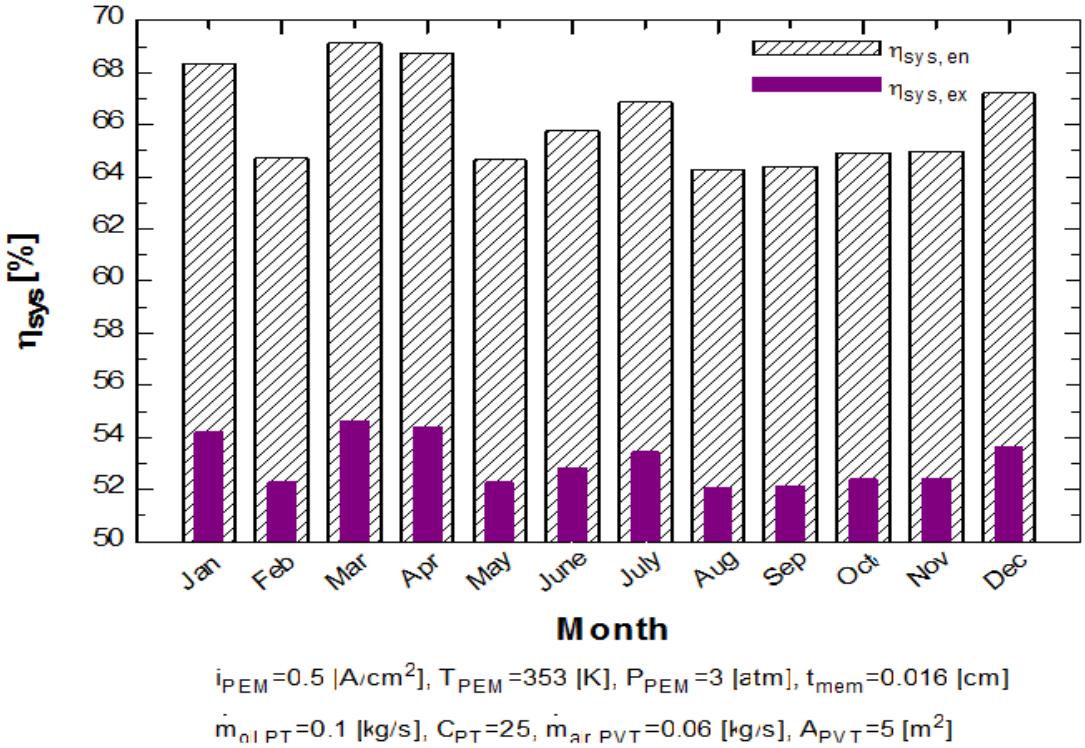

Fig. 4.46 Optimum energetic and exergetic efficiencies obtained by the hybrid system.

4.6 Summary of Results

In order to choose the optimum design of the absorption system, a comparison between the proposed systems based on their performance and efficiency is provided in this section.

Table 4.1 shows the values obtained for the energetic and exergetic COPs as well as the energetic and exergetic efficiencies of the proposed systems. PEMFCs integrated with double effect absorption cooling system result in the highest COP among the FPSC-, PTSC-, and PV/T-integrated systems followed by the PV/T integrated with the triple effect absorption cooling system. The low performance of the solar systems is due to the unavailability of solar irradiance in the evening.

In addition, PEMFC integrated with DEAS presents the optimum design economically as it provides the highest energetic and exergetic COPs as well as the highest energetic and exergetic efficiencies. The usage of the double effect absorption cooling system is more cost effective and more suitable for small cooling capacities. The factory cost of a 10 kW PEMFC stack is about 650 $/kW including materials and labor costs plus any balance of plant necessary for stack operation. Regarding the operating lifetime, the PEMFC system can operate up to 30,000 hours which ensures the continuous operation of the PEMFC system for 3-4 years. As a result, the system can provide the 10 kW cooling capacity so that no backup power from the grid is needed. Moreover, the maintenance cost of the system is low depending on the frequency of repairs and the replacement cost of components due to failure and wear out which are rarely occur. Also, regular maintenance could be done without turning off the PEMFC system, and the only time it would be turned off is for change out of the cell stack or every 30,000 hr. So, although the capital cost of the stationary PEMFC system is high, the running cost of the system is low [120].

However, the cost of the solar systems are less than that of fuel cells systems as the input fuel (solar energy) is considered free since it can be obtained from an available source in nature that is free of charge and is non-depleting. Moreover, solar energy can be used repeatedly without running down. In addition, the use of thermal storage systems in FPSC, PTSC and PV/T systems will greatly enhance the performance of these systems

so that they will be more practical and suitable for residential and commercial buildings in the UAE which is characterized by a sunny climate. The cost of a solar energy system depends on many factors such as system size, site work and infrastructure, heat transfer fluid medium, and whether thermal energy storage is included. Costs per unit area, however, are generally higher for smaller systems and lower for larger systems. So, although the PEMFCs system has the highest efficiency and performance, solar energy is still more cost effective.

The integration of PEMFCs, PTSCs and PV/Ts with a double effect absorption system results in improved COP in comparison with the use of PTSCs or PV/Ts with a triple effect system for the same cooling capacity of 10 kW. This is because the double effect system utilizes the beneficial output from all of these alternative sources of energy. This hybrid system is the optimum design from a performance point of view. However, economics and cost should be taken into account in considering the proposed system, especially for small scale units. As compared to the PEMFC system, the small increase in the energetic COP (from 2.70 to 2.94) is not a worthwhile investment in comparison to the increase in the system size and the variety in energy sources used which in turn affects the overall cost of the hybrid system. Thus, the hybrid system is not recommenced to be applied unless large cooling capacities are required.

Table 4.1Comparison between the proposed systems and conventional absorption systems based on their performance and efficiency for cooling load = 10 kW.

System	**Absorption System Configuration**	$\dot{Q}_{HG}$ (**kW**)	COP_{en}	COP_{ex}	$\eta_{sys,en}$ (%)	$\eta_{sys,ex}$ (%)	**Conventional Absorption System (COP_{en})**
PEMFC Based HVAC System	Double effect	14.8	2.70	2.30	63.41	53.60	1.00-1.40
FPSC Based HVAC System	Double effect	17.2	1.88	1.81	19.54	14.50	1.00-1.40
PTSC Based HVAC System	Triple effect	16.4	2.17	1.96	24.34	14.80	1.40-1.60
PV/T Based HVAC System	Triple effect	14.5	2.32	2.06	30.75	16.40	1.40-1.60
Hybrid Based HVAC System	Double effect	31.2	2.94	2.50	69.13	54.64	1.00-1.40

Chapter 5 Conclusions and Recommendations

Alternative cooling systems have been proposed by integrating selected renewable energy sources, PEMFC, FPSC, PTSC and PV/T collectors, with double effect and triple effect parallel flow absorption cooling systems that can solve the high energy demand and high emissions issues associated with conventional cooling systems. Thermodynamic (energy and exergy) analyses of the integrated systems have been performed. In addition, a parametric study has been conducted to investigate the effect of variation in design parameters on the systems' efficiency, performance, heat gain, and output power.

5.1 Conclusions

Energy and exergy analyses conducted for the PEMFC show that increasing the current density has a negative effect on both energy and exergy efficiencies of the PEMFC. Also, increasing the current density results in an increase in the power output and heat generated by the PEMFC as well as an increase in the irreversibility of the system. Moreover, both energetic and exergetic COPs of PEMFC-based HVAC cooling systems decrease with increased current density. The same behavior is observed by the energetic and exergetic efficiencies of the integrated system.

From the parametric study of the PEMFC, it is concluded that increasing the PEMFC operating temperature results in increasing the energy efficiency and power output. In contrast, increasing the membrane thickness causes the efficiency and power to be decreased. For the same increase in the operating temperature, the exergy efficiency increases while the irreversibility decreases. Also, a decrease in the energetic and exergetic COPs is observed when the PEMFC operating temperature is increased.

The monthly variation of the rate of heat generated by the FPSC results in a positive behavior for the heat generated against the solar irradiance and inlet water temperature. As a result, the thermal efficiency of the FPSC is increased with increasing the same variables while the exergetic efficiency is decreased. Regarding the variation of COPs and energetic and exergetic efficiencies of the integrated system, both energetic

and exergetic COPs as well as energetic and exergetic overall efficiencies are decreasing with increasing the solar irradiance and the inlet water temperature.

The parametric study of the FPSC integrated system shows that the rate of heat generated increases more rapidly to a certain limit at low mass flow rates of water at which it becomes almost constant for higher flow rates. In addition, increasing the collector area causes the rate of heat generated to increase. Moreover, increasing the mass flow rate of the inlet water causes the energetic efficiency to be increased. However, increasing the mass flow rate at higher rates does not have a great influence on the thermal efficiency of the solar system. On the other hand, increasing the collector area has a negative effect on the energetic efficiency of the solar collector unit. Energetic and exergetic COPs of the integrated systems are affected by the rate of water mass flowing into the system as they are decreased with increasing the mass flow rate. Nevertheless, the mass flow rate has insignificant improvement on the overall performance of the integrated system.

Energy and exergy analyses of the PTSC show that the highest rate of heat generation is obtained in August as the solar irradiance is maximum in this month. This in turn affects the energetic and exergetic efficiencies positively. However, both energetic and exergetic COPs of the PTSC-based HVAC cooling system are decreased with increasing solar irradiance.

The parametric study done for the PTSC shows that heat generation rate and energy and exergy efficiencies are increased by increasing the mass flow rate of the working fluid. However, increasing the mass flow rate of the working fluid results in decreasing the energetic and exergetic COPs of the system.

Results obtained from the analysis of the PV/T integrated system show that the efficiency of the PV/T collector is greatly influenced by the system construction and climatic parameters with the primary parameters being solar irradiance, inlet air temperature, and collector area. The power output from the PV/T collector increases with increasing solar irradiance and inlet air temperature while the heat generated by the PV/T collector is decreased. The electrical and exergetic efficiencies of the PV/T collector increase with increasing the solar irradiance while the energetic efficiency decreases. Regarding the overall integrated system performance, increasing the inlet air

temperature and solar irradiance causes the energetic and exergetic COPs to be increased, while it causes the overall energetic and exergetic efficiencies of the integrated system to decrease.

Results obtained from the parametric study conducted for the PV/T show that the power output and the heat generated are increased with increasing PV/T collector area while both energetic and exergetic COPs are decreased.

In the integrated PEMFC-PTSC-PV/T absorption cooling system, the maximum and minimum energetic and exergetic COPs and overall monthly energetic and exergetic efficiencies attained by the integrated system occur in March and August, respectively. The system shows considerable improvement compared to the conventional double effect absorption cooling system.

The comparison of the proposed systems shows that the PEMFC system integrated with a double effect absorption cooling system results in the highest COP among the FPSC-, PTSC- and PV/T-integrated systems, followed by the PV/T integrated with a triple effect absorption cooling system. The integration of PEMFCs, PTSCs and PV/Ts with a double effect absorption system results in improved COP in comparison to the use of PTSCs or PV/Ts with a triple effect system for the same cooling capacity of 10 kW. However, the hybrid system is not economically attractive, especially for small scale units unless a thermal storage medium is included.

5.2 Recommendations

It is recommended that comprehensive research and analysis on methods of fluid storage is conducted as it is a crucial unit in renewable energy systems. Thermal storage systems are the most appropriate methods of correcting the mismatch that occurs between the supply and demand of energy. Therefore, they are essential in overcoming the disadvantage of the intermittent nature of solar energy and variation in cooling demand.

For PTSCs, a tracking system can be implemented for better utilization of solar irradiance so that the efficiency of the system can be further enhanced, leading to the improvement of the overall performance of the integrated system.

Moreover, a detailed cost analysis of the integrated systems is highly recommended in order to study the systems' performance from an economic point of view.

Finally, results presented in this research can form the basis of further research toward the fulfillment of the UAE strategy in sustainable building operations.

REFERENCES

[1] M. Thirugnanasambandam, S. Iniyan, and R. Goic, "A review of solar thermal technologies," *Renewable and Sustainable Energy Reviews*, vol. 14, no. 1, pp. 312-322, Jan. 2010.

[2] APS Review Downstream Trends, "UAE - The Local Energy Market," 24-May-2010. [Online]. Available: www.entrepreneur.com/tradejournals/pub/0WDB.html.[Accessed: 27-May-2010].

[3] Gulf News, "UAE energy consumption beats global growth levels," 20-May-2008. [Online]. Available: http://gulfnews.com/business/oil-gas/uae-energy-consumption-beats-global-growth-levels-1.105925. [Accessed: 24-Feb-2010].

[4] Anne-Birte Stensgaard, "LG calls for reduction in GCC power consumption," 23-Aug-2005. [Online]. Available: http://www.ameinfo.com/66216.html. [Accessed: 24-Feb-2010].

[5] F. Agyenim, I. Knight, and M. Rhodes, "Design and experimental testing of the performance of an outdoor LiBr/H_2O solar thermal absorption cooling system with a cold store," *Solar Energy*, vol. 84, no. 5, pp. 735-744, May 2010.

[6] University of California, "Non-renewable Energy Sources," 25-Sep-2009. [Online]. Available: http://cnx.org/content/m16730/latest/. [Accessed: 02-Mar-2010].

[7] Nation Master, "CO_2 Emissions (most recent) by country," 2003. [Online]. Available: http://www.nationmaster.com/graph/env_co2_emi-environment-co2-emissions. [Accessed: 25-Feb-2010].

[8] P. Kasotia, "The health effects of global warming: developing countries are the most vulnerable.," 01-Jun-2007. [Online]. Available: http://www.un.org/wcm/content/site/chronicle/home/archive/issues2007/greenourworld/pid/21636. [Accessed: 21-Apr-2010].

[9] Douglas Fischer, "Can Alternative Energy Save the Economy and the Climate?," 13-Nov-2009. [Online]. Available: http://www.scientificamerican.com/article.cfm?id=copenhagen-consequences-investments-low-carbon. [Accessed: 28-Apr-2010].

[10] M. Cloutier, “Refrigeration Cycles.” [Online]. Available: http://web.me.unr.edu/me372/Spring2001/Refrigeration%20Cycles.pdf. [Accessed: 09-May-2010].

[11] H. Khemani, “Advantages and Disadvantages of Absorption Refrigeration over Vapor Compression Refrigeration System,” Bright Hub, 17-Mar-2010. [Online]. Available: http://www.brighthub.com/engineering/mechanical/articles/66476/p1. [Accessed: 09-May-2010].

[12] Smithsonian Institution, “Fuel Cell Basics,” 2008. [Online]. Available: http://americanhistory.si.edu/fuelcells/basics.htm. [Accessed: 24-Feb-2010].

[13] EG&G Technical Services, Inc., *Fuel Cell Handbook*, Seventh ed. Morgantown, West Virginia: National Energy Technology Laboratory, 2004.

[14] V. Ramani, “Fuel Cells,” *The Electrochemical Society Interface*, Spring 2006.

[15] FuelCell Energy, “Benefits of Fuel Cell Technology,” 2010. [Online]. Available: http://www.fuelcellenergy.com/benefits-fuel-cell-technology.php. [Accessed: 24-Feb-2010].

[16] W. Vielstich, H. Gasteiger, and A. Lamm, *Handbook of Fuel Cells – Fundamentals, Technology and Applications*, vol. 4: Fuel Cell Technology and Applications. John Wiley & Sons, Ltd, 2003.

[17] J. Larminie and A. Dicks, *Fuel Cell Systems Explained*. England: WILEY, 2000.

[18] C. Rayment and S. Sherwin, *Introduction to Fuel Cell Technology*. Notre Dame, U.S.A: University of Notre Dame, 2003.

[19] Z. Şen, *Solar Energy Fundamentals and Modeling Techniques*. London: Springer London, 2008.

[20] S. Kalogirou, “Solar thermal collectors and applications,” *Progress in Energy and Combustion Science*, vol. 30, no. 3, pp. 231-295, 2004.

[21] S. Kalogirou, *Solar Energy Engineering: Processes and Systems*. USA: Elsevier Science & Technology, 2009. [Online]. Available: <http://lib.myilibrary.com.ezproxy.aus.edu?ID=228560>

[22] F. Mahjouri, “Vacuum Tube Liquid-Vapor (Heat-Pipe) Collectors,” [Online]. Available: www.thermotechs.com. [Accessed: 18-Aug-2010].

[23] Event horizon solar, "Solar flat plate vs. evacuated tube collectors." [Online]. Available: http://eventhorizonsolar.com. [Accessed: 18-Aug-2010].

[24] A. Fernández-García, E. Zarza, L. Valenzuela, and M. Pérez, "Parabolic-trough solar collectors and their applications," *Renewable and Sustainable Energy Review*s, vol. 14, no. 7, pp. 1695-1721, Sep. 2010.

[25] National Renewable Energy Laboratory, "Parabolic-Trough Solar Water Heating," 2000. [Online]. Available: http://www.eren.doe.gov/femp/.

[26] Wikipedia, "Solar thermal collector," Jul-2010. [Online]. Available: http://en.wikipedia.org/wiki/Solar_thermal_collector.[Accessed: 22-Sep-2010].

[27] F. Sarhaddi, S. Farahat, H. Ajam, A. Behzadmehr, M. Mahdavi Adelis. "An improved thermal and electrical model for a solar photovoltaic thermal (PV/T) air collector". *Applied Energy*, vol. 87, no. 7,pp. 2328-2339, 2010.

[28] M. D. Islam, A. A. Alili, I. Kubo, and M. Ohadi, "Measurement of solar-energy (direct beam radiation) in Abu Dhabi, UAE," *Renewable Energy*, vol. 35, no. 2, pp. 515-519, Feb. 2010.

[29] L. El Chaar and L. A. Lamont, "Global solar radiation: Multiple on-site assessments in Abu Dhabi, UAE," *Renewable Energy*, vol. 35, no. 7, pp. 1596-1601, Jul. 2010.

[30] H. T. Chua, H. K. Toh, A. Malek, K. C. Ng, and K. Srinivasan, "A general thermodynamic framework for understanding the behaviour of absorption chillers," *International Journal of Refrigeration*, vol. 23, no. 7, pp. 491-507, Nov. 2000.

[31] T. Jaruwongwittaya and G. Chen, "A review: Renewable energy with absorption chillers in Thailand," *Renewable and Sustainable Energy Reviews*, vol. 14, no. 5, pp. 1437-1444, Jun. 2010.

[32] M. I. Karamangil, S. Coskun, O. Kaynakli, and N. Yamankaradeniz, "A simulation study of performance evaluation of single-stage absorption refrigeration system using conventional working fluids and alternatives," *Renewable and Sustainable Energy Reviews*, vol. 14, no. 7, pp. 1969-1978, Sep. 2010.

[33] P. Srikhirin, S. Aphornratana, and S. Chungpaibulpatana, "A review of absorption refrigeration technologies," *Renewable and Sustainable Energy Reviews*, vol. 5, no. 4, pp. 343-372, Dec. 2001.

[34] U. Eicker and D. Pietruschka, “Design and performance of solar powered absorption cooling systems in office buildings,” *Energy and Buildings*, vol. 41, no. 1, pp. 81-91, Jan. 2009.

[35] S. C. Kaushik and A. Arora, “Energy and exergy analysis of single effect and series flow double effect water–lithium bromide absorption refrigeration systems,” *International Journal of Refrigeration*, vol. 32, no. 6, pp. 1247-1258, Sep. 2009.

[36] M. B. Arun, M. P. Maiya, and S. S. Murthy, “Performance comparison of double-effect parallel-flow and series flow water–lithium bromide absorption systems,” *Applied Thermal Engineering*, vol. 21, no. 12, pp. 1273-1279, Aug. 2001.

[37] R. Gomri and R. Hakimi, “Second law analysis of double effect vapour absorption cooler system,” *Energy Conversion and Management*, vol. 49, no. 11, pp. 3343-3348, Nov. 2008.

[38] G. Rabah, “Second law comparison of single effect and double effect vapour absorption refrigeration systems,” *Energy Conversion and Management*, vol. 50, no. 5, pp. 1279-1287, May 2009.

[39] A. Hajizadeh Aghdam, F. Ranjbar and S.M. Seyed Mahmoudi, “Performance comparison of triple-effect parallel flow and series flow absorption refrigeration systems”, *Journal of Applied Sciences*, vol. 8, no. 16, pp. 2913-2918, 2008.

[40] Y. Kaita, “Simulation results of triple-effect absorption cycles,” *International Journal of Refrigeration*, vol. 25, no. 7, pp. 999-1007, Nov. 2002.

[41] G. Bizzarri and G. L. Morini, “Greenhouse gas reduction and primary energy savings via adoption of a fuel cell hybrid plant in a hospital,” *Applied Thermal Engineering*, vol. 24, no. 2-3, pp. 383-400, Feb. 2004.

[42] A. Ferguson and V. Ismet Ugursal, “Fuel cell modeling for building cogeneration applications,” *Journal of Power Sources*, vol. 137, no. 1, pp. 30-42, Oct. 2004.

[43] M. T. Gencoglu and Z. Ural, “Design of a PEM fuel cell system for residential application,” *International Journal of Hydrogen Energy*, vol. 34, no. 12, pp. 5242-5248, Jun. 2009.

[44] Lejda K. Fuel Cells as Source of Ecological Energy for Automotive Vehicles. Rzeszow University of Technology, Faculty of Mechanical Engineering and Aeronautics, Rzeszow, Poland. 2004.

[45] K. Kordesch et al., "Alkaline fuel cells applications," *Journal of Power Sources*, vol. 86, no. 1-2, pp. 162-165, Mar. 2000.

[46] I. Verhaert, M. De Paepe, and G. Mulder, "Thermodynamic model for an alkaline fuel cell," *Journal of Power Sources*, vol. 193, no. 1, pp. 233-240, Aug. 2009.

[47] J. Norland, "Fuel cells may reshape home HVAC," *The Air Conditioning, Heating and Refrigeration NEWS*, 2000. [Online]. Available: achrnews.com.[Accessed: 03-May-2010].

[48] Engleman R,"Commercial building applications for fuel cell gas turbine hybrids: analysis of absorption cooling potential using exhaust heat,".[Online]. Available:www.lti-global.com/pdfs/HybridEnergy.pdf.[Accessed: 05-May-2010].

[49] P. Hearn, "Will there be a fuel cell in your future HVAC application?," 01-Feb-2007. [Online]. Available: http://findarticles.com/p/articles/mi_m5PRD/is_4_12/ai_n24998240/. [Accessed: 28-Apr-2010].

[50] Kakaras E, Ginnakopoulos D, Rouvas A, Panopoulos D, "Demonstration of Fuel Cell Technology for Decentralised Co-generation in Greece," Department of Mechanical Engineering, National Technical University of Athens, Greece. 2004.

[51] Seong Je W, Dong Kwan K, Kyung Hoon K, "Fuel cell system and air conditioner using the same,"U.S. Patent 20080223067. 2008.

[52] Romey I, Behrens D, Schmitz S,"Proton Exchange Membrane Fuel Cells (PEMFC) for Decentral Co-Generation," University of Essen, Technology of Energy Supply and Energy Conversion Systems, Essen, Germany. 2004.

[53] T. E. Lipman, J. L. Edwards, and D. M. Kammen, "Fuel cell system economics: comparing the costs of generating power with stationary and motor vehicle PEM fuel cell systems," *Energy Policy*, vol. 32, no. 1, pp. 101-125, Jan. 2004.

[54] G. F. McLean, T. Niet, S. Prince-Richard, and N. Djilali, "An assessment of alkaline fuel cell technology," *International Journal of Hydrogen Energy*, vol. 27, no. 5, pp. 507-526, May 2002.

[55] G. Mulder, P. Coenen, A. Martens, and J. Spaepen, "The development of a 6 kW fuel cell generator based on alkaline fuel cell technology," *International Journal of Hydrogen Energy*, vol. 33, no. 12, pp. 3220-3224, Jun. 2008.

[56] E. De Geeter, M. Mangan, S. Spaepen, W. Stinissen, and G. Vennekens, "Alkaline fuel cells for road traction," *Journal of Power Sources*, vol. 80, no. 1-2, pp. 207-212, Jul. 1999.

[57] M. Duerr, S. Gair, A. Cruden, and J. McDonald, "Dynamic electrochemical model of an alkaline fuel cell stack," *Journal of Power Sources*, vol. 171, no. 2, pp. 1023-1032, Sep. 2007.

[58] D. Mohamed A., "Building air conditioning system using fuel cell: Case study for Kuwait," *Applied Thermal Engineering*, vol. 27, no. 17-18, pp. 2869-2876, Dec. 2007.

[59] F. Zink, Y. Lu, and L. Schaefer, "A solid oxide fuel cell system for buildings," *Energy Conversion and Manag*ement, vol. 48, no. 3, pp. 809-818, Mar. 2007.

[60] E. Baniasadi and A. A. Alemrajabi, "Fuel cell energy generation and recovery cycle analysis for residential application," *International Journal of Hydrogen Energy*, vol. 35, no. 17, pp. 9460-9467, Sep. 2010.

[61] K. Alanne, A. Saari, V. I. Ugursal, and J. Good, "The financial viability of an SOFC cogeneration system in single-family dwellings," *Journal of Power Sources*, vol. 158, no. 1, pp. 403-416, Jul. 2006.

[62] K. F. Fong, T. T. Chow, C. K. Lee, Z. Lin, and L. S. Chan, "Comparative study of different solar cooling systems for buildings in subtropical city," *Solar Energy*, vol. 84, no. 2, pp. 227-244, Feb. 2010.

[63] E. Erdil, M. Ilkan, and F. Egelioglu, "An experimental study on energy generation with a photovoltaic (PV)–solar thermal hybrid system," *Solar Energy*, vol. 33, no. 8, pp. 1241-1245, Aug. 2008.

[64] Nation Master,"Environment Statistics/ CO_2 Emissions (most recent) by country".[Online]. Available: http://www.nationmaster.com. [Accessed: 25-Feb-2010].

[65] D. S. Kim and C. A. Infante Ferreira, "Solar refrigeration options – a state-of-the-art review," *International Journal of Refrigeration*, vol. 31, no. 1, pp. 3-15, Jan. 2008.

[66] M. Qu, H. Yin, and D. H. Archer, "A solar thermal cooling and heating system for a building: Experimental and model based performance analysis and design," *Solar Energy*, vol. 84, no. 2, pp. 166-182, Feb. 2010.

[67] R. Yoshie, A. Satake, A. Mochida, S. Kato, and H. Yoshino, "Energy conservation effect of new HVAC system for condominiums with solar collectors integrated with the balcony handrail," *Energy and Buildings*, vol. 38, no. 11, pp. 1360-1367, Nov. 2006.

[68] M. Ortiz, H. Barsun, H. He, P. Vorobieff, and A. Mammoli, "Modeling of a solar-assisted HVAC system with thermal storage," *Energy and Buildings*, vol. 42, no. 4, pp. 500-509, Apr. 2010.

[69] D. Johnston, "Solar energy systems installed on Chinese-style buildings," *Energy and Buildings*, vol. 39, no. 4, pp. 385-392, Apr. 2007.

[70] S. Farahat, F. Sarhaddi, and H. Ajam, "Exergetic optimization of flat plate solar collectors," *Renewable Energy*, vol. 34, no. 4, pp. 1169-1174, Apr. 2009.

[71] J. D. Marcos, M. Izquierdo, and D. Parra, "Solar space heating and cooling for Spanish housing: Potential energy savings and emissions reduction," *Solar Energy*, vol. 85, no. 11, pp. 2622-2641, Nov. 2011.

[72] M. Mazloumi, M. Naghashzadegan, and K. Javaherdeh, "Simulation of solar lithium bromide–water absorption cooling system with parabolic trough collector," *Energy Conversion and Management*, vol. 49, no. 10, pp. 2820-2832, Oct. 2008.

[73] A. Mammoli, P. Vorobieff, H. Barsun, R. Burnett, and D. Fisher, "Energetic, economic and environmental performance of a solar-thermal-assisted HVAC system," *Energy and Buildings*, vol. 42, no. 9, pp. 1524-1535, Sep. 2010.

[74] Sophie Masson and Ming Qu. Overall system performance modeling: Solar thermal cooling/heating of the IW. Center for Building Performance and Diagnostics (CBPD). Advanced Building Systems Integration Consortium (ABSIC) Meeting; 2006.

[75] R. Z. Wang and X. Q. Zhai, "Development of solar thermal technologies in China," *Energy*, vol. 35, no. 11, pp. 4407-4416, Nov. 2010.

[76] F. Agyenim, I. Knight, and M. Rhodes, "Design and experimental testing of the performance of an outdoor LiBr/H2O solar thermal absorption cooling system with a cold store," *Solar Energy*, vol. 84, no. 5, pp. 735-744, May 2010.

[77] B. Parida, S. Iniyan, and R. Goic, "A review of solar photovoltaic technologies," *Renewable and Sustainable Energy Reviews*, vol. 15, no. 3, pp. 1625-1636, Apr. 2011.

[78] G. N. Tiwari, R. K. Mishra, and S. C. Solanki, "Photovoltaic modules and their applications: A review on thermal modelling," *Applied Energy*, vol. 88, no. 7, pp. 2287-2304, Jul. 2011.

[79] B. Norton et al., "Enhancing the performance of building integrated photovoltaics," *Solar Energy*, vol. 85, no. 8, pp. 1629-1664, Aug. 2011.

[80] H. I., "PV in buildings - the influence of pv on the design and planning process of a building," *Renewable Energy*, vol. 8, no. 1-4, pp. 467-470, May.

[81] M. D. Bazilian, H. Kamalanathan, and D. K. Prasad, "Thermographic analysis of a building integrated photovoltaic system," *Renewable Energy*, vol. 26, no. 3, pp. 449-461, Jul. 2002.

[82] A. S. Joshi and A. Tiwari, "Energy and exergy efficiencies of a hybrid photovoltaic–thermal (PV/T) air collector," *Renewable Energy*, vol. 32, no. 13, pp. 2223-2241, Oct. 2007.

[83] P. G. Charalambous, G. G. Maidment, S. A. Kalogirou, and K. Yiakoumetti, "Photovoltaic thermal (PV/T) collectors: A review," *Applied Thermal Engineering*, vol. 27, no. 2-3, pp. 275-286, Feb. 2007.

[84] T.T. Chow, "A review on photovoltaic/thermal hybrid solar technology," *Applied Energy*, vol. 87, no. 2, pp. 365-379, 2010.

[85] F. Sarhaddi, S. Farahat, H. Ajam, A. Behzadmehr, and M. Mahdavi Adeli, "An improved thermal and electrical model for a solar photovoltaic thermal (PV/T) air collector," *Applied Energy*, vol. 87, no. 7, pp. 2328-2339, Jul. 2010.

[86] Solutia, "Theminol 66 - High Performance Highly Stable Heat Transfer Fluid."[Online]. Available:http://www.therminol.com/pages/products/66.asp

[87] B. Viorel, "Model of a thermal energy storage device integrated into a solar assisted heat pump system for space heating," *Energy Conversion and Management*, vol. 44, no. 10, pp. 1589-1604, Jun. 2003.

[88] E. Cetin, A. Yilanci, H. K. Ozturk, M. Colak, I. Kasikci, and S. Iplikci, "A micro-DC power distribution system for a residential application energized by photovoltaic–wind/fuel cell hybrid energy systems," *Energy and Buildings*, vol. 42, no. 8, pp. 1344-1352, Aug. 2010.

[89] M. Medrano, J. Brouwer, V. McDonell, J. Mauzey, and S. Samuelsen, "Integration of distributed generation systems into generic types of commercial buildings in California," *Energy and Buildings*, vol. 40, no. 4, pp. 537-548, 2008.

[90] K. E. Herold, R. Radermacher, and S. A. Klein, *Absorption chillers and heat pumps*. USA: CRC Press, 1996.

[91] A. Şencan, K. A. Yakut, and S. A. Kalogirou, "Exergy analysis of lithium bromide/water absorption systems," *Renewable Energy*, vol. 30, no. 5, pp. 645–657, Apr. 2005.

[92] Y. L. Liu and R. Z. Wang, "Performance prediction of a solar/gas driving double effect LiBr–H2O absorption system," *Renewable Energy*, vol. 29, no. 10, pp. 1677–1695, Aug. 2004.

[93] G. P. Xu and Y. Q. Dai, "Theoretical analysis and optimization of a double-effect parallel-flow-type absorption chiller," *Applied Thermal Engineering*, vol. 17, no. 2, pp. 157–170, Feb. 1997.

[94] B. H. Gebreslassie, M. Medrano, and D. Boer, "Exergy analysis of multi-effect water–LiBr absorption systems: From half to triple effect," *Renewable Energy*, vol. 35, no. 8, pp. 1773–1782, Aug. 2010.

[95] G. Rabah, "Investigation of the potential of application of single effect and multiple effect absorption cooling systems," *Energy Conversion and Management*, vol. 51, no. 8, pp. 1629–1636, Aug. 2010.

[96] A. Hajizadeh Aghdam, S. M. S. Mahmoudi, and F. Ranjbar, "Perfromance Comparison of Triple-Effect Parallel Flow and Series Flow Absorption Refrigeration Systems," *Journal of Applied Sciences*, vol. 8, no. 16, pp. 2913–2918, 2008.

[97] M. Ay, A. Midilli, and I. Dincer, “Exergetic performance analysis of a PEM fuel cell,” *International Journal of Energy Research*, vol. 30, pp. 307–321, 2005.

[98] A. Yilanci, I. Dincer, and H. K. Ozturk, “Performance analysis of a PEM fuel cell unit in a solar–hydrogen system,” *International Journal of Hydrogen Energy*, vol. 33, no. 24, pp. 7538–7552, Dec. 2008.

[99] S. O. Mert, I. Dincer, and Z. Ozcelik, “Performance investigation of a transportation PEM fuel cell system,” *International Journal of Hydrogen Energy*, vol. 37, no. 1, pp. 623–633, Jan. 2012.

[100] H. Huisseune, A. Willockx, and M. De Paepe, “Semi-empirical along-the-channel model for a proton exchange membrane fuel cell,” *International Journal of Hydrogen Energy*, vol. 33, no. 21, pp. 6270–6280, Nov. 2008.

[101] M. M. Hussain, J. J. Baschuk, X. Li, and I. Dincer, “Thermodynamic analysis of a PEM fuel cell power system,” *International Journal of Thermal Sciences*, vol. 44, no. 9, pp. 903–911, Sep. 2005.

[102] M. Ay, A. Midilli, and I. Dincer, “Thermodynamic modelling of a proton exchange membrane fuel cell,” *Int. J. Exergy*, vol. 3, no. 1, pp. 16–44, 2006.

[103] A. Sözen, T. Menlik, and S. Ünvar, “Determination of efficiency of flat-plate solar collectors using neural network approach,” *Expert Systems with Applications*, vol. 35, no. 4, pp. 1533-1539, Nov. 2008.

[104] S. R. Dhariwal and U. S. Mirdha, “Analytical expressions for the response of flat-plate collector to various transient conditions,” *Energy Conversion and Management*, vol. 46, no. 11–12, pp. 1809-1836, Jul. 2005.

[105] D. Rojas, J. Beermann, S. A. Klein, and D. T. Reindl, “Thermal performance testing of flat-plate collectors,” *Solar Energy*, vol. 82, no. 8, pp. 746-757, Aug. 2008.

[106] W. Eisenmann, K. Vajen, and H. Ackermann, “On the correlations between collector efficiency factor and material content of parallel flow flat-plate solar collectors,” *Solar Energy*, vol. 76, no. 4, pp. 381-387, Apr. 2004.

[107] I. Luminosu and L. Fara, “Determination of the optimal operation mode of a flat solar collector by exergetic analysis and numerical simulation,” *Energy*, vol. 30, no. 5, pp. 731-747, Apr. 2005.

[108] B. Viorel, "Optimum fin geometry in flat plate solar collector systems," *Energy Conversion and Management*, vol. 47, no. 15–16, pp. 2397-2413, Sep. 2006.

[109] N. Akhtar and S. C. Mullick, "Computation of glass-cover temperatures and top heat loss coefficient of flat-plate solar collectors with double glazing," *Energy*, vol. 32, no. 7, pp. 1067-1074, Jul. 2007.

[110] S. Farahat, F. Sarhaddi, and H. Ajam, "Exergetic optimization of flat plate solar collectors," *Renewable Energy*, vol. 34, no. 4, pp. 1169-1174, Apr. 2009.

[111] Murat Öztürk et al, "Optical, Energetic and Exergetic Analyses of Parabolic Trough Collectors," *Chinese Phys. Lett*, vol. 24, no. 7, pp. 1787-1781, 2007.

[112] F. A. Al-Sulaiman, I. Dincer, and F. Hamdullahpur, "Exergy modeling of a new solar driven trigeneration system," *Solar Energy*, vol. 85, no. 9, pp. 2228-2243, Sep. 2011.

[113] S. K. Tyagi, S. Wang, M. K. Singhal, S. C. Kaushik, and S. R. Park, "Exergy analysis and parametric study of concentrating type solar collectors," *International Journal of Thermal Sciences*, vol. 46, no. 12, pp. 1304-1310, Dec. 2007.

[114] M. Li and L. L. Wang, "Investigation of evacuated tube heated by solar trough concentrating system," *Energy Conversion and Management*, vol. 47, no. 20, pp. 3591-3601, Dec. 2006.

[115] M J Brooks, I Mills, and T M Harms, "Performance of a parabolic trough solar collector," *Journal of Energy in Southern Africa*, vol. 17, no. 3, 2006.

[116] R. Kumar and M. A. Rosen, "A critical review of photovoltaic–thermal solar collectors for air heating," *Applied Energy*, vol. 88, no. 11, pp. 3603-3614, Nov. 2011.

[117] S. Dubey, S. C. Solanki, and A. Tiwari, "Energy and exergy analysis of PV/T air collectors connected in series," *Energy and Buildings*, vol. 41, no. 8, pp. 863-870, Aug. 2009.

[118] S. Dubey, G. S. Sandhu, and G. N. Tiwari, "Analytical expression for electrical efficiency of PV/T hybrid air collector," *Applied Energy*, vol. 86, no. 5, pp. 697-705, May 2009.

[119] S. Joshi, A. Tiwari, G. N. Tiwari, I. Dincer, and B. V. Reddy, "Performance evaluation of a hybrid photovoltaic thermal (PV/T) (glass-to-glass) system," *International Journal of Thermal Sciences*, vol. 48, no. 1, pp. 154-164, Jan. 2009.

[120] National Renewable Energy Laboratory, "1–10 kW Stationary Combined Heat and Power Systems Status and Technical Potential." Nov 2010. [Online]. Available:www.nrel.gov.

VITA

Amani Shaheen Ali Al Hammadi was educated in local schools and graduated in 2002. She completed her higher education at United Arab Emirates University in 2008. Her degree was a Bachelor of Science in Mechanical Engineering.

In 2009, Ms. Amani began a Master's program in Mechanical Engineering at the American University of Sharjah. She was awarded the Master of Science degree in Mechanical Engineering in 2013. Ms. Amani has worked at the Dubai Electricity and Water Authority (DEWA) as an Electromechanical Engineer since 2009.